NTNU

Norwegian University of
Science and Technology

Innovative power system event-detection and synchronous plant emulation technique for large wind power plant

Ryan Allen McGill

Innovative power system event-detection and synchronous plant emulation technique for large wind power plant

Ryan McGill

EWEM: 51008
NTNU: 471809
TU Delft: 4470605

21 June, 2017

European Wind Energy Masters Programme

MSc Technology-Wind Energy
Norwegian University of Science and Technology, Trondheim, NO

MSc Electrical Engineering
Delft University of Technology, Delft, NL

MSc Thesis Committee

Olimpo Anaya-Lara   Signature/Date:
Professor, NTNU

Pavol Bauer   Signature/Date:
Professor, TU Delft

Henk Polinder   Signature/Date:
Associate Professor, TU Delft

Raymundo Torres-Olguin   Signature/Date:
Ph.D., SINTEF Energy Research

Preface

This masters thesis was written in the 2016/17 academic year at the Department of Electric Power Engineering at the Norwegian University of Science and Technology in partial fulfilment of the degree MSc Technology-Wind Energy. The project was undertaken with direct supervision from Professor Olimpo Anaya-Lara of NTNU and Raymundo Torres-Olguin, Ph.D. of SINTEF Energy Research in Trondheim Norway. Under the canopy of the European Wind Energy Masters Programme, this document is also intended to satisfy the thesis report requirement toward the degree MSc Electrical Engineering from Delft University of Technology in Delft Netherlands. Professor Pavol Bauer and Associate Professor Henk Polinder represent the Electrical Sustainable Energy Department at the Delft University of Technology on the MSc Thesis Committee.

The subject matter of this thesis report investigates a synthetic inertia and dynamic stability technique for grid inter-connection of large VSC-HVDC connected offshore windfarms. Assuming traditional load frequency control on the AC grid for the short-term reallocation of power generation resources due to load disturbances, this technique ties the dynamic response of the windfarm to the dynamic response of a small synchronous generator at a point of common coupling. The report uses electromagnetic transient simulation to show that the windfarm can be made to react to onshore frequency events similar to any other synchronous generation source participating in power-frequency regulation. Simulation is also used to show that the windfarm can actively contribute to the frequency stability of the onshore AC grid.

Ryan McGill
4 June 2017
Trondheim

Abstract

As penetration of renewable energy sources increases, the proportion of synchronous generators with rotating masses directly coupled to the grid decreases. In the case of wind generation, the kinetic energy stored in the machine rotor is not available to perform the natural task of frequency support for the AC power system. New active control methods must therefore be developed to synthetically recouple this inertia characteristic to the grid. European offshore windpower is growing and the average distance to shore is increasing. Voltage Source Converter based HVDC (VSC-HVDC) is a promising method for transporting this power to the onshore AC grid over long distances. The fast power transfer capability of VSC-HVDC offers the opportunity for new control strategies to provide frequency support to the AC grid. The authors propose a method for using a VSC-HVDC transmission link to follow and amplify the traditional primary frequency response behaviour of a small synchronous generator connected at the point of common coupling. In terms of frequency support, the onshore grid will then see the HVDC connected offshore windfarm (OWF) and small synchronous generator together as one large synchronous generator with rotor inertia directly coupled to the grid (i.e. synthetic inertia). The method will therefore enable the OWF to provide frequency support services equivalent to that of a traditional power plant at the same rating. Electromagnetic transient simulation is used to investigate the proposed active control strategy. Fiber-optic technology is considered as a method of remote communication between the OWF and the small synchronous generator. A second communication-less method is also considered which utilizes a cascaded droop frequency to DC voltage control at the Grid Side VSC and then DC voltage to frequency at the Windfarm Side VSC. Simulation results are used to justify the proposed method.

Acronyms

PSCAD/EMT^{TM} Power System CAD, Electromagnetic Transient Simulation Software

GRF Generator Response Following

VSC-HVDC Voltage Source Converter, High Voltage Direct Current Transmission

PCC Point of Common Coupling

OWF Offshore Windfarm

LSG Aggregated Large Synchronous Generator and Strong Frequency Grid

SSG Small Synchronous Generator

WTG Aggregated Wind Turbine Generator and Weak Frequency Grid

WF-VSC Windfarm Side Voltage Source Converter

GS-VSC Grid Side Voltage Source Converter

INEC Inertia Emulation Controller

List of Tables

List of Figures

Contents

Chapter 1

Introduction

1.1   Background

In a traditional AC power system, frequency is an indicator of the global balance between generation and demand of active power [1]. Primary frequency control is a method for coordinating the load responses of a system of generators in an AC system. It stabilizes frequency excursions through adjustment of prime movers with a droop control [2]. When the active load of the system changes, the frequency adjusts inversely. This frequency deviation is the same across the entire AC system as frequency is a global variable. Each AC generator takes on a portion of the active load according to the global frequency deviation and a predefined Power-Frequency relationship specific to that generator. In turn, the Power-Frequency relationship of all the synchronous generators in the system defines the new steady state frequency of the system.

Inertial response is the rate of change of frequency as it approaches a new steady state according to a system active load change and the primary frequency control. This rate of change is a function of the stored kinetic energy of the total rotating mass directly coupled to the AC grid. In the moments leading up to a power system imbalance, the inherent inertial response of traditional synchronous machines limits the frequency rate of change [2]. It provides time for the primary frequency control to adjust prime movers and coordinate generation with demand but what happens when more non-synchronous generation sources are connected to the AC grid?

1.2   Problem Description

Larger penetration of renewables with power electronic interfaces reduces the amount of inertia directly coupled to the AC power grid in proportion to the active power being supplied. This leads to larger steady state frequency deviation and increased rate of change of frequency. Therefore, short term grid stability issues become more of a concern for grid operators [2]. This report will develop a synthetic inertia method for active power injection of VSC-HVDC

connected offshore windfarms proposed by Professor Olimpo Anaya-Lara. In this method, a small synchronous generator is installed at the wind farm power plant point of connection with the power grid. The challenge of this project is to design a wind farm controller that emulates and amplifies the response of this small generator. Electromagnetic transient simulation software will be used to demonstrate if the method can participate in load-frequency control and how it is limited by the dynamic frequency stability of the inter-connected AC grid.

1.3   Research Objectives

The proposed method, referred to as Generator Response Following, uses communication to imitate the dynamic response of a small synchronous generator employing load-frequency control. This small synchronous generator is connected at the point of common coupling with the offshore windfarm. The main challenge of this project is to design a wind farm controller that emulates and amplifies the response of this small generator.

Methods of communication are also an important topic. One available communication method is the fiber-optic line embedded in the HVDC cable as well as the windfarm cabling. Another important method identified in the literature that relies only on local measurements is the communicationless method. In order to be consistent with the existing research, the communicationless method will be used for load frequency regulation. The fiber-optic line will then be used to communicate information associated with the inertial response of the small synchronous generator.

Electromagnetic transient simulation software will be used to demonstrate the load-frequency regulation functionality of the communicationless method. The simulation results will then combine this functionality with the dynamics of the small synchronous generator tied to the offshore windfarm active power output. This report will seek to contribute to the existing research by exploring the stability benefits of the Generator Response Following concept combined with the communicationless method of load-frequency regulation.

1.4   Thesis Outline

This section outlines the report in two ways. 1.4.1 describes the theoretical development of the system as a linear progression. 1.4.2 describes the report in terms of the reference circuit and is intended to function more like an index than an outline. This reference circuit will be continually cited throughout the report.

1.4.1   Subject Matter

Chapter 2 first reviews the existing research to provide context. It attempts to define the research needs for this project in terms of what has already been attempted. Chapter 3 gives prerequisite information about modelling of the power electronic converters in the system.

Section 4.1 and chapters 5 and 6 are intended as prerequisite information outlining the development of the AC system. These chapters provide the background AC system behaviors that the synthetic inertia method seeks to mimic. Section 4.2 and chapter 7 then give the core material that has been developed in this project. Power flow and communication facilitating the synthetic inertia method are developed in section 4.2. The synthetic inertia method is then developed in chapter 7. Simulation results are presented in chapter 8. Chapter 9 relates everything back to what was learned in the literature review of chapter 2. It also gives some thoughts on practical application of the GRF concept.

1.4.2 Reference Circuit

Figure 1.1 is the onshore reference circuit and Figure 1.2 is the offshore reference circuit used for time domain simulation in this project. The circuit consists of a 400MW offshore windfarm (OWF) connected by a point-to-point VSC-HVDC connection to an onshore AC system at a Point of Common Coupling (PCC).

The onshore AC system is made up of an aggregated large synchronous generator (LSG, defined in 5.5) connected to the PCC by a 245kV transmission network represented by an equivalent π model with lumped parameters. This AC network has an effective short circuit ratio designed for voltage stability (defined in 4.1.3) and an effective inertia constant designed for frequency stability (defined in 6.1.3) to accommodate the connection of an HVDC link. The network has an X/R ratio typical for traditional 245kV AC transmission (defined in 4.1.1) and a stiffness typical for steam turbine generation (defined in 6.1.1). A small synchronous generator (SSG, defined in 7.1.3) is also connected at the PCC for interaction with the OWF. For simplicity, this simulation operates under the assumption of manual
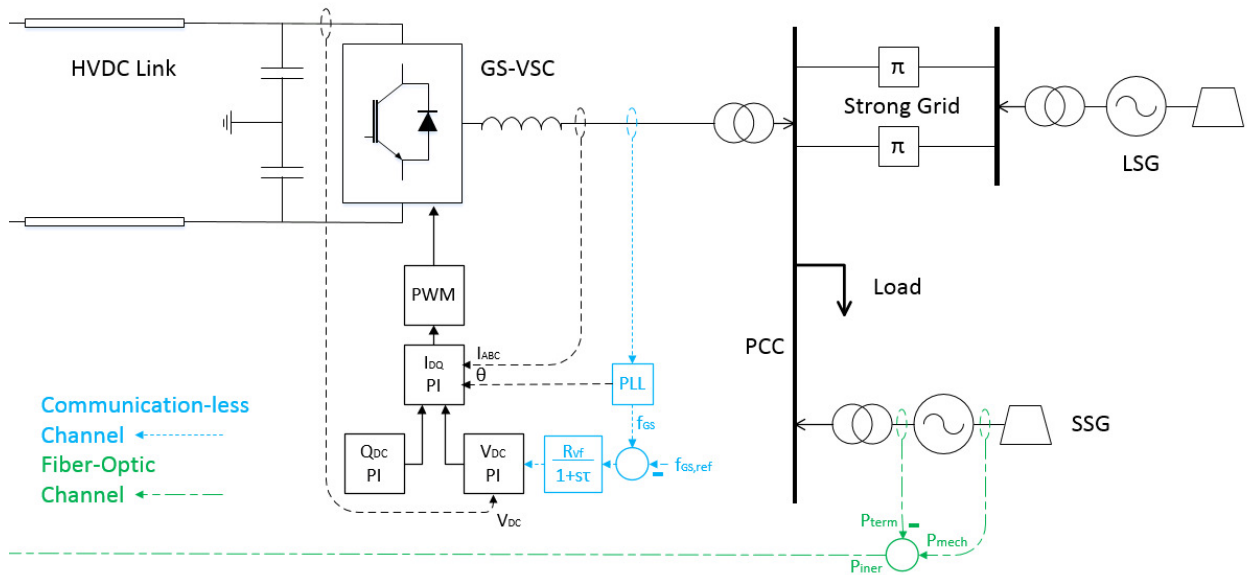
Figure 1.1: Onshore Reference Circuit
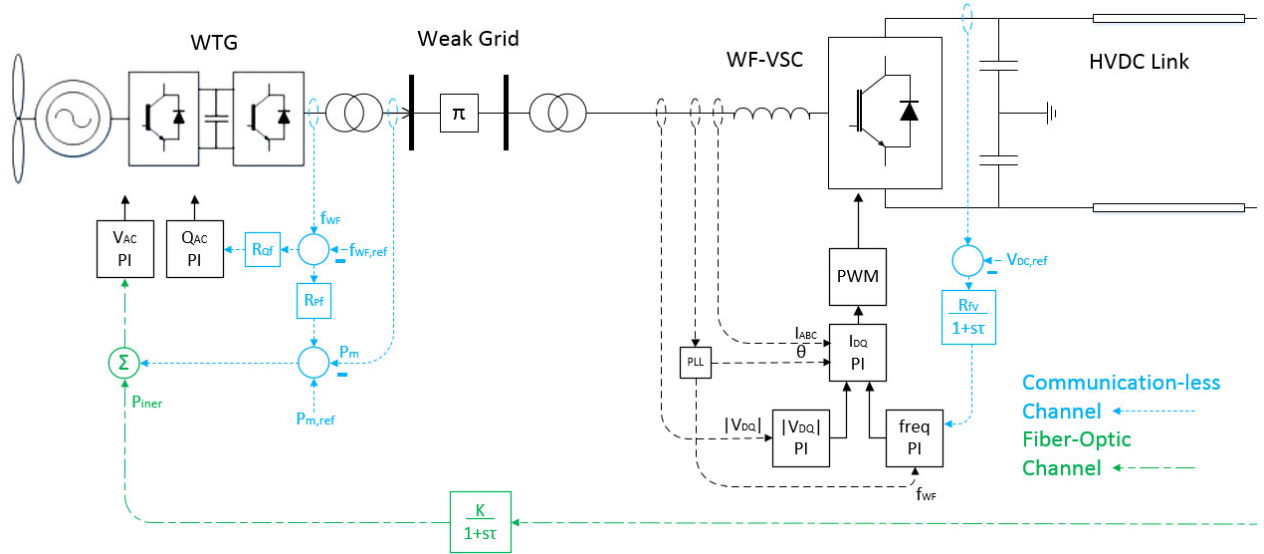
Figure 1.2: Offshore Reference Circuit

excitation from all contributing synchronous machines (see 5.3 & 5.4 for derivation and 5.5.2 for implementation).

The OWF is represented by an aggregated wind turbine generator (WTG, defined in 7.3.1). The offshore submarine cable network is modelled as an equivalent π network with lumped parameters. The network has an X/R ratio typical of a low voltage distribution network but with a higher capacitance due to the cables (defined in 4.2.2). The windfarm controller is designed to exploit these properties (refer to 7.3.2).

The VSC-HVDC converters are defined in chapter 3. They are represented with an average switching model rather than a standard switching model because this project is concerned with the time-scales associated with power flow dynamics not switching operations or voltage transients. Frequency is decoupled from power on the AC collection grid, this grid therefore follows the frequency dictated by the WF-VSC. The WF-VSC also provides a constant AC voltage magnitude at the terminals of the cable network and accepts the power flow sent from the WTG (refer to 4.2.3). The HVDC submarine line is made up of two cables in a bipolar configuration and is assumed to be 400km in length with a 500kV/500MW rating. It is operated as a voltage link at 400MW capacity (see 4.2 for operating characteristics). Power flow is assumed to be uni-directional from OWF to onshore network and the converters at either end of the link are assumed to be loss-less ($P_{AC} = P_{DC}$). The GS-VSC regulates the DC voltage of the line and operates independently of power flow (refer to 4.2.3).

Chapter 2

Literature Review

2.1   Synthetic Inertia from Wind Turbine Generators

In general, in order for windfarms to provide synthetic inertia services to the AC grid, the idea of using wind turbine generators has been proposed. One method of doing this is to operate the individual wind turbines below the maximum power operating point. This way, instantaneous increases in power output are made available to the wind turbine level control algorithm. This may be referred to as spinning reserve margin, wind generator de-load, power margin, power reserve, etc. Likewise, instantaneous decreases in power are available as the generator is producing more than minimum capability when tracking the maximum power point [2] [3]. Instantaneous surges of power may also be extracted from the kinetic energy of the rotor by rapid braking action or dynamic deloading of the turbine [4].
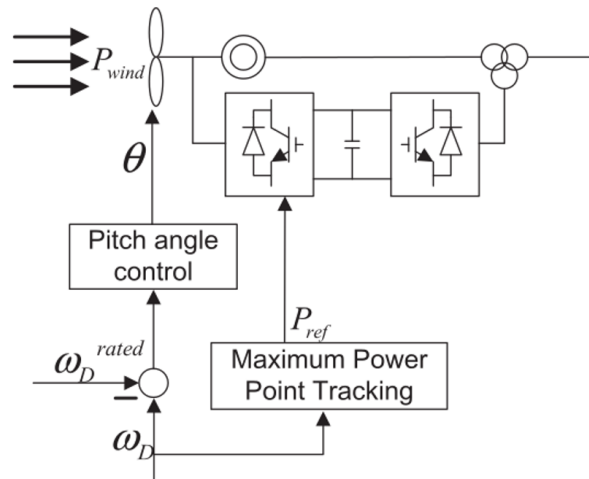
Figure 2.1: Synthetic Inertia from WTG by Active Power Control [4]

Supplementing the chosen mode of operation is a control loop at the wind turbine level, ready to increase or decrease the power output based on the measured frequency error input. In

the case of VSC-HVDC connected OWF's, variable frequency operation of the AC collection grid is then possible. [5] mentions that since the windfarm AC collection grid likely has no loads connected to it, changes in frequency may be accomplished fairly easily. [2] then describes that rapid, reliable communication may be set up with the onshore AC grid through a chain-link coordination of voltage droops. This is essentially an artificial coupling of the two AC grids.

This method may have disadvantages as well. While instantaneous surges of active power may be available for mimicking a short-term inertial response, this may be followed by more prolonged periods of reduced power output while the rotor kinetic energy supply is recharged. This may further compromise system stability during more serious disturbances [1]. WTG's also tend to have a limited inertia time constant when used for this purpose.

2.2   Problems and Opportunities with VSC-HVDC Connected Offshore Windfarms

Due to its fast power transfer capability, VSC-HVDC is becoming a popular electrical transmission technology. Other advantages over traditional thyristor based LCC technology include independent control of active and reactive power, small footprint and reduced harmonic filtering requirements [6]. Control methods for VSC-HVDC links are also customizable to the existing infrastructure. Application engineering is reduced and control methods may be tailored for strong versus weak systems at the sending end versus the receiving end [7]. Despite all advantages mentioned above, interfacing more power electronics with the grid brings disadvantages as well. VSC's contribute limited short circuit current, therefore reducing overall system strength [8]. Also, VSC's contribute no inertia, again reducing overall system stability. There is therefore an increasing interest by operators to request inertial and primary frequency response services from non-synchronous energy sources such as OWF's [2].

In Great Britain for example, installation of VSC connected OWF's is limited due to stability concerns. According to simulation, non-synchronous generator penetration is limited to 65% because of the estimated system stability limits. The authors of [8] suggest that VSC-HVDC control methods designed to mimic the inertial response of traditional synchronous generators may be a solution to this problem.

2.3   Frequency Control with VSC-HVDC

Typically, VSC-HVDC links are designed for active power control at the sending end converter and DC voltage control at the receiving end converter. Reactive power is then controlled at both ends in order to maintain the AC voltage and the reactive power at the required level. The VSC-HVDC link may be viewed as a fast, controllable, synchronous machine when connected to the AC grid through an AC filter. Frequency control may then be included in

the active power or DC voltage loop of the converter at the Point of Common Coupling (PCC). [9] proposes three methods; Fixed Frequency, Power-Frequency, DC Voltage-Frequency. The authors of [9] conclude that frequency performance is significantly improved by these methods, especially in isolated power systems. This section also includes a fourth method referred to as Inertia Emulation Control.
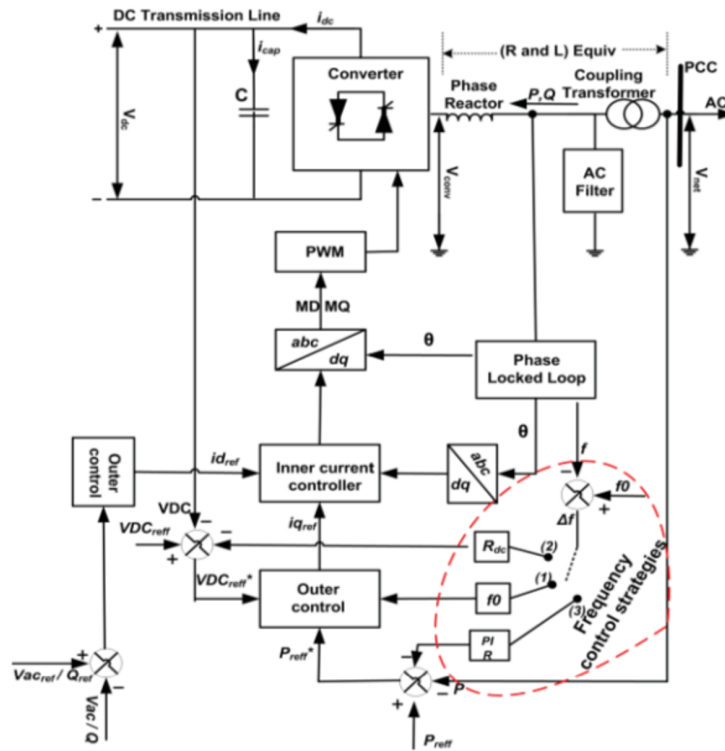
Figure 2.2: VSC-HVDC Frequency Control Methods [9]

2.3.1 Fixed Frequency Control Strategy

Fixed frequency is the simplest and may be used for isolated systems without any other means of frequency control. In this method, a fixed frequency reference is supplied to the outer control loop of the converter. Frequency errors will then result from changes in the power flow. The control loop will work to bring the frequency back to nominal [9].

2.3.2 Power-Frequency Control Strategy

In this method, the frequency control loop is added to the outer active power loop at the PCC. The method may employ proportional (droop) control of the steady state frequency or PI control for correction of the steady state frequency deviation as well [9].

The system dynamics equation can be adapted to include the effects of the converter. In general, grid connected synchronous generator interaction with system wide frequency

deviations can be described with the swing equation:

$$2H\frac{df}{dt} = P_m - P_e, \tag{2.1}$$

where H is the inertia time constant in seconds, f is the grid frequency in per unit, P_m is mechanical power in per unit and P_e is electrical power in per unit. The frequency dynamics of a grid connected VSC may be described similarly:

$$K_{DC}\frac{df}{dt} = P_{DES} - P_{DC}, \tag{2.2}$$

where P_{DES} is the desired change in power and P_{DC} is the actual change in power through the VSC due to a grid disturbance. K_{DC} is the slope of the P-f droop. (2.2) can now be solved for P_{DC} and added to (2.1) for a generalized dynamics equation that includes the effects of synchronous generation as well as the converter dynamics:

$$(2H + K_{DC})\frac{df}{dt} = (P_m + P_{DES}) - P_e. \tag{2.3}$$

A phase-locked loop is then used at the PCC to estimate the frequency and feed that information to the frequency controller [9].

2.3.3 V_{DC}-Frequency Control Strategy

In this method, the frequency control loop is added to the outer DC voltage loop at the PCC. Then when system frequency changes, instantaneous power is required from the DC link capacitor. This in-turn influences the DC voltage across that capacitor. V_{DC}-Frequency Control uses this DC voltage change and the capacitor energy equation to govern the dynamics of this interaction with a droop control [9]:

$$W_{cap} = \frac{1}{2}CV_{DC}^2 \tag{2.4}$$

where W_{cap} is the capacitor energy in per unit of rated power, C is the capacitance of the DC link capacitor in per unit and V_{DC} is the DC link voltage in per unit. The instantaneous power deviation can be included in this equation as the time derivative of energy:

$$\Delta P = \frac{dW_{cap}}{dt} = \frac{C}{2}\frac{dV_{DC}^2}{dt}. \tag{2.5}$$

Now, if we let (2.3) be represented by the standard P-f droop definition $\Delta f/\Delta P = -R_{Pf}$ and combine with (2.5), we arrive at:

$$\Delta f = -R_{Pf} \ \frac{C}{2} \frac{\Delta V_{DC}^2}{T_\Delta}. \tag{2.6}$$

The new voltage-frequency droop relationship is then

$$f - f_0 = -R_{Vf} \ \left[V_{DC}^2 - V_{0,DC}^2 \right] \tag{2.7}$$

where

$$R_{Vf} = \frac{R_{Pf}C}{2T_\Delta} \tag{2.8}$$

and is a function of the size of the DC link capacitor [9]. Notice the frequency deviation is proportional to the square of the voltage deviation. This non-linear relationship adds complexity to the small signal analysis of the system.

2.3.4   Inertia Emulation Control (INEC)

This method takes the DC Voltage-Frequency strategy one step further by allowing a desired emulation inertia to be specified. The derivation is also slightly different. The power dynamics between the AC and the DC side are calculated as follows [1]:

$$P_{in} - P_{out} = V_{DC} \ (I_{in} - I_{out}) \tag{2.9}$$

$$\Delta P = V_{DC} \ \Delta I_{DC} \tag{2.10}$$

where P_{in} and I_{in} are input from the VSC to the DC link capacitor and P_{out} and I_{out} are output from the DC link capacitor to the VSC. V_{DC} is the DC link voltage. Replacing ΔI_{DC} with the capacitor dynamics equation gives:

$$\Delta P = V_{DC} \ C \frac{dV_{DC}}{dt}. \tag{2.11}$$

In the per unit system, (2.11) can now be equated to the swing equation and an emulation inertia time constant H_{VSC} defined (see also (2.1)):

$$\frac{1}{f_0} \left[2H_{VSC} \frac{df}{dt} \right] = \frac{1}{S_{VSC}} \left[V_{DC} \ C \frac{dV_{DC}}{dt} \right]. \tag{2.12}$$

Integrating both sides yields:

$$\left[\frac{2H_{VSC}}{f_0}\right]\int df = \left[\frac{C}{S_{VSC}}\right]\int V_{DC}\ dV_{DC} \qquad (2.13)$$

and

$$\frac{2f\,H_{VSC}}{f_0} = \frac{CV_{0,DC}^2}{2\,S_{VSC}} + K_0, \qquad (2.14)$$

where K_0 is referred to as the integration constant. Finally, according to [1], by solving for K_0 the following relations can be made:

$$K_0 = 2H_{VSC} - \frac{CV_{0,DC}^2}{2\,S_{VSC}} \qquad (2.15)$$

where

$$H_{VSC} = \frac{f_0}{2\Delta f}\frac{CV_{0,DC}^2}{2\,S_{VSC}}\left[\left(\frac{\Delta V_{DC}}{V_{0,DC}} + 1\right)^2 - 1\right]. \qquad (2.16)$$

Then R_{Vf} from (2.7) can be replaced by:

$$R_{Vf} = \frac{Cf_0}{4S_{VSC}H_{VSC}} \qquad (2.17)$$

As with the DC Voltage-Frequency Control Strategy, a non-linear droop relationship exists. This adds complexity to the task of system design and analysis. The designer must make informed decisions about capacitor size, VSC power rating, VSC voltage and allowable VSC voltage variation and balance this with the desired inertia emulation.

A rule of thumb for VSC-HVDC voltage deviation limit is $\pm15\%$ to preserve stability [10]. Also, [1] explores the prospect of emulation inertia time constants in the range of zero to four seconds for capacitors of size 2mF and 5mF. Then for a larger emulation inertia time constant a larger capacitor is needed but this relationship is not linear and required capacitor size quickly becomes quite large.

The authors of [1] conclude that this method enhances AC system stability during frequency deviations as well as busbar load angle deviations. They also conclude the method does not hinder an important feature that HVDC transmission links already provide, which is to decouple the strong onshore AC grid from the weak OWF AC collection system.

2.4 Coordinated Control Strategies

2.4.1 VSC-HVDC Coordinated Control Strategy

This strategy combines the WTG Synthetic Inertia method described in Section 2.1 with the GS-VSC Inertia Emulation method (INEC Controller) described in Section 2.3.4. The purpose of this is to increase the size of the inertia emulation time constant while maintaining a reasonable size DC link capacitor. This can be achieved by supplying the energy requirement of the INEC controller from two sources; WTG rotor kinetic energy and DC link capacitor [10].

The INEC Controller energy requirement is communicated to the WTG installations by a chain-link coordination of voltage droops as described in Section 2.1. However, this time the voltage deviation of the DC link is initiated by the action of the INEC Controller draining energy (and therefore voltage) from the DC link capacitor at the GS-VSC. Simulation suggests the capacitor size was not improved and that further research is therefore required [4].

2.4.2 Wind-Thermal-Bundled DC Modulation

This strategy explores a coordination between the proportional power-frequency droop method of a VSC-HVDC described in Section 2.3.2 with the traditional primary frequency regulation (PFR) of a thermal power plant. The HVDC link and the thermal power plant are coupled together at one common bus to provide the necessary frequency support services for a wind farm. Note that this study takes place at the WF-VSC but is nevertheless relevant to the present discussion and could be adapted to the GS-VSC. It assumes a strong grid at the far end of the HVDC link and a weak grid at the point where the system is being analysed.

Traditional Primary Frequency Regulation has a feature called governor dead-band. This feature allows the governor to be programmed to ignore small frequency deviations. However, this dead-band must not be so large that it ignores significant disturbances. The frequency regulation range of traditional turbine governors is also small in comparison to the range required to regulate a wind farm on a weak grid. This is due to the significant variability of wind speeds [7].

Two operational modes are proposed: 1) Generator-Master, DC System-Slave and 2) DC System-Master, Generator-Slave. Mode 1 is realized with a small governor dead-band and a shallow slope for DC system droop. Mode 2 is realized with a large governor dead-band and a steep slope for DC system droop. The study compares mode 1, mode 2 and "PFR only" against collection grid frequency variability due to wind speed fluctuations. Results indicate that mode 1 yields the best operational performance of the three. Mode 1 results have the smallest maximum frequency deviation, the smallest steady state frequency deviation and a consistently stable post-disturbance steady state. This was verified in both islanded and interconnected mode. In contrast, mode 2 is found to yield the best results under fault conditions [7].

Method	Description / Implementation	Advantages	Disadvantages
Synthetic Inertia from WTG's	Artificial Coupling of Synthetic Inertia Through the HVDC Link	Much Research Available with Onshore Windfarms	Communication Required, Must Recharge Rotor Kinetic Energy
VSC Fixed Frequency Control	Implemented at the GS-VSC	Simple Design and Implementation	Intended for Small Isolated Systems, No Synthetic Inertial Response
VSC Power-Frequency Control (Proportional or PI)	Implemented at the GS-VSC	Simple Design and Implementation, PI can Influence Steady State Frequency	Very Little Synthetic Inertial Response
VSC Voltage-Frequency Control	Implemented at the GS-VSC	Some Synthetic Inertial Response	Synthetic Inertia Limited by Capacitor Size and Voltage Deviation Limits
Inertia Emulation Control	Implemented at the GS-VSC	Some Synthetic Inertial Response, Time Constant can be Specified	Synthetic Inertia Limited by Capacitor Size and Voltage Deviation Limits
VSC-HVDC Coordinated Control	Combine Inertia Emulation Control with Synthetic Inertia from WTG's	Some Synthetic Inertial Response, Time Constant can be Specified	No Improvement of Inertia and Capacitance Evident, Communication Required
Wind-Thermal-Bundled DC Modulation	Combine VSC Power-Frequency (Proportional) Control with Directly Coupled SG at WF-VSC	Good Inertial/Synthetic Inertial Response, Synchronous Generation Influences Steady State Frequency	Expensive and Site Specific because Synchronous Power Plant Required

Table 2.1: Control Strategies for the Purpose of Synthetic Inertia from VSC-HVDC Connected OWF's

2.5 Summary

This chapter explores various control strategies that have been proposed that enable VSC-HVDC connected offshore windfarms to provide synthetic inertia services to the onshore AC grid by way of active power injection and absorption. This includes dedicated control strategies at the grid-side VSC as well coordinated methods which utilize a combination of strategies across the decoupled asynchronous system to accomplish the desired outcome. Each method has advantages and disadvantages as can be seen in the Table 2.1 summary.

Based on the results of the present survey, a hypothetical optimized control strategy would have a synthetic inertial response which allows the designer to specify the inertia time constant. The designer would have the freedom to increase the size of the inertia time constant while keeping the DC link capacitor size within reason and without much dependence on DC voltage deviation limit. Ideally, this constant would be completely independent of capacitor size and DC voltage deviation. The method would also be able to contribute to the minimization of the steady state frequency deviation. The synthetic inertia design would be accomplished with minimal cost to the owner/operator and would not be site specific. All these items suggest there is still plenty of opportunity for research in this area. Furthermore, motivation is provided by the ever increasing need for non-synchronous generation to contribute to the stability of the AC system as a directly coupled synchronous plant would.

Chapter 3

Two-Level Voltage Source Converter

This project uses Three-Phase Full-Bridge Voltage Source Converters functioning as power converters at the grid side (GS-VSC) and the windfarm side (WF-VSC) of an HVDC link. These converters operate under a DC voltage link topology with the WF-VSC functioning as a Three Phase AC-to-DC Boost Rectifier and the GS-VSC functioning as a Current Controlled Voltage Source Inverter as defined in [11]. This chapter focuses on developing the AC to DC power flow transfer equation for a triangle carrier wave PWM modulation scheme in the linear region of operation. The power transfer equation for AC system interaction and VSC controller configuration is found in section 3.2.3. For converter control and development of power flow analysis as it relates to AC system interaction, refer to section 4.2. The power transfer equation for time domain implementation in electromagnetic transient simulation software can be found in section 3.3.1.

The converters are also employed to provide a cascaded droop, identified as a "communication-less" channel, for primary response to load changes on the AC grid (further detailed in section 4.2 and chapter 7). Section 3.1.3 defines the allowable limits of DC voltage magnitude for linear operation when using this communication-less channel.

This chapter is structured as follows. Section 3.1 gives some basic background about the amplitude modulation ratio. Section 3.2 then develops some theory for a standard switching model for controlling the VSC's at either end of the HVDC link. Last, the simplification of an average switching model is given in section 3.3. This is outlined and related to the standard switching model.

Derivations in this section use the following nomenclature:

- V_{AN}, V_{LL}, I_A, etc: RMS magnitude

- $\hat{V_{AN}}, \hat{I_A}$, etc: peak magnitude

- v_{AN}, i_A, v_{an}, i_a, etc: single-phase sinusoidal waveform with peak magnitude and frequency

- m_A: amplitude modulation ratio, peak magnitude

- $m_{a,b,c}$: amplitude modulation ratio, three-phase pulse width modulated output of the VSC controller with peak magnitude and frequency

3.1   Amplitude Modulation Ratio

3.1.1   Single Phase Perspective

In general, the phase voltage of a 2-level VSC is associated with $\frac{V_{DC}}{2}$. The variable m_A relates AC to DC voltage by equ. 8-56 of [12] for each individual converter leg:

$$(\hat{V}_{AN})_1 = m_A \frac{V_{DC}}{2} \ . \tag{3.1}$$

This project regulates $(\hat{V}_{AN})_1$ and V_{DC}, therefore (3.1) can be solved for m_A to observe the rated operating value:

$$m_A = \frac{2\,(\hat{V}_{AN})_1}{V_{DC}} = \frac{2 \times 200kV}{500kV} = 0.8 \tag{3.2}$$

and is within the linear region of operation. Note that (3.1) is also used in section 3.3 for implementation of the average switching model.

3.1.2   Three Phase Perspective

In general, the line to line voltage of a 2-level VSC is phase voltage $\times\sqrt{3}$ or $\frac{\sqrt{3}}{2}V_{DC}$. When operating in the linear modulation region, the relationship between V_{DC} and the RMS of V_{LL} can therefore be defined according to equ. 8-57 of [12] as

$$V_{LL} = \frac{\sqrt{3}}{2}\frac{1}{\sqrt{2}}\,m_A V_{DC} = 0.612\,m_A V_{DC} \ . \tag{3.3}$$

Once again, since our model is regulating DC voltage and AC voltage at both ends of the DC link, the equation can be solved for m_A:

$$m_A = \frac{V_{LL}}{0.612\,V_{DC}} = \frac{245kV}{0.612 \times 500kV} = 0.8 \tag{3.4}$$

and is consistent with (3.2). This can serve as a simple check for operating mode of the VSC.

3.1.3   Linear Operating Region of m_A

This project also uses a communication-less channel (see section 7.2.1) which changes v_{DC} at the GS-VSC according to the frequency. The amplitude modulation ratio can be used to define the limit of linear operation for this communication-less method. Solving (3.3) for v_{DC} and using rated V_{LL} and m_A at the upper limit of linear operation gives:

$$V_{DC,min} = \frac{V_{LL}}{0.612\,m_A} = \frac{245kV}{0.612 \times 1.0} = 400kV \ . \tag{3.5}$$

3.2   PWM Standard Switching Model

This project is implemented with an average switching model (see Section 3.3) which is based on a standard switching model with a bipolar switching scheme and a switching frequency of 1950Hz. Since this is a 50Hz system, the resulting frequency modulation ratio is $m_f = 39$. This is fairly large because we are working in a system with a very high power rating. This large m_f also facilitates the average model implementation as it allows the assumption that the PWM control waveform varies very little during a switching time period ([12] sec 8-2-1).

The bipolar switching scheme allows for fairly simple analysis compared to unipolar switching because only one control signal must be analysed ([12] sec 8-3-2). This can therefore easily be approximated into an average switching model implementation. Also, $m_f = 39$ is an odd number and a multiple of three in a three-phase system resulting in no harmonics at even multiples or triples of m_f.

Figure 3.1 is the standard switching model of the VSC plant. Figure 3.2 is a block diagram of the entire VSC system. It includes separate blocks for the VSC plant, the PWM (see also submodule of figure 3.1) and the PI controllers. Each of these blocks is explained in the following sections. Section 3.2.1 gives some preliminary background necessary for more detailed derivations later on. Section 3.2.2 explains the VSC plant in further detail with a standard switching model for the PWM. Section 3.2.3 gives the power equation in the DQ0 reference frame. Section 3.2.4 explains the current loop of the controller. Section 3.2.5 explains the outer loop of the controller.

3.2.1   Complex Vector Definitions

This section is intended to provide a background for justifying the VSC system derivation and the average switching model implementation used in this project. According to [11], a complex vector representation of a three phase system, with phase a on the positive real axis and at an arbitrary time (eg: $t = 0$) can be derived:
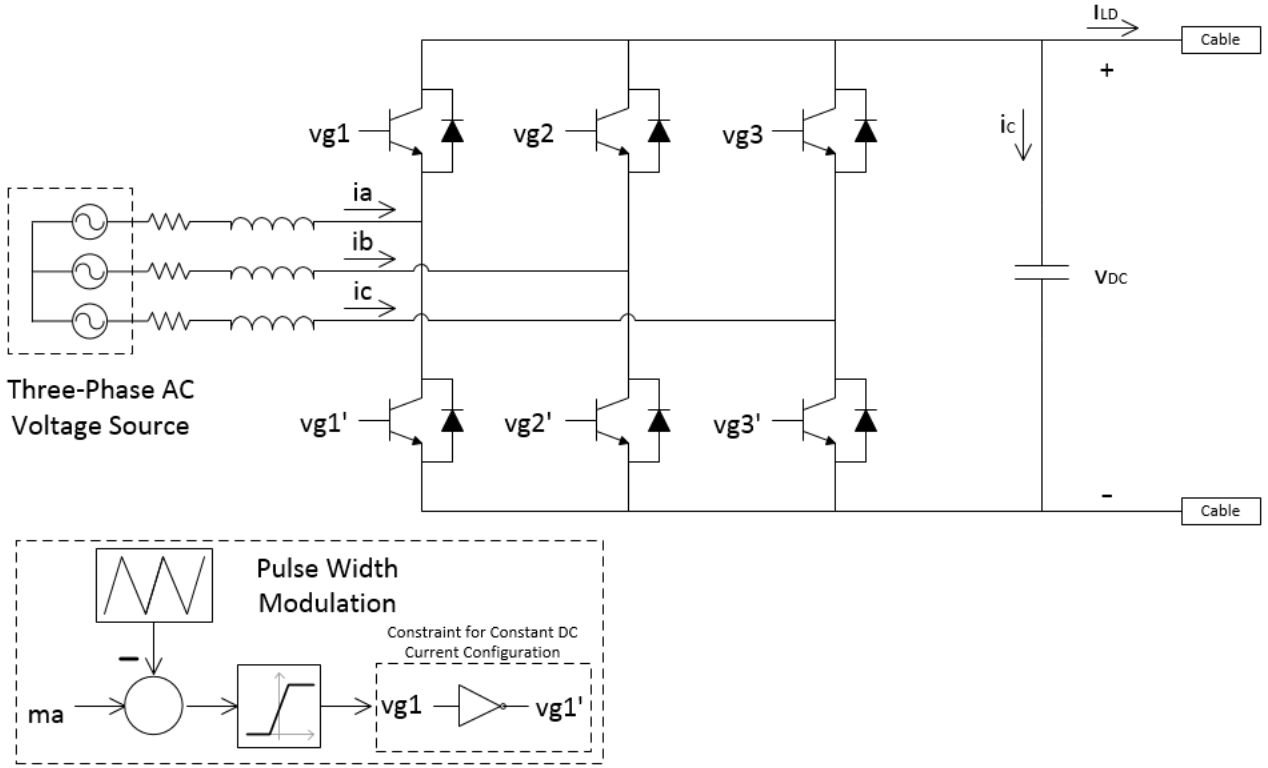
Figure 3.1: Standard Switching Model
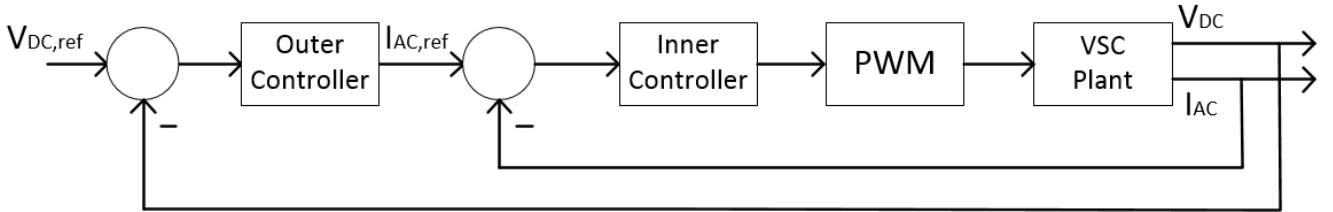
Figure 3.2: System Control Loop

$$\overline{X}(0) = X_a(0)\, e^{j0°} + X_b(0)\, e^{j120°} + X_c(0)\, e^{-j120°}$$
$$= X_a(0) + X_b(0)(\cos 120° + j \sin 120°) + X_c(0)(\cos 120° - j \sin 120°)$$
$$= \left[X_a(0) + X_b(0) \cos 120° + X_c(0) \cos 120° \right] + j \left[X_b(0) \sin 120° - X_c(0) \sin 120° \right]$$
$$= \left[X_a(0) - \frac{1}{2}X_b(0) - \frac{1}{2}X_c(0) \right] + j \left[\frac{\sqrt{3}}{2}X_b(0) - \frac{\sqrt{3}}{2}X_c(0) \right]$$

$$(3.6)$$

If we now assume a balanced three-phase system where $\hat{X}_a = \hat{X}_b = \hat{X}_c$ then the values of the three phases at any instant of time will always sum to zero. Therefore, we can simplify

(3.6) by putting the instantaneous $t = 0$ values into the equation (ie: $X_a(0) = \hat{X}_a$ and $X_b(0) = X_c(0) = -\frac{1}{2}\hat{X}_a$) and it will hold true for any instant of time:

$$
\begin{aligned}
\overline{X}(t) &= \left[\hat{X}_a - \frac{1}{2}\left(-\frac{1}{2}\hat{X}_a\right) - \frac{1}{2}\left(-\frac{1}{2}\hat{X}_a\right)\right] + j\left[\frac{\sqrt{3}}{2}\left(-\frac{1}{2}\hat{X}_a\right) - \frac{\sqrt{3}}{2}\left(-\frac{1}{2}\hat{X}_a\right)\right] \\
&= \left[\hat{X}_a + \frac{1}{4}\hat{X}_a + \frac{1}{4}\hat{X}_a\right] + j\left[-\frac{\sqrt{3}}{4}\hat{X}_a + \frac{\sqrt{3}}{4}\hat{X}_a\right] \\
&= \frac{3}{2}\hat{X}_a \, .
\end{aligned}
\tag{3.7}
$$

$\overline{X}(t)$ in (3.7) is essentially an $\alpha\beta$ transform expressed as a complex vector with α- as the real axis and β- as the imaginary axis. Since the result is a real value in a balanced three-phase system:

$$
\overline{X}(t) = Re\left[\overline{X}(t)\right] = \frac{3}{2}\hat{X}_a \qquad or \qquad \hat{X}_a = \frac{2}{3}Re\left[\overline{X}(t)\right] .
\tag{3.8}
$$

For amplitude invariance, a multiplier can be applied:

$$
\begin{aligned}
\overline{X}(t)\bigg|_{ampl\ invr} &= \frac{2}{3}\overline{X}(t) \\
&= \frac{2}{3}\left[X_a(t) + X_b(t)\,e^{j120°} + X_c(t)\,e^{-j120°}\right] \\
&= \frac{2}{3}\left[X_\alpha(t) + j\,X_\beta(t)\right]
\end{aligned}
\tag{3.9}
$$

This project uses a constant DC current switching configuration (see figure 3.1), therefore we need an equation for DC current as a function of a switching vector and an AC current vector [11]. First, we choose an arbitrary switching state represented by S1', S2 and S3' conducting. The amplitude invariant switching vector (figure 3.3, left side) representing this state is:

$$
\begin{aligned}
\overline{S} &= \frac{2}{3}\left[e^{j180°} + e^{j120°} + e^{j60°}\right] \\
&= \frac{2}{3}\left[-1 + e^{j120°} - e^{-j120°}\right] \\
&= \frac{4}{3}\,e^{j120°}
\end{aligned}
\tag{3.10}
$$

For this particular switching state, i_{DC} is momentarily equal to i_{BP} (figure 3.4). For analysis purposes, this means that $\overline{i_{BP}}$ is temporarily locked to the positive real axis (figure 3.3, right side) and has the amplitude invariant definition:
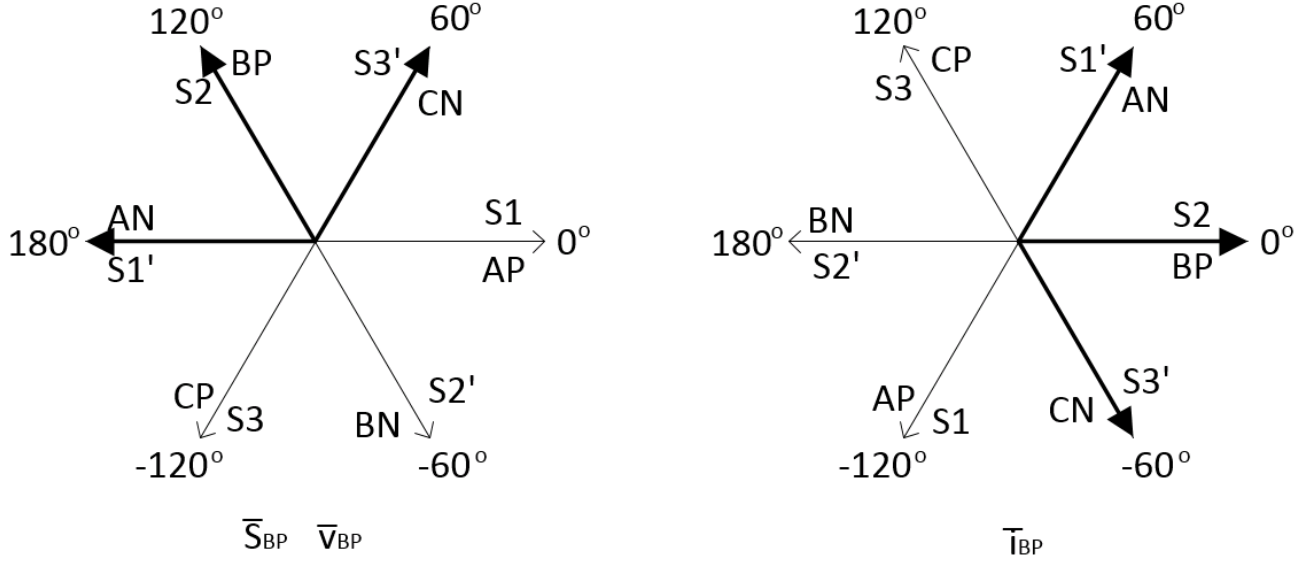
Figure 3.3: Space Vector Representation of Switching Configuration

$$
\begin{aligned}
\overline{i_{BP}} &= \frac{2}{3}\left[i_{AN}\,e^{j60^\circ} + i_{BP} + i_{CN}\,e^{-j60^\circ}\right] \\
&= \frac{2}{3}\left[i_{AP}\,e^{-j120^\circ} + i_{BP} + i_{CP}\,e^{j120^\circ}\right] \\
&= \frac{2}{3}\,e^{-j120^\circ}\left[i_{AP} + i_{BP}\,e^{j120^\circ} + i_{CP}\,e^{-j120^\circ}\right] \\
&= e^{-j120^\circ}\,\overline{i_{AP}}
\end{aligned}
\tag{3.11}
$$

where amplitude invariant $\overline{i_{AP}} = \frac{2}{3}\left[i_{AP} + i_{BP}\,e^{j120^\circ} + i_{CP}\,e^{-j120^\circ}\right]$. An equation for i_{DC} can now be found by combining amplitude invariant (3.10) and (3.11) [11]:

$$
\begin{aligned}
i_{DC} &= i_{BP} \\
&= Re\left[\overline{i_{BP}}\right] \\
&= Re\left[e^{-j120^\circ}\,\overline{i_{AP}}\right] \\
&= Re\left[\frac{3}{4}\left(\frac{4}{3}\,e^{-j120^\circ}\right)\overline{i_{AP}}\right] \\
&= \frac{3}{4}Re\left[\overline{S^*}\,\overline{i_{AP}}\right].
\end{aligned}
\tag{3.12}
$$

We also need an AC voltage vector ($\overline{v_{PH}}$) in phase with our switching vector. In the case of constant DC current switching configuration, the neutral of the AC voltage vector has ripple [11] and is seen here as $\frac{2}{3}$ magnitude phase to P and $\frac{1}{3}$ magnitude phase to N (see also figure 3.4):

$$\overline{v_{PH}} = \frac{2}{3}\left[v_{AN}\,e^{j180°} + v_{BP}\,e^{j120°} + v_{CN}\,e^{j60°}\right]$$

$$= \frac{2}{3}\left[-\frac{1}{3} + \frac{2}{3}\,e^{j120°} - \frac{1}{3}\,e^{-j120°}\right]v_{DC}$$

$$= \frac{2}{3}\,e^{j120°}\,v_{DC} \tag{3.13}$$

$$= \frac{1}{2}\,\overline{S}\,v_{DC}$$

3.2.2 Derive VSC System Equations

Kirchoff's Voltage Law applied to phase one of Figure 3.4 yields

$$e_1 = L\frac{di_1}{dt} + R_l i_1 + v_{AN} + v_{Nn} \, . \tag{3.14}$$
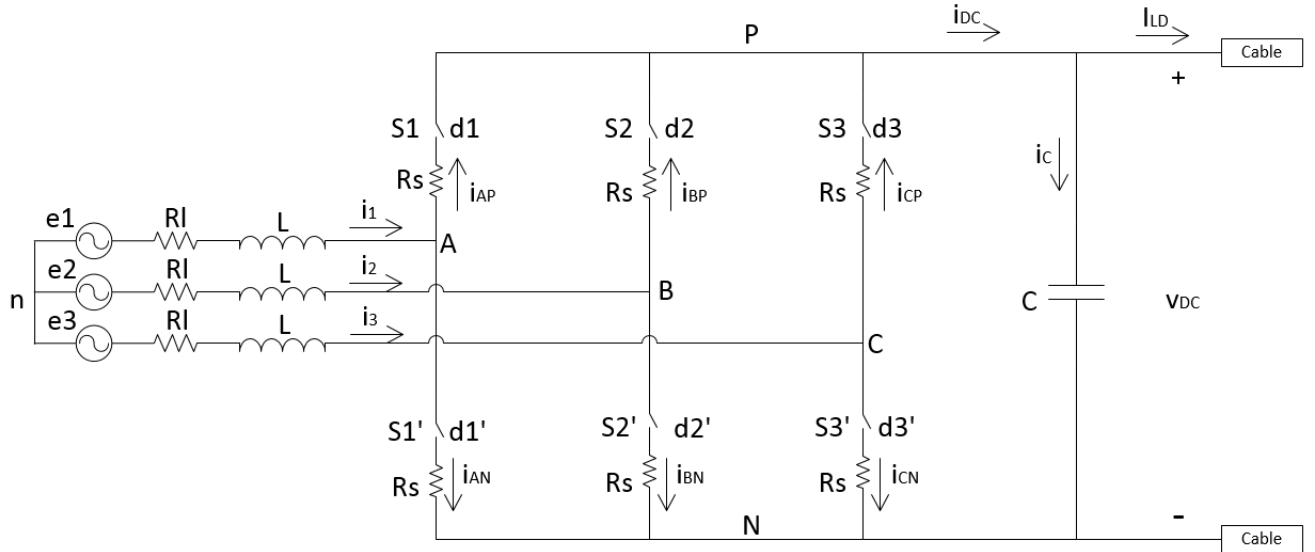
Figure 3.4: Standard Switching Model for VSC System Analysis

In Figure 3.4, if switch S_1 is closed $d_1 = 1$ and if switch S_1 is open $d_1 = 0$. This same logic applies to all three phases. The DC current configuration constraint from Figure 3.1 (ie: $v'_{g1} = NOT(v_{g1})$) can also be expressed here in the form

$$d_1 + d'_1 = 1 \, . \tag{3.15}$$

Observing the DC current configuration constraint, v_{AN} from (3.14) changes discretely with the switching of S_1 as follows:

$$\left[v_{AN} = R_s i_1 + v_{DC} \right]_{S_1 \ closed} \qquad or \qquad \left[v_{AN} = R_s i_1 \right]_{S_1 \ open} . \tag{3.16}$$

Combining these gives

$$\begin{aligned} v_{AN} &= (R_s i_1 + v_{DC}) \, d_1 + (R_s i_1) \, d_1' \\ &= (d_1 + d_1') \, R_s i_1 + d_1 v_{DC} \\ &= R_s i_1 + d_1 v_{DC} . \end{aligned} \tag{3.17}$$

Putting v_{AN} back into (3.14):

$$\begin{aligned} e_1 &= L \frac{di_1}{dt} + R_l i_1 + R_s i_1 + d_1 v_{DC} + v_{Nn} \\ &= L \frac{di_1}{dt} + (R_l + R_s) \, i_1 + d_1 v_{DC} + v_{Nn} . \end{aligned} \tag{3.18}$$

Repeating for all three phases and replacing $(R_l + R_s)$ with R :

$$\begin{aligned} e_1 &= L \frac{di_1}{dt} + R \, i_1 + d_1 v_{DC} + v_{Nn} \\ e_2 &= L \frac{di_2}{dt} + R \, i_2 + d_2 v_{DC} + v_{Nn} \\ e_3 &= L \frac{di_3}{dt} + R \, i_3 + d_3 v_{DC} + v_{Nn} \end{aligned} \tag{3.19}$$

If a balanced three-phase system is now assumed:

$$\begin{aligned} e_1 + e_2 + e_3 &= 0 \\ i_1 + i_2 + i_3 &= 0 \\ \frac{di_1}{dt} + \frac{di_2}{dt} + \frac{di_3}{dt} &= 0 \end{aligned} \tag{3.20}$$

then the three phases of (3.19) can be summed and the result is:

$$(d_1 + d_2 + d_3) \, v_{DC} + 3 v_{Nn} = 0$$

$$v_{Nn} = -\frac{v_{DC}}{3} \sum_{n=1}^{3} d_n \tag{3.21}$$

Putting this v_{Nn} back into (3.14) and expressing in general terms:

$$e_k = L\frac{di_k}{dt} + R\,i_k + d_k v_{DC} - \frac{v_{DC}}{3}\sum_{n=1}^{3} d_n$$

$$= L\frac{di_k}{dt} + R\,i_k + v_{DC}\left[d_k - \frac{1}{3}\sum_{n=1}^{3} d_n\right]$$

(3.22)

where subscript k indicates 1, 2 or 3. Note, the elements in the square brackets are discrete, making the equation time variant. Since we need time invariant equations for control modelling we must convert to the $\alpha\beta$- static reference frame and then the dq- rotating reference frame (Figure 3.5):
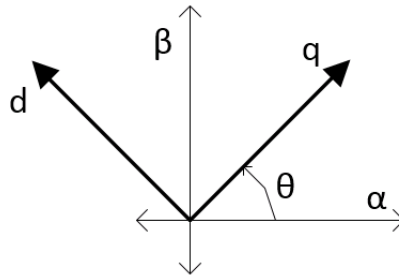
Figure 3.5: $\alpha\beta$ and dq Coordinate Systems

With no invariance multipliers, the inverse $\alpha\beta$ transform for the $\alpha\beta$ coordinate system defined in Figure 3.5 is [6]:

$$\begin{bmatrix} X_a \\ X_b \\ X_c \end{bmatrix} = \begin{bmatrix} 1 & 0 \\ -1/2 & -\sqrt{3}/2 \\ -1/2 & +\sqrt{3}/2 \end{bmatrix} \begin{bmatrix} X_\alpha \\ X_\beta \end{bmatrix}$$

(3.23)

or in equation form

$$X_a = X_\alpha$$
$$X_b = -\frac{1}{2}X_\alpha - \frac{\sqrt{3}}{2}X_\beta$$
$$X_c = -\frac{1}{2}X_\alpha + \frac{\sqrt{3}}{2}X_\beta$$

(3.24)

These can now be used to simplify the discrete portion of (3.22):

$$d_k - \frac{1}{3}\sum_{n=1}^{3} d_n = d_k - \frac{1}{3}\left\{ d_\alpha + \left[-\frac{1}{2}d_\alpha - \frac{\sqrt{3}}{2}d_\beta\right] + \left[-\frac{1}{2}d_\alpha + \frac{\sqrt{3}}{2}d_\beta\right]\right\}$$

$$= d_k$$

(3.25)

which can be put back into the AC equation for a simplified (3.22) in general terms:

$$e_k = L\frac{di_k}{dt} + R\,i_k + v_{DC}\,d_k \; . \tag{3.26}$$

Converting all three phases of (3.26) to the $\alpha\beta$ reference frame:

$$e_\alpha = L\frac{di_\alpha}{dt} + R\,i_\alpha + v_{DC}\,d_\alpha$$

$$\left[-\frac{1}{2}e_\alpha - \frac{\sqrt{3}}{2}e_\beta \right] = L\frac{d}{dt}\left[-\frac{1}{2}i_\alpha - \frac{\sqrt{3}}{2}i_\beta \right] + R\left[-\frac{1}{2}i_\alpha - \frac{\sqrt{3}}{2}i_\beta \right] + v_{DC}\left[-\frac{1}{2}d_\alpha - \frac{\sqrt{3}}{2}d_\beta \right]$$

$$\left[-\frac{1}{2}e_\alpha + \frac{\sqrt{3}}{2}e_\beta \right] = L\frac{d}{dt}\left[-\frac{1}{2}i_\alpha + \frac{\sqrt{3}}{2}i_\beta \right] + R\left[-\frac{1}{2}i_\alpha + \frac{\sqrt{3}}{2}i_\beta \right] + v_{DC}\left[-\frac{1}{2}d_\alpha + \frac{\sqrt{3}}{2}d_\beta \right] \tag{3.27}$$

and separating the second and third part of (3.27) into their respective vector axes:

$$e_\alpha = L\frac{di_\alpha}{dt} + R\,i_\alpha + v_{DC}\,d_\alpha$$

$$-\frac{1}{2}\left[e_\alpha = L\frac{di_\alpha}{dt} + R\,i_\alpha + v_{DC}\,d_\alpha \right] - \frac{\sqrt{3}}{2}\left[e_\beta \;= L\frac{di_\beta}{dt} + R\,i_\beta + v_{DC}\,d_\beta \right] \tag{3.28}$$

$$-\frac{1}{2}\left[e_\alpha = L\frac{di_\alpha}{dt} + R\,i_\alpha + v_{DC}\,d_\alpha \right] + \frac{\sqrt{3}}{2}\left[e_\beta \;= L\frac{di_\beta}{dt} + R\,i_\beta + v_{DC}\,d_\beta \right]$$

we see repeated instances of the same equation independent of the vector direction. We can now summarize with a complex vector representation:

$$\overline{e_{\alpha\beta}} = L\frac{d}{dt}\,\overline{i_{\alpha\beta}} + R\,\overline{i_{\alpha\beta}} + v_{DC}\,\overline{d_{\alpha\beta}} \; . \tag{3.29}$$

Now (3.29) can be converted to the dq rotating reference frame by setting $X_{dq} = X_{\alpha\beta}\,e^{j\theta}$ or $X_{\alpha\beta} = X_{dq}\,e^{-j\theta}$ where $j\theta = j\omega t$:

$$\overline{e_{dq}}\,e^{-j\theta} = L\frac{d}{dt}\left[\overline{i_{dq}}\,e^{-j\theta} \right] + R\,\overline{i_{dq}}\,e^{-j\theta} + v_{DC}\,\overline{d_{dq}}\,e^{-j\theta}$$

$$\overline{e_{dq}}\,e^{-j\theta} = L\frac{d\overline{i_{dq}}}{dt}\,e^{-j\theta} + j\omega L\,\overline{i_{dq}}\,e^{-j\theta} + R\,\overline{i_{dq}}\,e^{-j\theta} + v_{DC}\,\overline{d_{dq}}\,e^{-j\theta} \tag{3.30}$$

$$\overline{e_{dq}} = L\frac{d\overline{i_{dq}}}{dt} - j\omega L\,\overline{i_{dq}} + R\,\overline{i_{dq}} + v_{DC}\,\overline{d_{dq}}$$

or when split up into individual axes

$$e_d = L\frac{di_d}{dt} - \omega L\, i_q + R\, i_d + v_{DC}\, d_d$$

$$e_q = L\frac{di_q}{dt} + \omega L\, i_d + R\, i_q + v_{DC}\, d_q \tag{3.31}$$

Solving for current and expressing in the Laplace domain we have our AC side VSC system equations:

$$i_d = \left[\frac{1}{sL+R}\right]\left[e_d - v_{DC}\, d_d + \omega L\, i_q\right]$$

$$i_q = \left[\frac{1}{sL+R}\right]\left[e_q - v_{DC}\, d_q - \omega L\, i_d\right] \tag{3.32}$$

which are given in block diagram form in Figure 3.6 ([6], figure 5 of [13]).
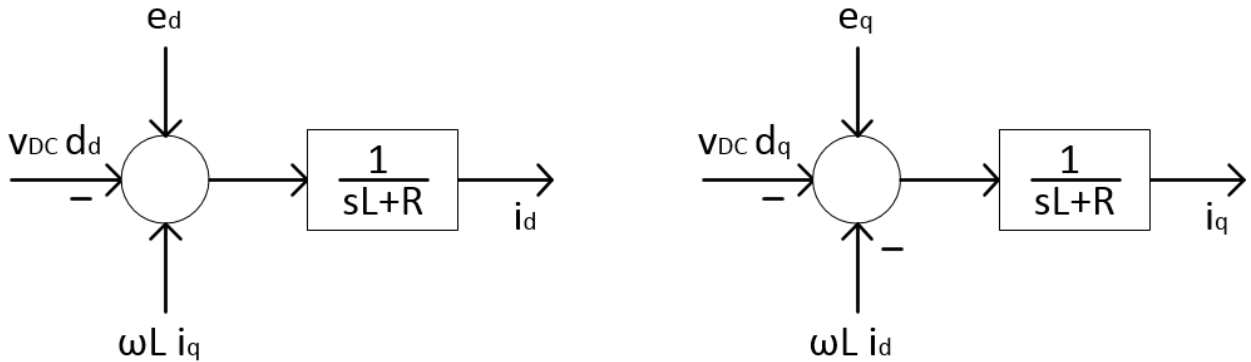
Figure 3.6: VSC Plant, AC Side Block Diagram

The effects of capacitor dynamics must also be included in the VSC system representation. According to (3.12) and Kirchoff's Current Law on the DC side of Figure 3.4

$$i_{DC} = i_C + I_{LD}$$

$$C\frac{dv_{DC}}{dt} = \frac{3}{4}Re\left[\overline{i_{\alpha\beta}}\, \overline{S_{\alpha\beta}^*}\right] - I_{LD}\,. \tag{3.33}$$

This is also converted to the dq- rotating reference frame defined in figure 3.5:

$$C\frac{dv_{DC}}{dt} = \frac{3}{4}Re\left[\overline{i_{dq}}\,e^{-j\theta}\,\overline{S_{dq}^*}\,e^{j\theta}\right] - I_{LD}$$

$$= \frac{3}{4}Re\left[\overline{i_{dq}}\,(cos\theta - j\sin\theta)\,\overline{S_{dq}^*}\,(cos\theta + j\sin\theta)\right] - I_{LD}$$

$$= \frac{3}{4}Re\left[\overline{i_{dq}}\,\overline{S_{dq}^*}\,(cos^2\theta + \sin^2\theta)\right] - I_{LD} \tag{3.34}$$

$$= \frac{3}{4}Re\left[\overline{i_{dq}}\,\overline{S_{dq}^*}\right] - I_{LD}\,.$$

Solving for v_{DC} and expressing in the Laplace domain we have:

$$v_{DC} = \left[\frac{1}{sC}\right]\left[\frac{3}{4}Re\left[\overline{i_{dq}}\,\overline{S_{dq}^*}\right] - I_{LD}\right] \tag{3.35}$$

but we need to express (3.35) in terms of individual dq- axes. Since we now know that i_{DC} is the same in the $\alpha\beta$- as in the dq- domain, we can change from $\overline{S}$ to d as in Figure 3.4 and (3.15):

$$i_{DC} = \frac{3}{4}Re\left[\overline{i_{dq}}\,\overline{S_{dq}^*}\right] = \sum_{n=1}^{3}\left[i_n d_n\right] \tag{3.36}$$

The elements on the right side of (3.36) can be converted to the dq- reference frame with the inverse transform equations of (3.24). Note that since we are now developing an equation for implementation in the time domain, the invariance multiplier has been neglected:

$$= \left[i_q d_q\right] + \left[-\frac{1}{2}i_q - \frac{\sqrt{3}}{2}i_d\right]\left[-\frac{1}{2}d_q - \frac{\sqrt{3}}{2}d_d\right] + \left[-\frac{1}{2}i_q + \frac{\sqrt{3}}{2}i_d\right]\left[-\frac{1}{2}d_q + \frac{\sqrt{3}}{2}d_d\right]$$

$$= i_q d_q + \frac{1}{4}i_q d_q + \frac{\sqrt{3}}{4}i_q d_d + \frac{\sqrt{3}}{4}i_d d_q + \frac{3}{4}i_d d_d + \frac{1}{4}i_q d_q - \frac{\sqrt{3}}{4}i_q d_d - \frac{\sqrt{3}}{4}i_d d_q + \frac{3}{4}i_d d_d$$

$$= \frac{6}{4}i_q d_q + \frac{6}{4}i_d d_d$$

$$= \frac{3}{2}\left(i_q d_q + i_d d_d\right)\,. \tag{3.37}$$

Now putting (3.37) into (3.35) according to (3.36) we have our DC side VSC system equation:

$$v_{DC} = \left[\frac{1}{sC}\right]\left[\frac{3}{2}\left(i_q d_q + i_d d_d\right) - I_{LD}\right]\,. \tag{3.38}$$

This is given in block diagram form in figure 3.7 ([6], figure 5 of [13]).
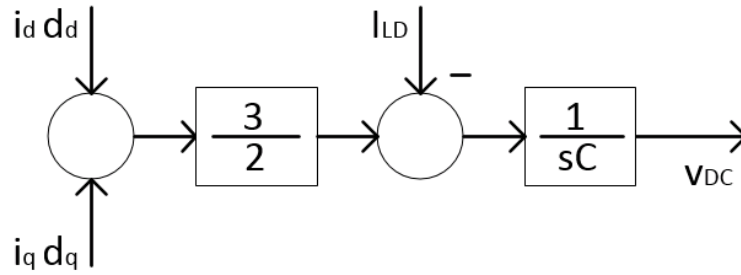
Figure 3.7: VSC Plant, DC Side Block Diagram

3.2.3 VSC Power Equation in DQ0 Reference Frame

Last, we need equations for P and Q. The standard apparent power relationship can be used $(S = P + jQ = 3VI^*)$:

$$
\begin{aligned}
3VI^* &= 3\left[\frac{\overline{e_{dq}}}{\sqrt{2}}\right]\left[\frac{\overline{i_{dq}^*}}{\sqrt{2}}\right] \\
&= 3\left[\frac{e_q + je_d}{\sqrt{2}}\right]\left[\frac{i_q - ji_d}{\sqrt{2}}\right] \\
&= \frac{3}{2}\left[e_q i_q - je_q i_d + je_d i_q + e_d i_d\right] \\
P + jQ &= \frac{3}{2}\left\{\left[e_q i_q + e_d i_d\right] + j\left[e_d i_q - e_q i_d\right]\right\}.
\end{aligned}
\tag{3.39}
$$

If we lock our d-axis to the system voltage vector then $e_d = \sqrt{2}E$ and $e_q = 0$. Our equation now simplifies to:

$$
\begin{aligned}
P &= \frac{3}{2} e_d i_d = \frac{3}{2} \times \sqrt{2}E\, i_d \\
Q &= \frac{3}{2} e_d i_q = \frac{3}{2} \times \sqrt{2}E\, i_q
\end{aligned}
\tag{3.40}
$$

where P and Q can be controlled independently of each other by i_d and i_q respectively.

3.2.4 Inner Loop Controller

The inner current loop PI block of the VSC controller in figure 3.2 is associated with fast time constants relative to the outer loop. Therefore the goal of the inner loop is zero error. Modulus Optimum is a control strategy which can facilitate this goal [6, 14]. It is a conventional analogue controller tuning method for low order controlled plants.

Notice in Figure 3.6 that i_d is dependant on multiple inputs (e_d and $d_d\,v_{DC}$) and a cross-coupling component ($\omega L\,i_q$). Feed forward measurements can be put into the inner loop to simplify and decouple these dependencies before the control signal m_a is sent to the PWM [6, 13]. This feed forward can be observed in Figure 3.8 and adds some beneficial features to the overall converter control scheme. It decouples i_d from i_q allowing independent control of, for example, active power and reactive power as suggested in (3.40). It also decouples i_d from e_d (and i_q from e_q) leaving dependencies between current and voltage isolated to the DC side of the power converter. This allows DC power at WF-VSC to be controlled independently of DC voltage magnitude at GS-VSC and allows for the VSC operational characteristics described in section 4.2.1.
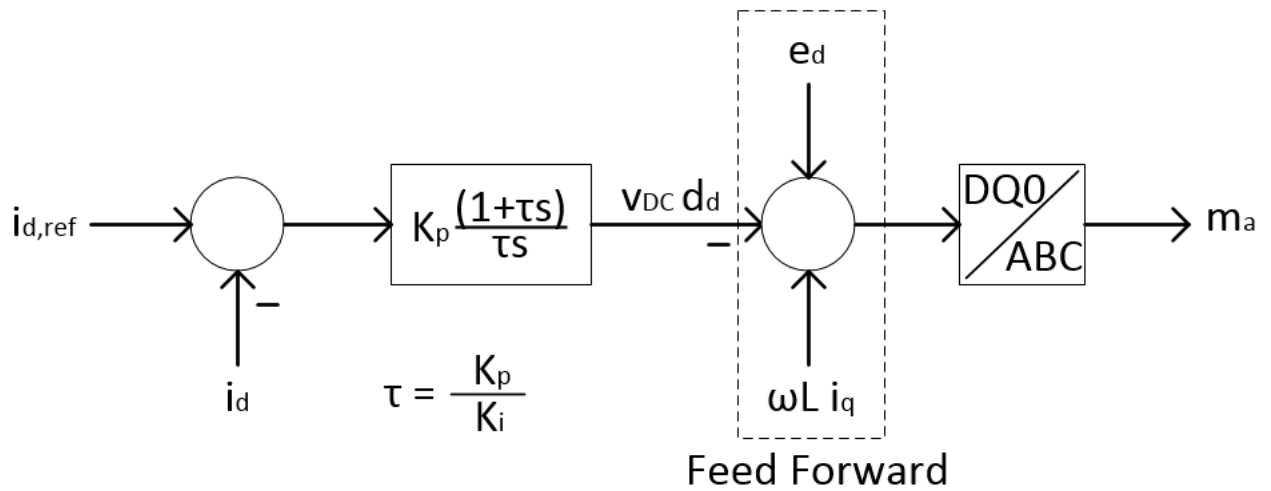
Figure 3.8: Current Inner Loop Controller

3.2.5   Outer Loop Controller

The outer loop PI block of the VSC controller in figure 3.2 is associated with slower time constants relative to the inner loop. The goal of the outer loop is to optimize system behavior with respect to disturbance signals. Symmetrical Optimum is a control strategy which can be used toward this goal [6, 14]. This loop does not require feed forward modifications as the inner loop did. It is fairly straightforward with a reference signal, a feedback signal and a PI controller.

In this project, at GS-VSC, the d-axis outer loop is used to control v_{DC} and the q-axis outer loop is used to control reactive power. At WF-VSC, the d-axis is used to regulate AC voltage and the q-axis is used to regulate frequency. This is further detailed in section 4.2 and chapter 7. Figure 3.9 is a diagram of the voltage magnitude outer loop controller at WF-VSC. In this diagram v_{DQ} represents the magnitude of the DQ reference frame voltage vector or $\sqrt{e_d^2 + e_q^2}$.

The other outer loop controllers function as part of the "communication-less" channel and are found in section 4.2.
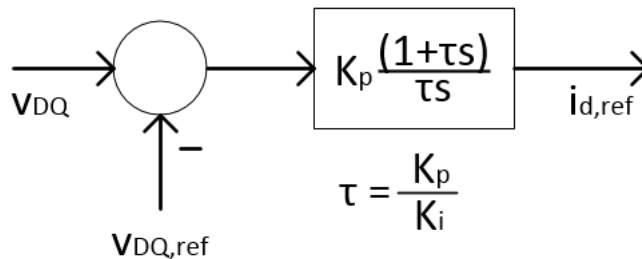
Figure 3.9: Voltage Magnitude Controller at WF-VSC

3.3 Implementation with PWM Average Switching Model

Since the VSC is implemented in a Constant DC Current configuration (Figure 3.1), the average switching model is implemented with DC current sources and AC voltage sources (Figure 3.10). The DC current sources depend on AC current measurements and the AC voltage sources depend on DC voltage measurements.

3.3.1 VSC Power Equation in ABC Reference Frame

The three-phase power equation can be used to find the average model implementation of current. Assuming no converter losses, the three-phase power equation is

$$V_{DC}\, I_{DC} = v_{an}\, i_a + v_{bn}\, i_b + v_{cn}\, i_c \tag{3.41}$$

where the lower-case variables represent the individual sinusoidal waveforms. For the purpose of representing the average model implementation in one single equation, (3.1) can now be used to replace all the AC voltage components in (3.41). Also, the control system outputs a three-phase sinusoidal amplitude modulation ratio with a peak of $m_A = 0.8$. The variable $m_{a,b,c}$ can be used to represent this three-phase signal:

$$V_{DC}\, I_{DC} = m_{a,b,c} \frac{V_{DC}}{2} \left[i_a + i_b + i_c \right]. \tag{3.42}$$

Next, V_{DC} cancels and (3.42) becomes

$$I_{DC} = \frac{m_{a,b,c}}{2} \left[i_a + i_b + i_c \right]. \tag{3.43}$$

Implementation of the average model plant in Figure 3.10 can now be summed up with (3.1) and (3.43).
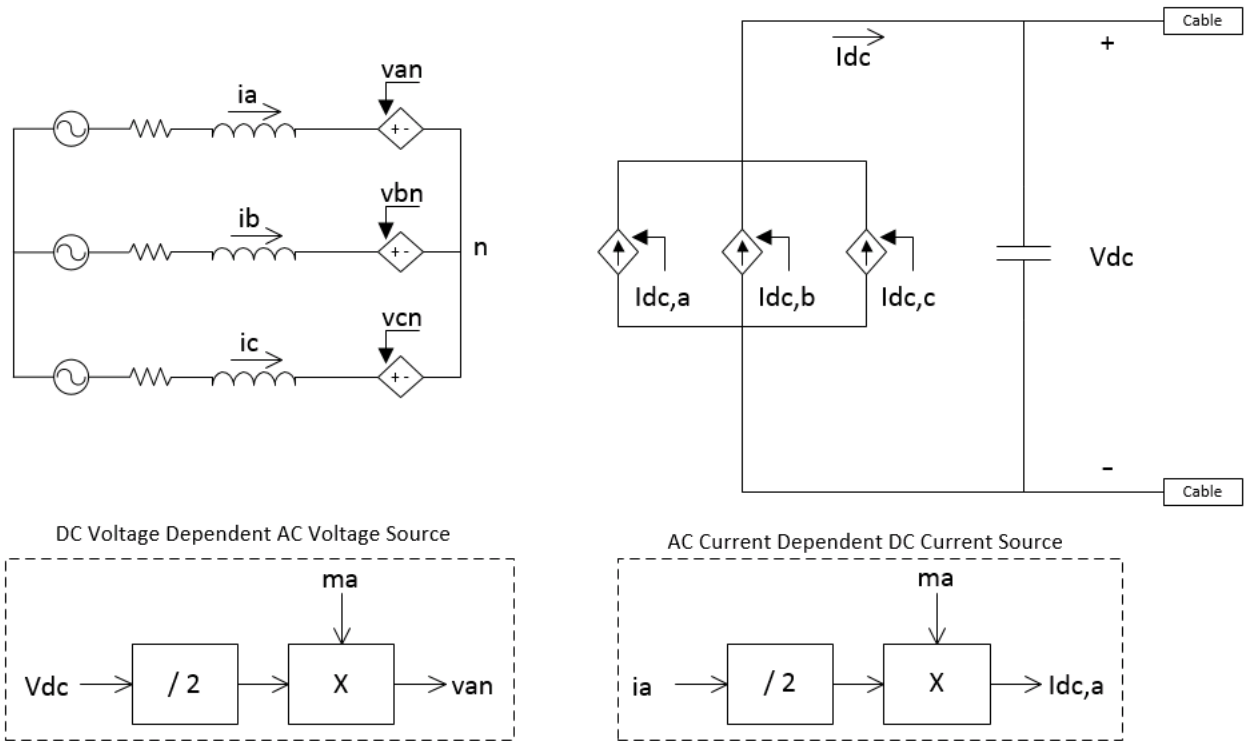
Figure 3.10: Average Switching Model

Chapter 4

Power Flow and Voltage

The onshore AC network in this project is a load bus supplied by the aggregated large synchronous generator (LSG) through a network of transmission lines. The system is designed for voltage stability and maintains constant rated voltage at the load bus. Section 4.1 develops the power transfer characteristics and voltage stability criteria required for the onshore AC network. The load bus also serves as a point of common coupling (PCC) for a VSC-HVDC link. The HVDC link relies on the voltage and frequency stability of the onshore AC network in order to operate. Section 4.2 develops the power flow control strategy for the converters so that they can interact correctly with the AC systems located at either end of the DC link. This includes designing the DC circuit to facilitate the windfarm controller design in chapter 7.

4.1   AC Power Flow and Voltage

This section develops the onshore AC system design as it relates to power flow and voltage stability. First a general AC power flow equation is developed. Then section 4.1.1 reduces the equation for a primarily inductive network which is relevant for the onshore AC system. Section 4.1.2 reduces the equation for a primarily resistive network which is relevant for the offshore AC system. Section 4.1.3 then outlines the voltage strength required for AC/DC system interaction. Last, section 4.1.4 gives a development of the AC voltage stability at the load bus.

Figure 4.1 is a diagram for the purpose of AC power flow analysis. R_T and X_T represent the Thevenin impedance of the network between the generator transmission bus and the load.

First, load current can be found as a function of voltage and impedance:
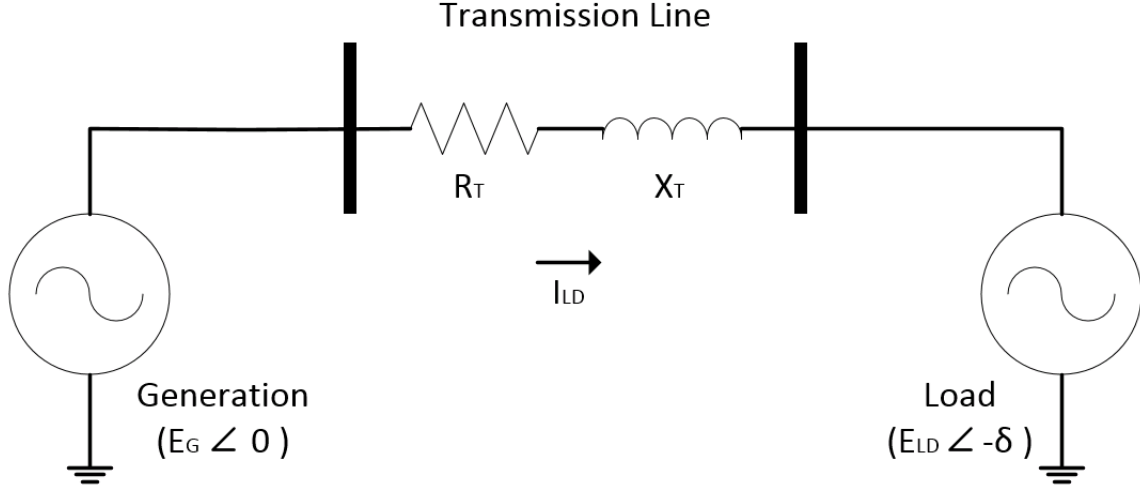
Figure 4.1: AC Power Flow

$$
\begin{aligned}
I_{LD} &= \frac{E_G \angle 0 - E_{LD} \angle^- \delta}{R_T + jX_T} \\
&= \frac{E_G - E_{LD}(\cos \delta - j \sin \delta)}{R_T + jX_T} \\
&= \frac{(E_G - E_{LD} \cos \delta) + jE_{LD} \sin \delta}{R_T + jX_T} \times \frac{R_T - jX_T}{R_T - jX_T} \\
&= \frac{(E_G R_T - E_{LD} R_T \cos \delta + E_{LD} X_T \sin \delta) + j(E_{LD} R_T \sin \delta - E_G X_T + E_{LD} X_T \cos \delta)}{R_T^2 + X_T^2}.
\end{aligned}
\tag{4.1}
$$

Apparent power output at the generator can then be found as:

$$
\begin{aligned}
S_G &= E_G I_{LD}^* \\
&= \left[\frac{E_G(E_G R_T - E_{LD} R_T \cos \delta + E_{LD} X_T \sin \delta)}{R_T^2 + X_T^2} \right] \\
&\quad - j \left[\frac{E_G(E_{LD} R_T \sin \delta - E_G X_T + E_{LD} X_T \cos \delta)}{R_T^2 + X_T^2} \right] \\
&= \left[\frac{E_G(E_G R_T - E_{LD}(R_T \cos \delta - X_T \sin \delta))}{R_T^2 + X_T^2} \right] \\
&\quad + j \left[\frac{E_G(E_G X_T - E_{LD}(R_T \sin \delta + X_T \cos \delta))}{R_T^2 + X_T^2} \right] \\
&= P_G + jQ_G
\end{aligned}
\tag{4.2}
$$

and can be quite tedious to work with. Further simplifications are typically used. One way to characterize an AC network is with an X/R ratio with X and R as the Thevenin equivalent of

the network. A high X/R ratio indicates that X $\gg$ R and can be referred to as an inductive network. A low X/R ratio indicates that R $\gg$ X and can be referred to as a resistive network.

4.1.1 Inductive Network

As X/R ratio increases, R approaches zero relative to X. As a result, for an inductive network, R_T in figure 4.1 is considered negligible and (4.2) can be simplified to:

$$S_G = P_G + jQ_G$$
$$= \left[\frac{E_G E_{LD}}{X_T} \sin \delta \right] + j \left[\frac{E_G(E_G - E_{LD} \cos \delta)}{X_T} \right] . \tag{4.3}$$

High X/R ratio typically indicates a high voltage transmission network and as voltage rating increases X/R ratio increases (Table 6.1 of [15]). As can be observed in (4.3), an inductive network exhibits a strong dependency between frequency and active power. It also exhibits a strong dependency between voltage and reactive power. In traditional AC transmission systems, this inductive quality is used for enhancing stability of the system. Load sharing is implemented based on the fact that frequency remains virtually constant across the whole network. By automatically reassigning load changes according to this global frequency and a proportional controller (referred to as a droop controller) at any one individual generation source, load mismatches can be reassigned dynamically. This subject is explored further in chapter 6.

In this project, the X and R values of the AC transmission line were taken from Table 6.1 of [15] as typical values for 230kV overhead lines. These values are $0.050 \, \Omega/\text{km}$ resistance and $0.488 \, \Omega/\text{km}$ inductive reactance resulting in $X/R = 9.76$ for the onshore AC network at frequency 50Hz. This is considered adequate to neglect R_T and perform power flow calculations with the equation given in 4.3. Also, according to 10.6.1 (pg. 529) of [15], phase angle of the Thevenin equivalent impedance θ_T has an effect on AC/DC system control stability. It indicates resistive load and improves the damping effect of the system. Typical values fall between 75° and 85°. The phase angle of the Thevenin impedance used in this project is $\theta_T = 84.1°$ and falls within this range.

4.1.2 Resistive Network

As X/R ratio decreases, X approaches zero relative to R. As a result, for a resistive network, X_T in figure 4.1 is considered negligible and (4.2) can be simplified to:

$$S_G = P_G + jQ_G$$
$$= \left[\frac{E_G(E_G - E_{LD} \cos \delta)}{R_T} \right] + j \left[\frac{-E_G E_{LD}}{R_T} \sin \delta \right] . \tag{4.4}$$

Low X/R ratio typically indicates a low voltage distribution network ([16], Section 3.4.1). In this case, active power is more strongly dependent on voltage. Frequency is independent of both active and reactive power and inductance is negligible making it a local variable. This suggests more active control requirements in a resistive network with no global frequency variable to follow.

However, according to ([16], Section 3.4.3), reactive power can be coupled to frequency by associated it with load angle δ. This subject is explored further with wind farm controller design in chapter 7.

4.1.3   Voltage Strength

According to chapter 5 of [17] and 10.6 of [15], AC system voltage strength has a significant influence on AC/DC system interaction. In a strong voltage AC system, voltage fluctuations and harmonic resonances are minimized and the system is more resilient to voltage stability issues. Short Circuit Ratio is a means of quantifying the AC system voltage strength relative to the DC system. It is defined as:

$$SCR = \frac{\text{Short Circuit Level of AC System, MVA}}{\text{Power Rating of DC Converter, MW}} \tag{4.5}$$

where Short Circuit Level of the AC system is a function of system voltage rating E_{base} and Thevenin equivalent impedance of the transmission system Z_T:

$$SCL = \frac{E_{base}^2}{Z_T} \ . \tag{4.6}$$

The resulting short circuit ratio is:

$$SCR = \frac{E_{base}^2}{P_C \, Z_T} \tag{4.7}$$

where P_C is the DC power rating of the Grid Side VSC (GS-VSC). Section 5.1 (pg. 151) of [17] suggests $SCR \geq 10$ and section 10.6.1 (pg. 529) of [15] suggests $SCR \geq 5$ for a strong voltage AC network. This requires a Thevenin impedance magnitude of:

$$
\begin{aligned}
Z_T &\leq \frac{E_{base}^2}{P_C \times SCR} \\
&\leq \frac{(245kV)^2}{400MW \times (5 \text{ or } 10)} \\
&\leq 15 \text{ or } 30 \, \Omega \ .
\end{aligned}
\tag{4.8}
$$

The onshore AC transmission network in this project is two overhead lines in parallel. Their characteristics can be found in section 4.1.1 and they are 70km in length. The Thevenin

resistance is therefore $R_T = 1.75\,\Omega$ and the inductive reactance is $X_T = 17.1\,\Omega$. The total Thevenin line impedance is then $Z_T = 17.2\,\Omega$ and is sufficient to meet the criteria for a strong voltage onshore AC network.

4.1.4 Voltage Stability at Load Bus

In this project the load bus is located directly at the point of common coupling (PCC). In general, this load bus must be able to maintain voltage stability for minor load changes in order for the system to function properly. Practically, this means that small variations in load cannot cause significant variations in voltage at the load bus. For this project, the load was chosen to be a simple resistor and load changes were modelled as changes in that resistance. A capacitor was also to used to facilitate the voltage stability at the load bus.

Voltage stability of the load bus is expressed by plotting load voltage E_{LD} as a function of active power consumed by the load P_{LD}. In order to do this, the load in figure 4.1 can be analysed in terms of load impedance. This load impedance can then be expressed in terms of voltage E_{LD}, active power P_{LD} and reactive power Q_{LD} for the purpose of plotting the characteristic. Figure 4.2 is figure 4.1 adapted for this purpose. In the figure, ϕ is the power factor angle of the load, δ is not needed for this derivation. The following is a derivation for E_{LD} as a function of E_G, P_{LD} and Q_{LD} according to [18]. It is based on chapter 14 of [15].

The vector form of $\overline{I_{LD}}$ can be found as:

$$\overline{I_{LD}} = \frac{\overline{E_G}}{\overline{Z_T} + \overline{Z_{LD}}} \tag{4.9}$$

where $\overline{Z_T}$ is the Thevenin equivalent impedance of the line. However, it is more convenient to express these quantities in terms of magnitude. Since E_G is the reference voltage with an angle of zero and assuming R_T to be negligible (ie: lossless line):

$$
\begin{aligned}
I_{LD} &= \frac{E_G}{\sqrt{(Z_{LD}\cos\phi)^2 + (X_T + Z_{LD}\sin\phi)^2}} \\
&= \frac{E_G}{X_T}\frac{1}{\sqrt{F}}
\end{aligned}
\tag{4.10}
$$

where:

$$
\begin{aligned}
F &= \left[\frac{Z_{LD}}{X_T}\cos\phi\right]^2 + \left[1 + \frac{Z_{LD}}{X_T}\sin\phi\right]^2 \\
&= 1 + 2\frac{Z_{LD}}{X_T}\sin\phi + \left(\frac{Z_{LD}}{X_T}\right)^2(\cos^2\phi + \sin^2\phi) \\
&= 1 + 2\frac{Z_{LD}}{X_T}\sin\phi + \left(\frac{Z_{LD}}{X_T}\right)^2
\end{aligned}
\tag{4.11}
$$
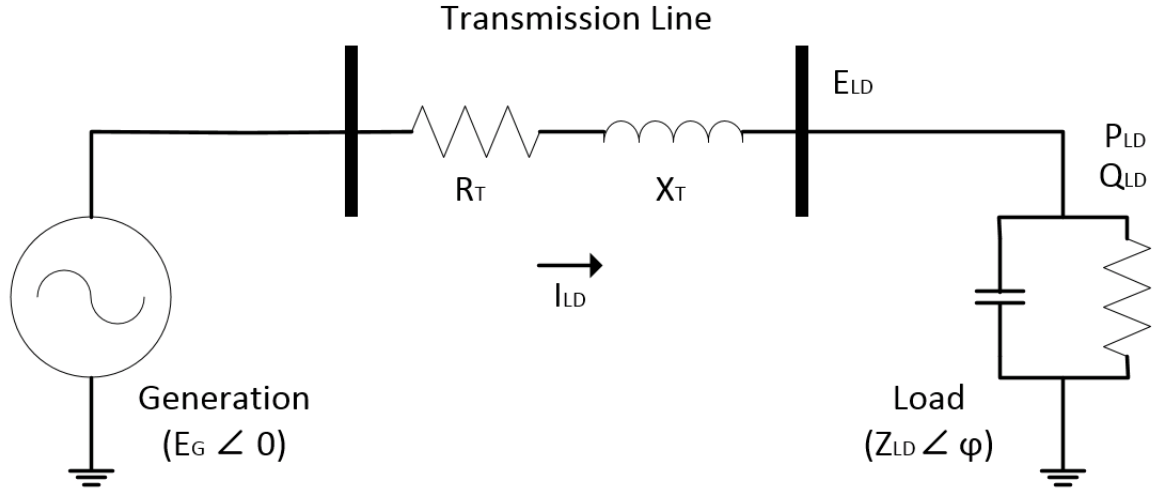
Figure 4.2: Load Bus AC Voltage Stability

and is also found in 14.1.1 of [15]. Load voltage is then:

$$
\begin{aligned}
E_{LD} &= I_{LD}\,Z_{LD} \\
&= \frac{E_G\,Z_{LD}}{X_T\,\sqrt{F}} \; .
\end{aligned}
\tag{4.12}
$$

Power consumed by the load is:

$$
\begin{aligned}
P_{LD} &= E_{LD}\,I_{LD}\,\cos\phi \\
&= \left(\frac{E_G}{X_T}\right)^2 \frac{Z_{LD}}{F}\,\cos\phi \; .
\end{aligned}
\tag{4.13}
$$

The following substitutions can now be made for an expression in terms of E_{LD}, P_{LD} and Q_{LD}:

$$
\begin{aligned}
Z_{LD} &= \frac{E_{LD}^2}{\sqrt{P_{LD}^2 + Q_{LD}^2}} \\
\cos\phi &= \frac{P_{LD}}{\sqrt{P_{LD}^2 + Q_{LD}^2}} \\
\sin\phi &= \frac{Q_{LD}}{\sqrt{P_{LD}^2 + Q_{LD}^2}} \; .
\end{aligned}
\tag{4.14}
$$

Putting (4.11) and (4.14) into (4.13) gives:

$$P_{LD} = \left(\frac{E_G}{X_T}\right)^2 \frac{Z_{LD}\,\cos\phi}{1 + 2\,\frac{Z_{LD}}{X_T}\,\sin\phi + \left(\frac{Z_{LD}}{X_T}\right)^2}$$

$$= \left(\frac{E_G}{X_T}\right)^2 \frac{E_{LD}^2\,P_{LD}}{P_{LD}^2 + Q_{LD}^2} \frac{1}{1 + 2\,\frac{Z_{LD}}{X_T}\,\sin\phi + \left(\frac{Z_{LD}}{X_T}\right)^2}$$

$$\frac{(E_G\,E_{LD})^2}{X_T^2\,(P_{LD}^2 + Q_{LD}^2)} = 1 + \frac{2\,E_{LD}^2\,Q_{LD}}{X_T\,(P_{LD}^2 + Q_{LD}^2)} + \left(\frac{E_{LD}^2}{X_T\,\sqrt{P_{LD}^2 + Q_{LD}^2}}\right)^2$$

$$(E_G\,E_{LD})^2 = X_T^2\,(P_{LD}^2 + Q_{LD}^2) + 2\,E_{LD}^2\,Q_{LD}\,X_T + E_{LD}^4$$

$$0 = E_{LD}^4 + E_{LD}^2\left[2\,Q_{LD}\,X_T - E_G^2\right] + \left[X_T^2\,(P_{LD}^2 + Q_{LD}^2)\right]\,. \tag{4.15}$$

The quadratic formula can now be used to find E_{LD}^2 and then E_{LD}:

$$E_{LD}^2 = \frac{E_G^2}{2} - Q_{LD}\,X_T \pm \sqrt{\left(Q_{LD}\,X_T - \frac{E_G^2}{2}\right)^2 - X_T^2\,(P_{LD}^2 + Q_{LD}^2)}$$

$$= \frac{E_G^2}{2} - Q_{LD}\,X_T \pm \sqrt{Q_{LD}^2\,X_T^2 - E_G^2\,Q_{LD}\,X_T + \frac{E_G^4}{4} - X_T^2\,(P_{LD}^2 + Q_{LD}^2)}$$

$$= \frac{E_G^2}{2} - Q_{LD}\,X_T \pm \sqrt{\frac{E_G^4}{4} - E_G^2\,Q_{LD}\,X_T - P_{LD}^2\,X_T^2} \tag{4.16}$$

$$E_{LD} = \sqrt{\frac{E_G^2}{2} - Q_{LD}\,X_T \pm \sqrt{\frac{E_G^4}{4} - E_G^2\,Q_{LD}\,X_T - P_{LD}^2\,X_T^2}}\,.$$

This is the equation for the PV characteristic of the load bus in terms of source voltage and power consumed by the load. For the purpose of plotting the PV curve, it is convenient to know the maximum deliverable power. This can be obtained by taking the inner square root from (4.16), setting it to zero and solving for P_{LD} (note that Q_{LD} can be removed from the equation as well by replacing with $P_{LD}\,\tan\phi$):

$$0 = \frac{E_G^4}{4} - E_G^2\,(P_{LD}\,\tan\phi)\,X_T - P_{LD}^2\,X_T^2$$

$$= P_{LD}^2 + P_{LD}\left[\frac{E_G^2\,\tan\phi}{X_T}\right] - \left[\frac{E_G^4}{4\,X_T^2}\right]$$

$$P_{LD,max} = -\frac{E_G^2\,\tan\phi}{2\,X_T} \pm \sqrt{\left(\frac{E_G^2\,\tan\phi}{2\,X_T}\right)^2 + \frac{E_G^4}{4\,X_T^2}} \tag{4.17}$$

$$= \frac{E_G^2}{2\,X_T}\left(\sqrt{\tan^2\phi + 1} - \tan\phi\right)\,.$$

Figure 4.3 is a PV curve of the voltage stability at the PCC for the onshore AC network according to (4.16) and (4.17). The dashed lines indicate the nominal load operating condition. The load corresponds to LSG rated capacity at $3 \times 463 = 1389$ MW. Since we are concerned with voltage stability due to power flow we consider resistance negligible

and use the Thevenin inductive reactance of $X_T = 17.1\,\Omega$ from section 4.1.3. The voltage at the source terminals (ie: at LSG) is rated voltage of $E_G = 245$kV. A capacitor rated $20\,\mu F$ is also used to improve the power transfer capability by changing the load power factor angle to $\phi = {}^-11.83°$. As the figure suggests, small changes in load will not cause significant deviations in voltage.
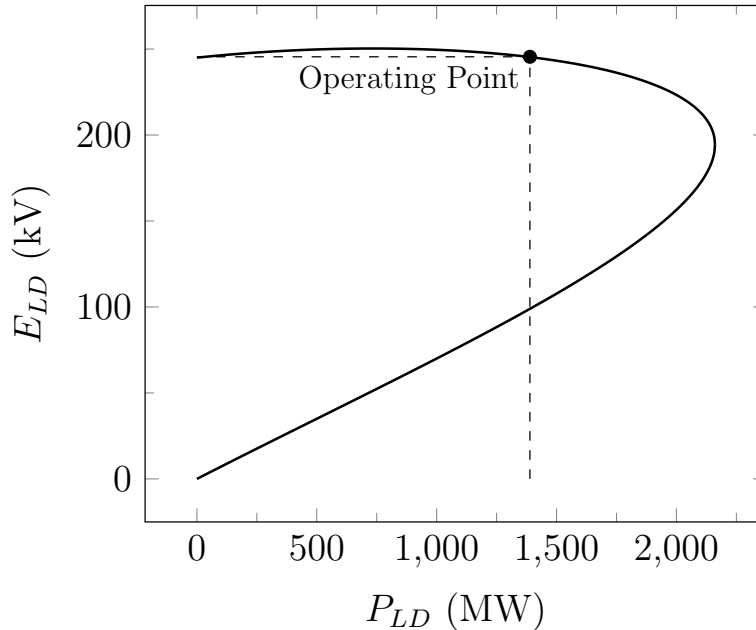
Figure 4.3: PV Curve at PCC for Onshore AC System Rated Load

4.2   DC Power Flow and Voltage

As stated in chapter 3, this project uses Three-Phase Full-Bridge Voltage Source Converters functioning as power converters at the grid side (GS-VSC) and the windfarm side (WF-VSC) of an HVDC link.   These converters operate under a DC voltage link topology with the WF-VSC functioning as a Three Phase AC-to-DC Boost Rectifier and the GS-VSC functioning as a Current Controlled Voltage Source Inverter as defined in [11]. This section develops the power flow analysis method as it relates to AC system interaction and VSC controller configuration. The AC to DC power transfer equation for this purpose can be found in section 3.2.3. For more details on the AC to DC power conversion method, refer to chapter 3. The present development also depends heavily on the windfarm controller design outlined in chapter 7 and is intended to facilitate that design.

Figure 4.4 is a diagram for the purpose of DC power flow analysis and is based on section 17-2-3 of [12]. In figure 4.4, R_{DC} is the DC resistance of the transmission line conductor, WF-VSC is the rectifier and GS-VSC is the inverter. P_d and V_d represent regulated quantities and will be discussed in section 4.2.1. Since V_d is the regulated voltage at GS-VSC, the voltage at WF-VSC will be slightly higher due to DC current flowing through the line resistance:

$$V_{WF} = V_d + I_d R_{DC} \, . \tag{4.18}$$

Rearranging gives us an equation for DC current in terms of the converter voltages:

$$I_d = \frac{V_{WF} - V_d}{R_{DC}} \, . \tag{4.19}$$
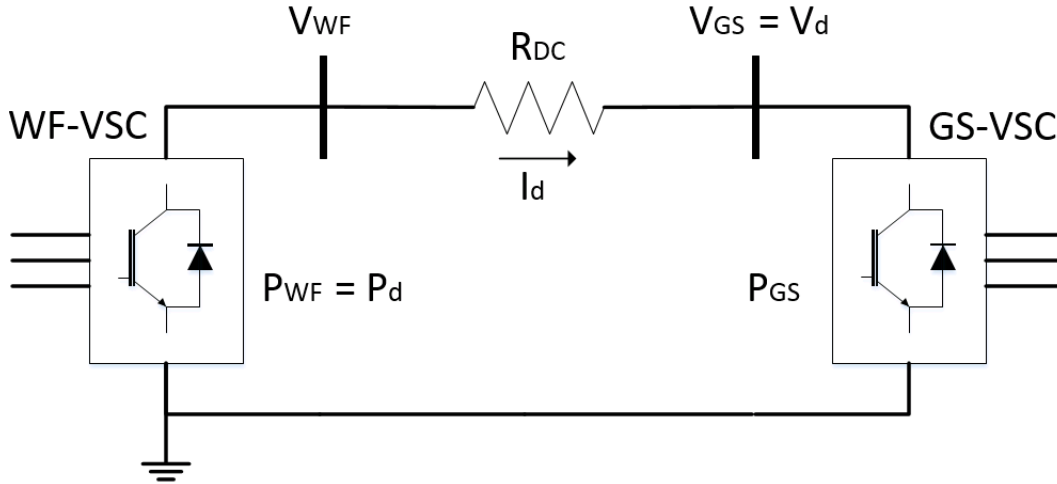
Figure 4.4: DC Power Flow

P_d is the regulated power at WF-VSC. Expressing this in terms of current and voltage gives:

$$P_d = V_{WF} I_d \, . \tag{4.20}$$

Combining (4.18) with (4.20) gives us a relationship for regulated power at WF-VSC in terms of DC current and regulated voltage at GS-VSC:

$$
\begin{aligned}
P_d &= (V_d + I_d R_{DC}) \, I_d \\
&= V_d I_d + I_d^2 R_{DC} \, .
\end{aligned} \tag{4.21}
$$

This can now be solved for I_d, giving us DC current in terms of regulated quantities:

$$
\begin{aligned}
0 &= I_d^2 R_{DC} + V_d I_d - P_d \\
&= I_d^2 + \left[\frac{V_d}{R_{DC}} \right] I_d - \left[\frac{P_d}{R_{DC}} \right] \\
I_d &= \sqrt{ \left(\frac{V_d}{2 R_{DC}} \right)^2 + \left(\frac{P_d}{R_{DC}} \right) } - \frac{V_d}{2 R_{DC}} \, .
\end{aligned} \tag{4.22}
$$

If we wish to know the power delivered to the AC grid at GS-VSC, (4.22) can be multiplied by V_d:

$$P_{GS} = V_d I_d$$

$$= V_d \left\{ \sqrt{\left(\frac{V_d}{2R_{DC}}\right)^2 + \left(\frac{P_d}{R_{DC}}\right)} - \frac{V_d}{2R_{DC}} \right\}. \qquad (4.23)$$

4.2.1   Control Mode of the Voltage Source Converters

Since the VSC has the advantage of being able to instantaneously change AC voltage magnitude and phase, power flow is regulated by controlling these quantities. One typical method for regulating power flow of a point-to-point VSC-HVDC link is with constant power control at the sending (rectifier) end and constant DC voltage control at the receiving (inverter) end of the link ([17], Chapter 10). This means the power flow is controlled by the outer loop of the sending end VSC control algorithm which in this project is the WF-VSC. Since we are coordinating power flow with the windfarm controller, which will be receiving information via the "communication-less" channel (see chapter 7) and injecting power based on the availability of the wind resource, this is the natural controller configuration option. The DC voltage magnitude of the HVDC line is then controlled by the outer loop of the receiving end VSC control algorithm which is the GS-VSC in this project.

According to chapter 10 of [17] and section 2.4 of [19] this operating mode has a $V_d - P_d$ characteristic as shown in figure 4.5.
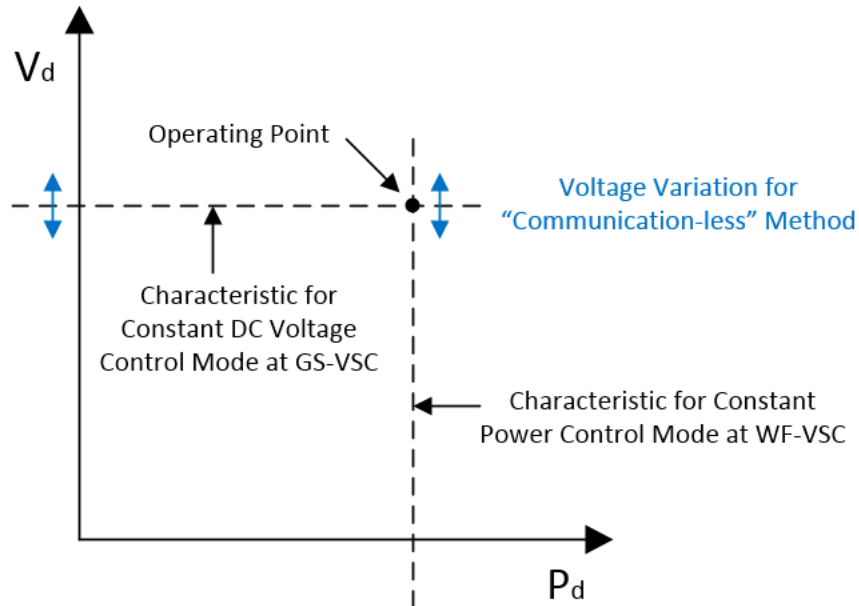
Figure 4.5: VSC-HVDC Link Operating Mode

In the figure, WF-VSC is able to maintain constant power regardless of the voltage magnitude at GS-VSC. Likewise, GS-VSC is able to maintain constant DC voltage regardless of the power flow at WF-VSC. The former is identified in blue and is an important characteristic for implementation of the "communication-less" channel in chapter 7 because power needs to flow to the onshore AC grid while information is sent to the offshore windfarm through the DC voltage magnitude. This is made possible because the design of the inner loop controller of the VSC in section 3.2.4 decouples current from voltage on the AC side of the converter. The operational mode is therefore limited only by DC side dependencies. Also, since this is a DC voltage link topology, the DC side circuit is of a voltage character and current can change instantaneously to accommodate the voltage variations. A simple $V_d - I_d$ relationship can be seen in figure 4.6 for varying V_d and a spectrum of P_d's. The figure is a plot of (4.22) with P_d at various values (400MW base), $R_{DC} = 0.0928$ p.u. (400km cable) and V_d ranging from 0.85 p.u. to 1.15 p.u. (500kV base). It is an example of the range of DC current required for the "communication-less" functionality of the operational mode, it is inversely proportional to voltage and is nearly linear.

In this example, the rated current is 0.921 p.u. and the efficiency of the transmission line is 92.1% (P_{GS} from (4.23) divided by P_d). The dashed lines indicate the nominal load operating point (1). In this project, a decrease in frequency is accompanied by an increase in DC voltage (figure 4.7) and an increase in power output. Therefore, an under-frequency event would cause the operating point in figure 4.6 to move from (1) to the right along the nominal $V_d - I_d$ characteristic to (2) which is a decrease in DC line current. After the "communication-less" signal reaches the WTG, power flow will then be increased which is an increase in RMS current from the windfarm. This also moves the entire characteristic in figure 4.6 up to operating point (3) which is an increase in DC line current. Regulation constants must therefore be chosen carefully so when load disturbances occur, the final RMS current will equal the DC line current at WF-VSC. This is discussed further in 4.2.4.

4.2.2   Power Flow Analysis for AC System Interaction

According to [19] section 2.3.1, VSC controller configuration for the purpose of power flow analysis can fall into two categories. Configuration for connection to an active AC grid and configuration for connection to a passive AC grid. An active AC grid is the traditional AC network with synchronous generation sources injecting power into the system and is typically inductive. This corresponds to the onshore AC network in this project. A passive AC grid has voltage magnitude and frequency defined by the VSC connection. This may be, for example, an island, an offshore platform, a distributed generation system or a VSC-HVDC connected wind farm. It is a network that relies on the VSC to convert the power so that it can be injected into the larger active AC grid. In this project, the VSC-HVDC connected offshore windfarm is a passive AC grid.

According to [17] the typical method for analysing power flow is with the inductive network equation (4.3) above where the Thevenin reactance X_T in (4.3) is the reactance of the VSC smoothing inductor and the Thevenin resistance R_T is negligible. In general, active power flow creates a voltage angle δ_{ind} across the inductor which decreases in the direction of the
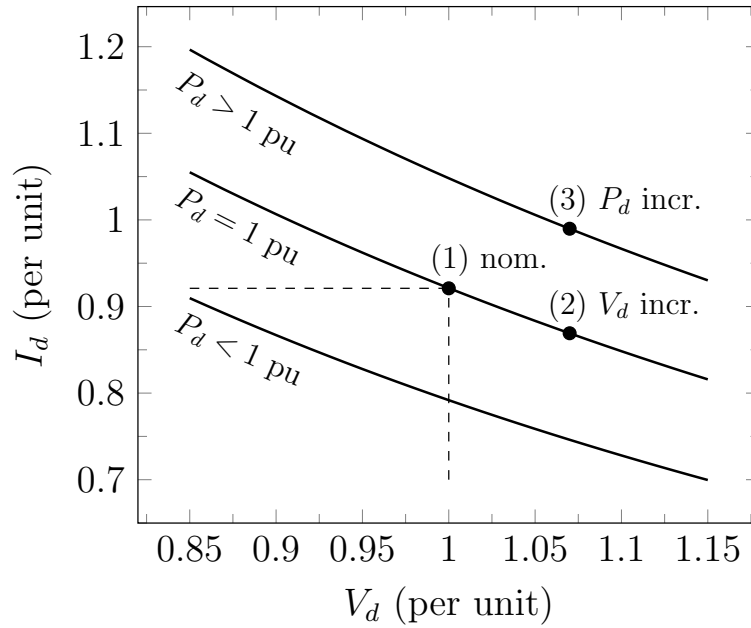
Figure 4.6: DC Current for VSC-HVDC Link Operating Mode

power flow. In this method, δ_{ind} is then the quantity that is regulated by the PWM to influence power flow. This type of scenario also closely associates voltage magnitude with reactive power. In general, reactive power flow creates a voltage magnitude difference Δv_{ind} across the inductor ($E_G - E_{LD}$ in (4.3)) which decreases in the direction of the reactive power flow. This variable Δv_{ind} is then the quantity that is regulated by the PWM to influence reactive power flow. This method assumes an active AC grid (as defined above) interacting with the sending end VSC. However, since this project has a windfarm (ie: passive AC grid) at the WF-VSC, another method must be developed.

For the purpose of power flow analysis and outer loop controller configuration at the WF-VSC, this project makes some assumptions about the windfarm AC collection network. The windfarm is rated 400MW, therefore it is assumed to operate at 33kV line to line. It is assumed to have 80 wind turbine generators rated 5MW each. Since the windfarm is represented by an aggregated wind turbine generator (WTG) in this project, the aggregated cable connecting the windfarm to the WF-VSC is assumed to be 80 36kV submarine cables connected in parallel and 5km in length. Assuming Nexans Medium Voltage 36kV XLPE submarine power cables with fiber-optic connections and 200A ampacity [20], we have an X/R ratio of roughly 0.25. Although there is also extra capacitance in the offshore network due to the AC submarine cabling, simulation has shown that this X/R ratio is adequate to base a WF-VSC power flow analysis and outer loop controller configuration on the resistive power flow equation in (4.4). The windfarm controller design in chapter 7 introduces a method for controlling active power flow over the AC submarine cable network according to (4.4) by controlling voltage magnitude.

4.2.3 Implementation of the VSC Controllers

The active power control method introduced in chapter 7 depends on a constant AC voltage magnitude from the WF-VSC. The d-axis outer loop controller of the WF-VSC is therefore assigned the task of maintaining constant AC voltage magnitude with a simple proportional-integral controller (see figure 3.9). This is a constant power mode of operation where active power is controlled by the windfarm controller at the WTG. The d-axis outer loop controller of GS-VSC can therefore function in constant DC voltage mode as the first leg of the cascaded droop "communication-less" channel (section 4.2.1) taking Δf of the active AC grid, translating to Δv_{DC} and combining with the DC voltage regulation of the HVDC link. Figure 4.7 is a diagram of the DC voltage regulator and the first leg of the "communication-less" channel. See figure 1.1 for a view of the complete onshore reference circuit.
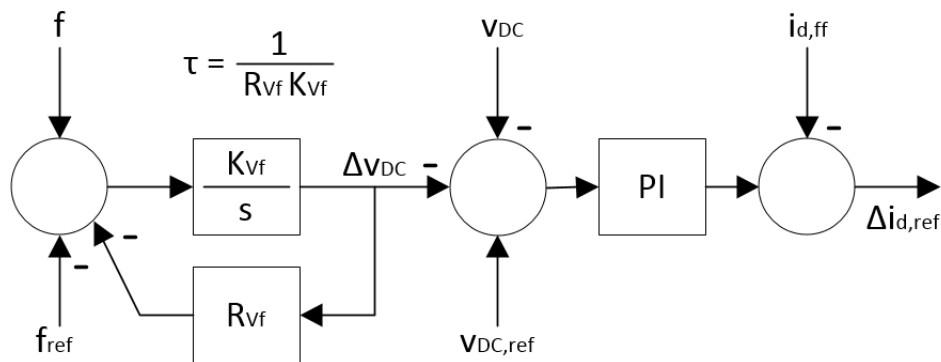
Figure 4.7: GS-VSC Outer Loop Controller

In figure 4.7, a feed-forward $(i_{d,ff})$ has been placed at the output of the PI controller. Figure 4.8 is a diagram of what this feed forward is accomplishing. According to [6, 14] it allows us to regulate small signal Δv_{DC} rather than v_{DC} $(V_{DC} + \Delta v_{DC})$ at the GS-VSC, greatly reducing the gain required from the PI controller and therefore enhancing the stability of the system. The nodal equation describing this scenario has been given as the DC side VSC system equation in (3.38). The feed forward then sets i_{DC} $(I_{DC} + \Delta i_{DC})$ equal to DC line current I_{LD}, removing steady state DC quantities from the voltage regulation.

Analytically, $i_{d,ff}$ from figure 4.7 can be found by combining the time invariant rotating reference frame quantities of the VSC power transfer equation (3.40) with the regulated quantities of the grid side power equation (4.23) and solving for DC current (note that subscript "$_d$" representing regulated quantities in (4.23) has been replaced by subscript "$_{DC}$"):

$$V_{DC}\,I_{DC} = \frac{3}{2}\,e_d\,i_d$$
$$I_{DC} = \frac{3}{2}\,\frac{e_d\,i_d}{V_{DC}}\,. \tag{4.24}$$
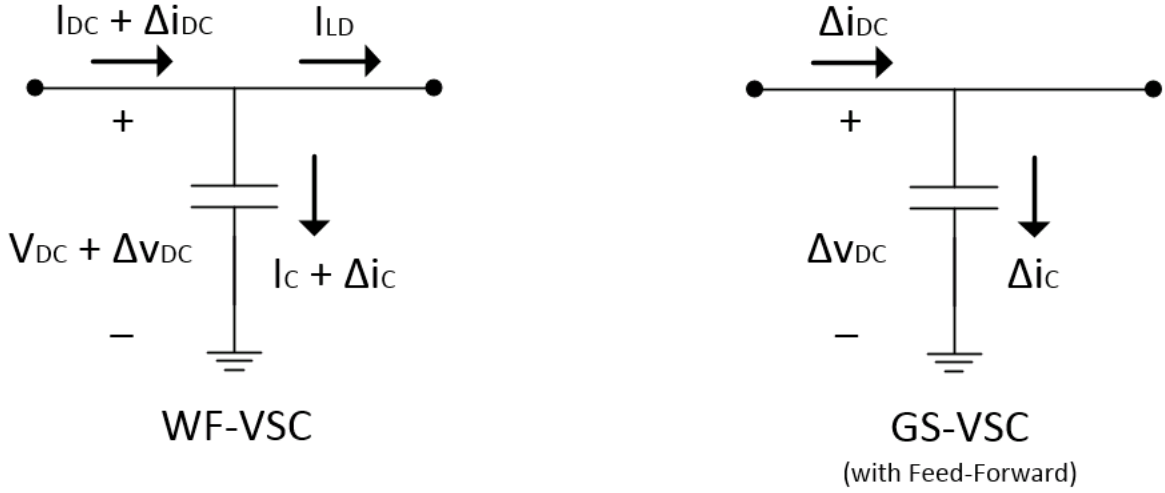
Figure 4.8: Nodal Analysis at VSC Converters

Putting (4.24) back into the DC side VSC system equation, setting the DC quantities equal to each other (ie: capacitor current is zero at steady state), and solving for i_d now gives us a time invariant rotating reference frame d-axis current reference which can serve as a feed-forward enhancing the stability of the system:

$$
\begin{aligned}
0 &= I_{DC} - I_{LD} \\
&= \frac{3}{2} \frac{e_d\, i_d}{V_{DC}} - I_{LD} \\
i_{d,ff} &= \frac{2}{3} \frac{V_{DC}\, I_{LD}}{e_d} \, .
\end{aligned}
\tag{4.25}
$$

This feed forward from figure 4.7 reduces the DC side VSC system equation (3.38) to a linearized small signal version of the original [6, 14]:

$$
\Delta v_{DC} = \frac{1}{sC} \left[\frac{3}{2} \frac{e_{d,0}}{V_{DC,0}} \right] \Delta i_d
\tag{4.26}
$$

where e_d and i_d come from VSC power transfer equation (3.40), V_{DC} is the regulated quantity V_d in the grid side power flow equation (4.23) and subscript "0" denotes an initial value.

The windfarm controller design in chapter 7 also introduces a method for coupling frequency of the passive AC grid to reactive power by using the voltage angle δ. This gives frequency full independence from voltage and active power, enabling it to function as a communication channel across the AC collection grid (and then as an input at WTG indicating how much power to inject). Since the windfarm controller associates frequency with reactive power, the q-axis outer loop controller of the WF-VSC can be used to regulate the frequency of the passive AC grid. It can also function as the second leg of the "communication-less" channel

taking Δv_{DC}, translating to Δf and combining with the frequency regulation. Figure 4.9 is a diagram of the second leg of the "communication-less" channel. The feed-forward block removes voltage difference due to current flow through the resistance of the transmission line and allows an estimate of the voltage magnitude at GS-VSC. In other words, we need to look at V_d from figure 4.4 to get the onshore frequency information from the first leg of the "communication-less" channel. Solving (4.18) for V_d gives us:

$$V_d = V_{WF} - I_d R_{DC} \tag{4.27}$$

which is the feed-forward in figure 4.9. Reactive power is regulated by the windfarm controller at the WTG. See figure 1.2 for a view of the complete offshore reference circuit.
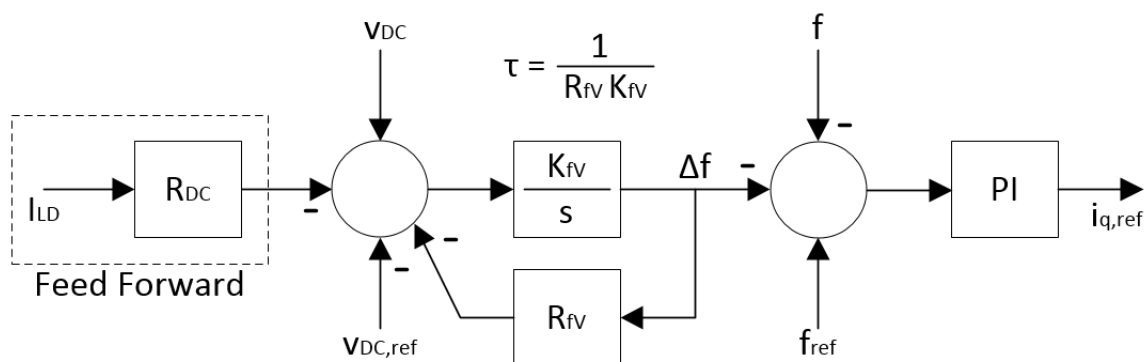
Figure 4.9: WF-VSC Outer Loop Controller

4.2.4 Selection of Regulation Constants for Communication-less Channel

The regulation constants in figures 4.7 & 4.9 must be chosen correctly. The HVDC link is being operated in a constant current operating mode. The feed-forward ($i_{d,ff}$) in figure 4.7 is ensuring steady state $I_{LD} = I_{DC}$ at the GS-VSC (figure 4.8, right) but there is nothing ensuring the same at WF-VSC (figure 4.8, left). Therefore, if $I_{LD} \neq I_{DC}$ at the WF-VSC, current will flow through the capacitor at steady state ($I_C = I_{DC} - I_{LD}$). This will cause voltage to change linearly across the WF-VSC capacitor ($V_{DC} = \frac{1}{C} \int I_C \, dt$) and it will be difficult for power flow to maintain steady state stability.

In this project, we wish the OWF to have a primary frequency response to load disturbances at the PCC with the onshore AC grid. In order to do this, the "communication-less" channel causes the operating point to move from (1) to (2) in figure 4.6. The distance between (1) and (2) and therefore the change in DC line current I_{LD} at WF-VSC is determined by R_{Vf} at GS-VSC. The power flow response from the WTG then causes the operating point to move from (2) to (3) in figure 4.6. The distance between (2) and (3) and therefore the change in converter current I_{DC} *and* DC line current I_{LD} at WF-VSC is determined by the total cascaded droop:

$$R_{WTG} = R_{Vf}\,R_{fV}\,R_{Pf} \tag{4.28}$$

where R_{Vf} is the onshore frequency to DC voltage transition at GS-VSC, R_{fV} is the DC voltage to offshore frequency transition at WF-VSC and R_{Pf} is the offshore frequency to power flow transition at WTG. If R_{Vf} is chosen correctly, converter current I_{DC} and DC line current I_{LD} at WF-VSC will find the same steady state after the load disturbance. The process of selecting R_{Vf} is done experimentally in section 8.4. R_{WTG} is also chosen in chapter 8 based on theoretical calculation. R_{fV} and R_{Pf} must then be chosen so that (4.28) remains true.

In general, R_{fV} needs to be chosen so that offshore frequency deviations are larger than onshore frequency deviations. This is because the offshore grid is a weak frequency network and the onshore grid is a strong frequency network. Therefore the deviations must be larger in order to be meaningful. Simulation has shown that $R_{fV} = 1$ is a reasonable choice. It puts offshore frequency deviations on the same scale as DC voltage deviations.

The K integration constants in figures 4.7 & 4.9 can be chosen according to the circuit time constants governing the speed of transition. In this project, they are selected so that the droop time constants are larger than the capacitor time constant at GS-VSC:

$$
\begin{aligned}
\tau &= C\,R_{DC,base} \\
&= C\,\frac{(500\ \text{kV})^2}{400\ \text{MW}} \\
&= 70\,\mu F \times 625\,\Omega \\
&= 43.75\ \text{ms}\,.
\end{aligned}
\tag{4.29}
$$

It is possible that a correctly tuned R_{Vf} is not enough to ensure stable steady state power flow for multiple load disturbance scenarios. The design may need to be tuned for the most commonly expected scenario. It may then be possible to enhance the stability of the control system by performing sample and hold operations after the new steady state has been reached. These can be installed at the point labelled Δv_{DC} in figure 4.7 and at the point labelled Δf in figure 4.9 and will have the effect of permanently changing $v_{DC,ref}$ and f_{ref} respectively. Although this will not solve the $I_{LD} \neq I_{DC}$ problem at WF-VSC, it may stabilize the system long enough for secondary controls to intervene by renormalizing the system. Further investigation is needed.

Chapter 5

Machine Stability

Since this project utilizes the dynamics associated with load frequency control (see chapter 6) the Large Synchronous Generator(LSG) and the Small Synchronous Generator(SSG) must be designed to supply the load while maintaining rotor dynamic stability during frequency excursions. The SSG must also be able to synchronize to the LSG during the starting sequence (see section 7.1.3).

This chapter therefore develops a small signal plant matrix for the synchronous machine under the assumption of manual excitation. A block diagram representation of the synchronous generator system is presented for the purpose of understanding small signal disturbance withstand capability. A MATLAB program has also been written according to the development in this chapter. The program analyzes small signal stability for the synchronous generator design used in this project. See Appendix A for the code listing from this program.

This project focuses on small signal stability and assumes a stable system with regards to transient stability. The following sections are a development of the small signal stability transfer function of a synchronous generator. This development assumes a strong voltage and a strong frequency power system (see 4.1.3 & 6.1.2).

According to [15] equ. 2.2, AC system dynamic stability associated with a synchronous machine can be summarized into two components:

$$\Delta T_e = \frac{\partial T_e}{\partial \delta}\, \Delta \delta + \frac{\partial T_e}{\partial \omega}\, \Delta \omega$$
$$= K_S\, \Delta \delta + K_D\, \Delta \omega \qquad (5.1)$$

where $K_S \Delta \delta$ is the torque in phase with rotor angle perturbations and is referred to as synchronizing torque. Lack of sufficient synchronizing torque results in rotor angle drift and is non-oscillatory. This will appear in an eigenvalue analysis as a positive real number. $K_D \Delta \omega$ is the torque in phase with speed deviations and is referred to as damping torque. Lack of sufficient damping torque will result in oscillatory instability. This will appear in an eigenvalue analysis as a complex conjugate pair with a positive real component. According

to pg. 23 of [15] stability problems in a system with manually excited machines will be due to lack of synchronizing torque.

5.1 Network Equations

Network equations will now be used in the development of the synchronous machine small signal plant matrix. This is so other impedances such as transformer windings between the machine and the transmission bus are included in the stability analysis. This also allows us to include the state variable δ in our calculation. We can adapt (4.3) for this purpose:

$$P_e = \frac{E_e E_B}{X_T} \sin \delta \tag{5.2}$$

where subscript "$_e$" refers to the machine air gap, subscript "$_B$" refers to the transmission bus and subscript "$_T$" refers to the thevenin impedance between the machine air gap and the transmission bus. See also Figure 5.1 (note that E_t refers to the machine terminal voltage).
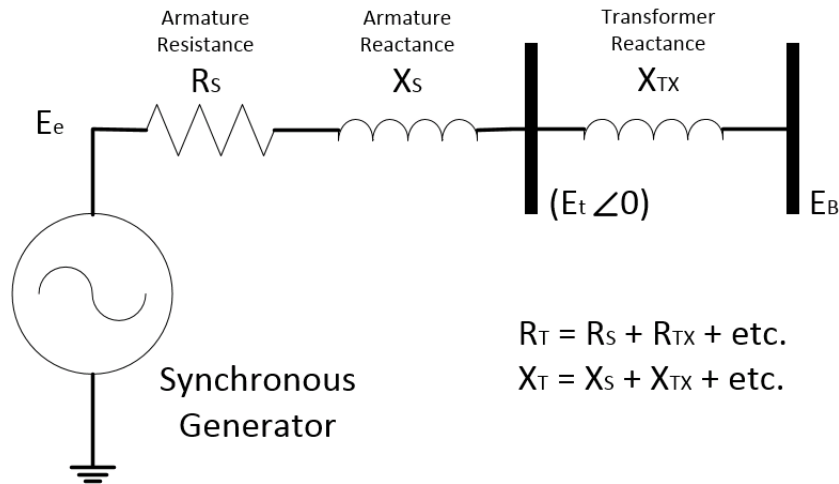
Figure 5.1: Circuit Diagram for Synchronizing Torque Calculation

With regards to network analysis, R_S can be considered negligible making air gap power P_e roughly equivalent to terminal power (section 12.3 of [15]). Also, in the per unit system, electrical torque T_e is considered interchangeable with P_e (section 11.1 of [15]). Therefore we can say:

$$T_e = \frac{E_e E_B}{X_T} \sin \delta \tag{5.3}$$

where δ is the total angle between the machine air gap and the transmission bus (ie: machine load angle plus network voltage angle) as defined in Figure 5.2. Note that Figure 5.2 is an overexcited (leading power factor) generator according to (fig. 6.17a of [21]).
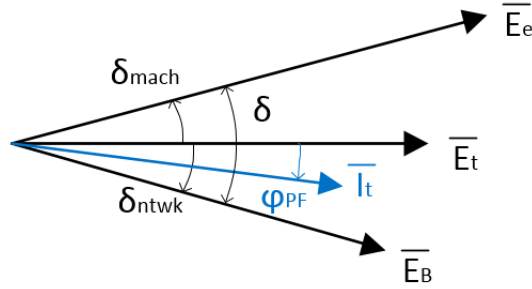
Figure 5.2: Vector Diagram for Synchronizing Torque Calculation

Assuming constant voltage and linearizing about a final steady state load angle δ_f we have our synchronizing torque (equ. 12.72, 12.76 of [15]):

$$
\begin{aligned}
\Delta T_e\bigg|_{\Delta\delta} &= \frac{\partial T_e}{\partial \delta}\Delta\delta \\
&= \left[\frac{E_e E_B}{X_T}\cos\delta_f\right]\Delta\delta
\end{aligned}
\tag{5.4}
$$

and our synchronizing torque coefficient is defined as:

$$
K_S = \frac{E_e E_B}{X_T}\cos\delta_f \; .
\tag{5.5}
$$

5.2 Equations of Motion

The swing equation for generators is:

$$
J\frac{\mathrm{d}\omega}{\mathrm{d}t} = T_m - T_e
\tag{5.6}
$$

where J is the moment of inertia of the rotor, T_m is the mechanical torque, T_e is the electrical torque and ω is the speed of the rotor. If we express this in per unit and introduce a new variable $H = \frac{1}{2}J\omega^2$ where $\omega = 1$ p.u. we can say:

$$
2H\frac{\mathrm{d}\omega}{\mathrm{d}t} = T_m - T_e
\tag{5.7}
$$

where H is referred to as the inertia constant (see also 6.1.2 & 7.1.1). Then introducing another variable $M = 2H$, solving for ω and expressing as small signal in the Laplace domain according to (equ. 3.209, 12.75 of [15]) we have:

$$\Delta\omega = \frac{1}{Ms}\left[\Delta T_m - \Delta T_e\right]$$
$$= \frac{1}{Ms}\left[\Delta T_m - K_S\Delta\delta - K_D\Delta\omega\right] \tag{5.8}$$

where M is the start time of the machine, ΔT_e is as defined in 5.1 and K_S is as defined in 5.5. The variable K_D can be associated with natural damping characteristics of the machine such as amortisseur windings which are neglected in the present derivation. It can also be associated with the natural damping effect of the load flow in the network. In this case, chapter 11 of [15] gives it the variable name "D" and suggests it is typically on the order of 1 to 2 p.u with load as base. Damping torque will also appear in section 5.3 as a function of the machine field circuit. $\Delta\delta$ is now just a matter of integrating (5.8):

$$\Delta\delta = \frac{\omega_{base}}{s}\Delta\omega \tag{5.9}$$

and can be found in (equ. 3.210, 12.77 of [15]). The ω_{base} multiplier is necessary for integration in the per unit system (see also [15] equ. 3.88). A block diagram of (5.8) and (5.9) is given in Figure 5.3. The functions represented in (5.8) and (5.9) are two of the three equations required to represent a synchronous machine with manual excitation. In state space matrix form ($\Delta\dot{x} = A\Delta x + b\Delta u$) these are:

$$\begin{bmatrix}\Delta\dot{\omega} \\ \Delta\dot{\delta}\end{bmatrix} = \begin{bmatrix}-\frac{K_D}{M} & -\frac{K_S}{M} \\ \omega_{base} & 0\end{bmatrix}\begin{bmatrix}\Delta\omega \\ \Delta\delta\end{bmatrix} + \begin{bmatrix}\frac{1}{M} \\ 0\end{bmatrix}\Delta T_m \tag{5.10}$$

where K_S is given in (5.5) and K_D is as described above. Section 5.3 will develop the third equation required for manual excitation analysis.

5.3   Field Circuit Equations

Dynamics of the synchronous machine field circuit must now be included. The goal of this section is to expand (5.10) to include the state variable $\Delta\psi_{fd}$ and the input variable ΔE_{fd} according to [15] section 12.3.2. First, section 3.6 of [15] points out that it is common practice to align the q-axis of the rotating reference frame with the machine q-axis quantities. This simplifies rotor circuit analysis and provides a means to keep track of rotor position. Figure 5.4 is an adaptation of Figure 5.2 for this purpose. In the figure, $\overline{E_e}$ has been replaced with $\overline{E_q}$ representing the air gap voltage aligned with the q-axis.

A few more assumptions are also necessary to further simplify this analysis. As stated earlier, the effects of amortisseur windings will be neglected for the present study. Manual excitation will also be assumed which means field voltage is considered constant (ie: $\Delta E_{fd} = 0$). According to [15] Section 5.1.2 $\frac{d\psi}{dt}$ on the stator can be neglected when studying rotor dynamics because the dynamic time constants associated with the rotor are much longer than
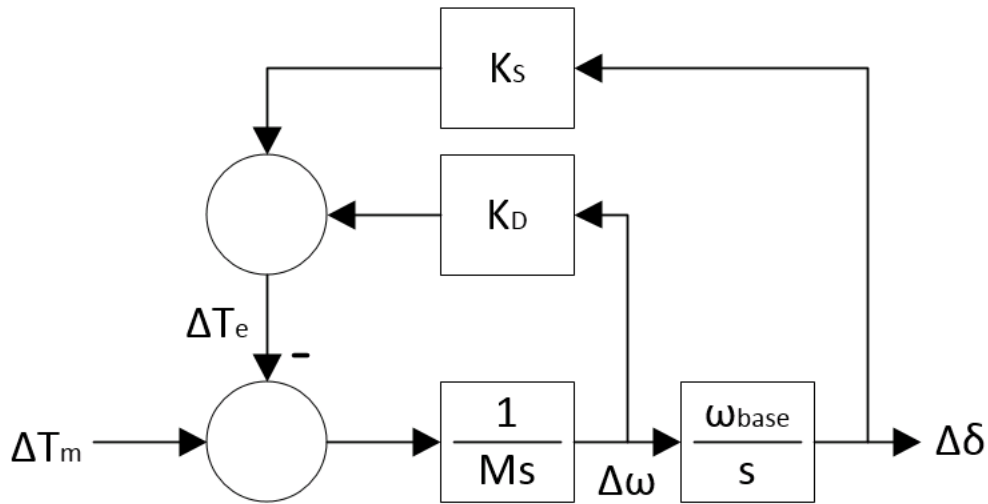
Figure 5.3: Small Signal Transfer Function of Synchronous Generator Mechanical System

the transient time constants associated with the stator. Rotor speed can also be considered constant ($\omega_r = 1$ p.u.) when used in stator equations to counter the effect of neglecting $\frac{\mathrm{d}\psi}{\mathrm{d}t}$ in the stator equations.
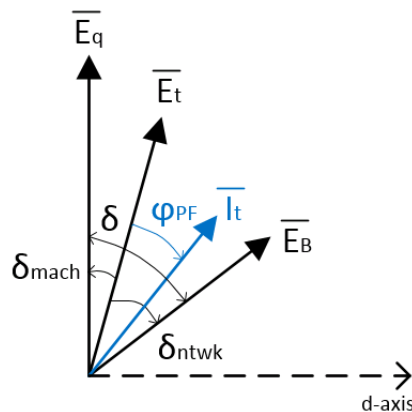
Figure 5.4: Vector Diagram for Field Circuit Calculation (dq-Reference Frame)

This section is structured as follows. In 5.3.1 a small signal equation for air gap torque which includes field circuit dynamics is found. Then in 5.3.2 the field circuit dynamics equation is found. In 5.3.3 the equations are combined with the equation of motion for a new system representation under the assumption of manual excitation.

5.3.1   Derive Small Signal Air Gap Torque

The following is a derivation of e_d and e_q (associated with machine terminal voltage $\overline{E_t}$) in terms of network equations and then in terms of internal machine flux linkage equations. These are then combined in order to find i_d and i_q in terms of state variables δ and ψ_{fd}. After that, i_d, i_q, ψ_{ad} and ψ_{aq} are linearized and a new equation for small signal air gap torque ΔT_e is found which includes the effects of field circuit dynamics (again assuming manual excitation).

The network equations according to Figure 5.4 are:

$$
\begin{aligned}
\overline{E_t} &= \overline{E_B} + (R_{ntwk} + jX_{ntwk})\overline{I_t} \\
(e_d + je_q) &= (E_{Bd} + jE_{Bq}) + (R_{ntwk} + jX_{ntwk})(i_d + ji_q) \\
&= (E_B \sin\delta + R_{ntwk}\,i_d - X_{ntwk}\,i_q) + j(E_B \cos\delta + R_{ntwk}\,i_q + X_{ntwk}\,i_d) \ .
\end{aligned}
\tag{5.11}
$$

Separating into d-axis and q-axis we have:

$$
\begin{aligned}
e_d &= E_B \sin\delta + R_{ntwk}\,i_d - X_{ntwk}\,i_q \\
e_q &= E_B \cos\delta + R_{ntwk}\,i_q + X_{ntwk}\,i_d \ .
\end{aligned}
\tag{5.12}
$$

According to [22] equ. 2.59, the machine armature voltage equation (adapted for generators) as a function of internal flux linkage is:

$$
\overline{E_t} = \frac{\mathrm{d}\overline{\psi}}{\mathrm{d}t} - R_S\overline{I_t}
\tag{5.13}
$$

or split up into the d- and q- axes (equ. 5.15 of [22]):

$$
\begin{aligned}
e_d &= {}^-R_S i_d - \omega_r \psi_q + \frac{\mathrm{d}\psi_d}{\mathrm{d}t} \\
e_q &= {}^-R_S i_q + \omega_r \psi_d + \frac{\mathrm{d}\psi_q}{\mathrm{d}t}
\end{aligned}
\tag{5.14}
$$

where ψ_d and ψ_q are the stator flux linkage. However, as noted earlier, we will be neglecting $\frac{\mathrm{d}\psi}{\mathrm{d}t}$ in stator equations and setting $\omega_r = 1$ p.u. in stator equations to compensate:

$$
\begin{aligned}
e_d &= {}^-R_S i_d - \psi_q \\
e_q &= {}^-R_S i_q + \psi_d \ .
\end{aligned}
\tag{5.15}
$$

We know from [22] equ. 5.15 that stator flux linkage is equal to air gap mutual flux linkage minus armature leakage (again adapted for generators):

$$\psi_d = \psi_{ad} - L_S\, i_d$$
$$\psi_q = \psi_{aq} - L_S\, i_q \tag{5.16}$$

where ψ_{ad}, ψ_{aq} are the air gap mutual flux linkage and L_S is the armature leakage inductance. By definition, air gap mutual flux linkage is a shared mutual inductance between stator and rotor, therefore (with rotor field circuit on the d-axis only) we have:

$$\psi_{ad} = L_{ad}(i_{fd} - i_d)$$
$$\psi_{aq} = L_{aq}(^-i_q) \, . \tag{5.17}$$

where i_d, i_q are opposite direction because this is a generator. We now have just one more variable to get rid of. The field current i_{fd} can be expressed in terms of field circuit d-axis flux linkage ψ_{fd} which is one of our state variables and is by definition associated with it's own self inductance as well as the d-axis mutual inductance associated with the armature (see also [22] equ. 5.30 and [15] equ. 12.88):

$$\begin{aligned}
\psi_{fd} &= (L_{ad} + L_{fdl})i_{fd} - L_{ad}\, i_d \\
&= L_{ad}(i_{fd} - i_d) + L_{fdl}\, i_{fd} \\
&= \psi_{ad} + L_{fdl}\, i_{fd}
\end{aligned} \tag{5.18}$$

where L_{fdl} is the field circuit leakage inductance. We can now solve (5.17, d-axis) and (5.18) for i_{fd} and set them equal giving us an equation for ψ_{ad} independent of field current:

$$\begin{aligned}
i_d + \frac{\psi_{ad}}{L_{ad}} &= \frac{\psi_{fd} - \psi_{ad}}{L_{fdl}} \\
L_{fdl}\, i_d + \frac{L_{fdl}}{L_{ad}}\psi_{ad} &= \psi_{fd} - \psi_{ad} \\
\psi_{ad}\left[1 + \frac{L_{fdl}}{L_{ad}}\right] &= \psi_{fd} - L_{fdl}\, i_d \\
\psi_{ad}\left[\frac{1}{L_{fdl}} + \frac{1}{L_{ad}}\right] &= \frac{\psi_{fd}}{L_{fdl}} - i_d \\
\psi_{ad} &= L'_{ad}\left[\frac{\psi_{fd}}{L_{fdl}} - i_d\right]
\end{aligned} \tag{5.19}$$

where:

$$L'_{ad} = L_{ad} \,||\, L_{fdl} \, . \tag{5.20}$$

If we now put (5.17, q-axis) and (5.19) into (5.16) for stator flux linkage in terms of armature current and field flux linkage:

$$\psi_d = \frac{L'_{ad}}{L_{fdl}} \psi_{fd} - (L'_{ad} + L_S) i_d \tag{5.21}$$

$$\psi_q = {}^-(L_{aq} + L_S) i_q \, ,$$

then (5.21) can be put into (5.15) for machine terminal voltage in terms of armature current and field flux linkage:

$$e_d = {}^-R_S i_d + (L_{aq} + L_S) i_q$$

$$e_q = {}^-R_S i_q + \frac{L'_{ad}}{L_{fdl}} \psi_{fd} - (L'_{ad} + L_S) i_d \, . \tag{5.22}$$

We now have two sets of machine terminal voltage equations. The equations associated with the network are given in (5.12). The equations associated with machine flux linkage are given in (5.22). Combining these allows us to find current in terms of state variables. First we combine the e_d equations (remember $\omega_r = 1$ p.u. in the stator equations and is not shown) and solve for i_q:

$$E_B \sin \delta + R_{ntwk} \, i_d - X_{ntwk} \, i_q = {}^-R_S i_d + (L_{aq} + L_S) i_q$$

$$i_q (L_{aq} + L_S + X_{ntwk}) = E_B \sin \delta + i_d (R_S + R_{ntwk})$$

$$i_q = \frac{E_B \sin \delta + i_d (R_S + R_{ntwk})}{L_{aq} + L_S + X_{ntwk}} \, . \tag{5.23}$$

Then we combine the e_q equations and solve for i_d:

$$E_B \cos \delta + R_{ntwk} \, i_q + X_{ntwk} \, i_d = {}^-R_S i_q + \frac{L'_{ad}}{L_{fdl}} \psi_{fd} - (L'_{ad} + L_S) i_d$$

$$E_B \cos \delta + i_d (L'_{ad} + L_S + X_{ntwk}) = \frac{L'_{ad}}{L_{fdl}} \psi_{fd} - i_q (R_S + R_{ntwk}) \tag{5.24}$$

$$i_d = \frac{\frac{L'_{ad}}{L_{fdl}} \psi_{fd} - i_q (R_S + R_{ntwk}) - E_B \cos \delta}{L'_{ad} + L_S + X_{ntwk}} \, .$$

Putting (5.23) into (5.24) removes i_q. If we define a few supplementary variables, the equation will be simpler to work with (again, $\omega_r = 1$ p.u. for stator reactances and is not shown):

$$R_T = R_S + R_{ntwk}$$

$$X_{Td} = L'_{ad} + L_S + X_{ntwk}$$

$$X_{Tq} = L_{aq} + L_S + X_{ntwk} \tag{5.25}$$

$$D = R_T^2 + X_{Td} X_{Tq} \, .$$

Now we solve for i_d:

$$E_B \cos \delta + i_d \, X_{Td} = \frac{L'_{ad}}{L_{fdl}} \, \psi_{fd} - \frac{E_B \sin \delta + i_d \, R_T}{X_{Tq}} \, R_T$$

$$E_B \cos \delta + i_d \, X_{Td} = \frac{L'_{ad}}{L_{fdl}} \, \psi_{fd} - \frac{E_B R_T}{X_{Tq}} \, \sin \delta - i_d \, \frac{R_T^2}{X_{Tq}}$$

$$i_d \left[X_{Td} + \frac{R_T^2}{X_{Tq}} \right] = \frac{L'_{ad}}{L_{fdl}} \, \psi_{fd} - E_B \cos \delta - \frac{E_B R_T}{X_{Tq}} \, \sin \delta \qquad (5.26)$$

$$i_d \, D = X_{Tq} \frac{L'_{ad}}{L_{fdl}} \, \psi_{fd} - E_B (X_{Tq} \cos \delta + R_T \, \sin \delta)$$

$$i_d = \frac{1}{D} \left[X_{Tq} \frac{L'_{ad}}{L_{fdl}} \, \psi_{fd} - E_B (X_{Tq} \cos \delta + R_T \, \sin \delta) \right]$$

where L'_{ad} is defined in (5.20) and R_T, X_{Td}, X_{Tq} and D are defined in (5.25). Just like with (5.26), q-axis current can be found by putting (5.24) into (5.23) to eliminate i_d:

$$i_q \, X_{Tq} = E_B \sin \delta + \frac{R_T}{X_{Td}} \left[\frac{L'_{ad}}{L_{fdl}} \, \psi_{fd} - i_q \, R_T - E_B \cos \delta \right]$$

$$i_q \, X_{Tq} = E_B \sin \delta + \frac{R_T}{X_{Td}} \frac{L'_{ad}}{L_{fdl}} \, \psi_{fd} - i_q \, \frac{R_T^2}{X_{Td}} - \frac{E_B R_T}{X_{Td}} \, \cos \delta$$

$$i_q \left[X_{Tq} + \frac{R_T^2}{X_{Td}} \right] = \frac{R_T}{X_{Td}} \frac{L'_{ad}}{L_{fdl}} \, \psi_{fd} - \frac{E_B R_T}{X_{Td}} \, \cos \delta + E_B \sin \delta \qquad (5.27)$$

$$i_q \, D = R_T \frac{L'_{ad}}{L_{fdl}} \, \psi_{fd} - E_B (R_T \, \cos \delta - X_{Td} \sin \delta)$$

$$i_q = \frac{1}{D} \left[R_T \frac{L'_{ad}}{L_{fdl}} \, \psi_{fd} - E_B (R_T \, \cos \delta - X_{Td} \sin \delta) \right] .$$

Again, L'_{ad} is defined in (5.20) and R_T, X_{Td}, X_{Tq} and D are defined in (5.25). Machine terminal current in (5.26) and (5.27) is now a function of state variables ψ_{fd} and δ. This can be linearized for small signal analysis:

$$\Delta i_d = \frac{\partial i_d}{\partial \delta} \, \Delta \delta + \frac{\partial i_d}{\partial \psi_{fd}} \, \Delta \psi_{fd}$$

$$= m_1 \, \Delta \delta + m_2 \, \Delta \psi_{fd}$$

$$\Delta i_q = \frac{\partial i_q}{\partial \delta} \, \Delta \delta + \frac{\partial i_q}{\partial \psi_{fd}} \, \Delta \psi_{fd} \qquad (5.28)$$

$$= n_1 \, \Delta \delta + n_2 \, \Delta \psi_{fd}$$

where:

$$
\begin{aligned}
m1 &= \frac{E_{Bf}}{D}\left[X_{Tq}\sin\delta_f - R_T\cos\delta_f\right] \\
m2 &= \frac{X_{Tq}}{D}\frac{L'_{ad}}{L_{fdl}} \\
n1 &= \frac{E_{Bf}}{D}\left[R_T\sin\delta_f + X_{Td}\cos\delta_f\right] \\
n2 &= \frac{R_T}{D}\frac{L'_{ad}}{L_{fdl}}
\end{aligned}
\tag{5.29}
$$

and subscript "f" denotes the final steady state value. Air gap mutual flux linkage ψ_{ad} and ψ_{aq} from (5.19) and (5.17) can now be linearized:

$$
\begin{aligned}
\Delta\psi_{ad} &= \frac{\partial\psi_{ad}}{\partial\psi_{fd}}\Delta\psi_{fd} + \frac{\partial\psi_{ad}}{\partial i_d}\Delta i_d \\
&= \frac{L'_{ad}}{L_{fdl}}\Delta\psi_{fd} - L'_{ad}\Delta i_d \\
\Delta\psi_{aq} &= \frac{\partial\psi_{aq}}{\partial i_q}\Delta i_q \\
&= {}^{-}L_{aq}\Delta i_q
\end{aligned}
\tag{5.30}
$$

and combined with (5.28) for a function in terms of state variables:

$$
\begin{aligned}
\Delta\psi_{ad} &= \frac{L'_{ad}}{L_{fdl}}\Delta\psi_{fd} - L'_{ad}\left[m_1\,\Delta\delta + m_2\,\Delta\psi_{fd}\right] \\
&= \frac{L'_{ad}}{L_{fdl}}\Delta\psi_{fd} - L'_{ad}\,m_1\,\Delta\delta - L'_{ad}\,m_2\,\Delta\psi_{fd} \\
&= {}^{-}L'_{ad}\,m_1\,\Delta\delta + L'_{ad}\left(\frac{1}{L_{fdl}} - m_2\right)\Delta\psi_{fd} \\
\Delta\psi_{aq} &= {}^{-}L_{aq}\left[n_1\,\Delta\delta + n_2\,\Delta\psi_{fd}\right] \\
&= {}^{-}L_{aq}\,n_1\,\Delta\delta - L_{aq}\,n_2\,\Delta\psi_{fd}
\end{aligned}
\tag{5.31}
$$

where L'_{ad} is defined in (5.20) and m_1, m_2, n_1 and n_2 are defined in (5.29). We now have all the pieces necessary to calculate small signal air gap torque. In (5.3) we have already equated terminal power P_t with air gap power P_e and air gap electrical torque T_e which can now be expressed as a function of air gap mutual flux linkage and armature current ([22] equ. 5.20, [15] equ. 12.93):

$$
T_e = \psi_{ad}\,i_q - \psi_{aq}\,i_d \,.
\tag{5.32}
$$

The linearized version is ([15] equ. 12.112):

$$\Delta T_e = \frac{\partial T_e}{\partial \psi_{ad}} \Delta \psi_{ad} + \frac{\partial T_e}{\partial i_q} \Delta i_q + \frac{\partial T_e}{\partial \psi_{aq}} \Delta \psi_{aq} + \frac{\partial T_e}{\partial i_d} \Delta i_d$$

$$= i_{qf} \Delta \psi_{ad} + \psi_{adf} \Delta i_q - i_{df} \Delta \psi_{aq} - \psi_{aqf} \Delta i_d$$

$$= i_{qf} \left[^- L'_{ad} m_1 \Delta \delta + L'_{ad} \left(\frac{1}{L_{fdl}} - m_2 \right) \Delta \psi_{fd} \right]$$

$$+ \psi_{adf} \left[n_1 \Delta \delta + n_2 \Delta \psi_{fd} \right] - i_{df} \left[^- L_{aq} n_1 \Delta \delta - L_{aq} n_2 \Delta \psi_{fd} \right] - \psi_{aqf} \left[m_1 \Delta \delta + m_2 \Delta \psi_{fd} \right]$$

$$= K_1 \Delta \delta + K_2 \Delta \psi_{fd} \tag{5.33}$$

where:

$$K_1 = {}^- i_{qf} L'_{ad} m_1 + \psi_{adf} n_1 + i_{df} L_{aq} n_1 - \psi_{aqf} m_1$$

$$K_2 = i_{qf} L'_{ad} \left(\frac{1}{L_{fdl}} - m_2 \right) + \psi_{adf} n_2 + i_{df} L_{aq} n_2 - \psi_{aqf} m_2 \;. \tag{5.34}$$

As before, subscript "$_f$" denotes the final steady state value, L'_{ad} is defined in (5.20) and m_1, m_2, n_1 and n_2 are defined in (5.29). The $K_D \Delta \omega$ component has been neglected for the present analysis and will be recombined into the complete equation in 5.3.3.

5.3.2 Derive Field Circuit Dynamics Equation

Similar to (5.13), the machine field voltage equation is ([22] equ. 5.22, [15] equ. 3.89):

$$e_{fd} = \frac{\mathrm{d}\psi_{fd}}{\mathrm{d}t} + R_{fd} i_{fd}$$

$$\frac{\mathrm{d}\psi_{fd}}{\mathrm{d}t} = e_{fd} - R_{fd} i_{fd} \;. \tag{5.35}$$

Expressing in per unit and converting e_{fd} to the stator base according to [15] equ. 12.85 we have:

$$\frac{\mathrm{d}\psi_{fd}}{\mathrm{d}t} = \omega_{base} \left[\frac{R_{fd}}{L_{adu}} E_{fd} - R_{fd} i_{fd} \right] \;. \tag{5.36}$$

where subscript "$_u$" denotes unsaturated (remember again that $\omega_r = 1$ p.u. in stator equations and is not shown). Solving (5.18) for i_{fd} and combining with (5.36) then gives:

$$\frac{\mathrm{d}\psi_{fd}}{\mathrm{d}t} = \omega_{base} \left[\frac{R_{fd}}{L_{adu}} E_{fd} - R_{fd} \frac{\psi_{fd} - \psi_{ad}}{L_{fdl}} \right]$$

$$= \omega_{base} \frac{R_{fd}}{L_{fdl}} \left[\psi_{ad} - \psi_{fd} \right] + \omega_{base} \frac{R_{fd}}{L_{adu}} E_{fd} \;. \tag{5.37}$$

This can now be linearized by taking $\Delta\psi_{ad}$ from (5.31). Expressing in terms of state variables and input variables gives:

$$
\begin{aligned}
\frac{\mathrm{d}}{\mathrm{d}t}\Delta\psi_{fd} &= \omega_{base}\frac{R_{fd}}{L_{fdl}}\left[\Delta\psi_{ad} - \Delta\psi_{fd}\right] + \omega_{base}\frac{R_{fd}}{L_{adu}}\Delta E_{fd} \\
&= \omega_{base}\frac{R_{fd}}{L_{fdl}}\left[-L'_{ad}\,m_1\,\Delta\delta + L'_{ad}\left(\frac{1}{L_{fdl}} - m_2\right)\Delta\psi_{fd} - \Delta\psi_{fd}\right] + \omega_{base}\frac{R_{fd}}{L_{adu}}\Delta E_{fd} \\
&= {}^-\omega_{base}\frac{R_{fd}}{L_{fdl}}\left[L'_{ad}\,m_1\,\Delta\delta + \left(1 - \frac{L'_{ad}}{L_{fdl}} + L'_{ad}\,m_2\right)\Delta\psi_{fd}\right] + \omega_{base}\frac{R_{fd}}{L_{adu}}\Delta E_{fd}\ .
\end{aligned}
$$

$$(5.38)$$

5.3.3 Manually Excited Synchronous Machine System in State Space Matrix Form

The equations represented in (5.8), (5.9), (5.33) and (5.38) can now be assembled into one state space system representation with three state variables and two input variables. First, (5.33) and damping torque is put into (5.8) for a new equation of motion which includes field circuit dynamics:

$$
\begin{aligned}
\Delta\omega &= \frac{1}{Ms}\left[\Delta T_m - \Delta T_e\right] \\
&= \frac{1}{Ms}\left[\Delta T_m - K_1\Delta\delta - K_D\Delta\omega - K_2\Delta\psi_{fd}\right]\ .
\end{aligned}
$$

$$(5.39)$$

Now (5.9), (5.38) and (5.39) are the three equations that can be combined for a system representation in state space matrix form ([15] equ. 12.115):

$$
\begin{bmatrix} \Delta\dot{\omega} \\ \Delta\dot{\delta} \\ \Delta\dot{\psi}_{fd} \end{bmatrix} = \begin{bmatrix} a_{11} & a_{12} & a_{13} \\ a_{21} & 0 & 0 \\ 0 & a_{32} & a_{33} \end{bmatrix} \begin{bmatrix} \Delta\omega \\ \Delta\delta \\ \Delta\psi_{fd} \end{bmatrix} + \begin{bmatrix} b_{11} & 0 \\ 0 & 0 \\ 0 & b_{32} \end{bmatrix} \begin{bmatrix} \Delta T_m \\ \Delta E_{fd} \end{bmatrix}
$$

$$(5.40)$$

where:

$$a_{11} = -\frac{K_D}{M}$$

$$a_{12} = -\frac{K_1}{M}$$

$$a_{13} = -\frac{K_2}{M}$$

$$a_{21} = \omega_{base}$$

$$a_{32} = {}^{-}\omega_{base}\,\frac{R_{fd}}{L_{fdl}}\,L'_{ad}\,m_1$$

$$a_{33} = {}^{-}\omega_{base}\,\frac{R_{fd}}{L_{fdl}}\left(1 - \frac{L'_{ad}}{L_{fdl}} + L'_{ad}\,m_2\right)$$

$$b_{11} = \frac{1}{M}$$

$$b_{32} = \omega_{base}\,\frac{R_{fd}}{L_{adu}}\;.$$

(5.41)

5.4   Manually Excited Synchronous Machine System in Block Diagram Form

A block diagram of synchronizing and damping torque feedback has already been given in Figure 5.3. The field circuit contribution to synchronizing and damping torque is not quite as obvious. The field circuit voltage equation in (5.40) can be rearranged to facilitate a better understanding of it's role in small signal stability ([15] equ. 12.119):

$$s\,\Delta\psi_{fd} = a_{32}\,\Delta\delta + a_{33}\,\Delta\psi_{fd} + b_{32}\,\Delta E_{fd}$$

$$\Delta\psi_{fd}\,(s - a_{33}) = a_{32}\,\Delta\delta + b_{32}\,\Delta E_{fd}$$

$$\Delta\psi_{fd} = \frac{1}{s - a_{33}}\left[a_{32}\,\Delta\delta + b_{32}\,\Delta E_{fd}\right]$$

$$= \frac{b_{32}}{s - a_{33}}\left[\Delta E_{fd} + \frac{a_{32}}{b_{32}}\,\Delta\delta\right]$$

$$= \frac{K_3}{1 + T_3\,s}\left[\Delta E_{fd} - K_4\,\Delta\delta\right]$$

(5.42)

where:

$$K_3 = -\frac{b_{32}}{a_{33}}$$

$$T_3 = -\frac{1}{a_{33}}$$

$$K_4 = -\frac{a_{32}}{b_{32}}\;.$$

(5.43)

The equations in (5.9), (5.39) and (5.42) can now be combined for a system representation in the Laplace domain. Figure 5.5 is a block diagram of the synchronous machine system. Notice how the simplifying assumption of manual excitation removes the ΔE_{fd} input by setting it to zero.
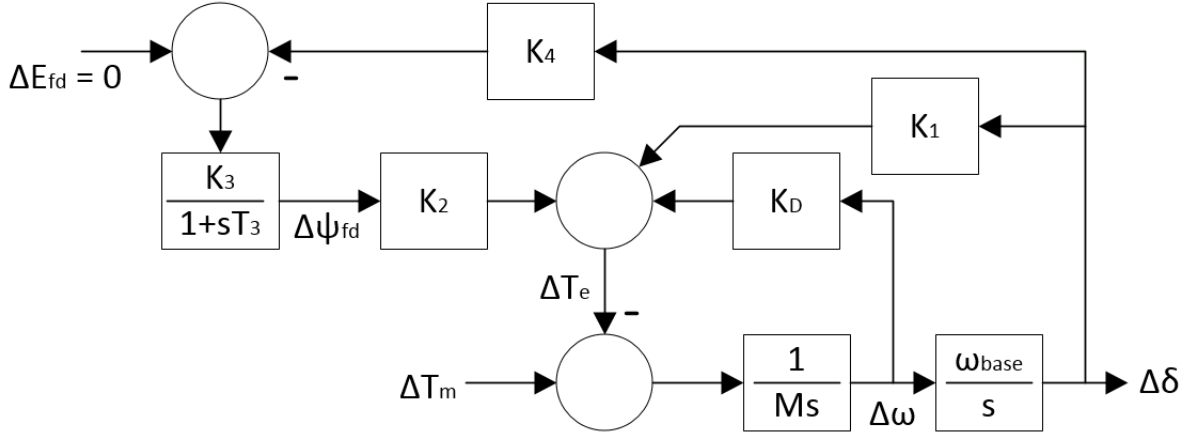
Figure 5.5: Small Signal Transfer Function of Synchronous Generator Mechanical and Field Circuit

5.4.1   Stability Criteria Due to Field Circuit

According to Figure 5.5, since we are assuming manual excitation operation $\Delta E_{fd} = 0$, air gap torque associated with the field circuit reduces to ([15] equ. 12.130):

$$\left.\frac{\Delta T_e}{\Delta \delta}\right|_{\Delta \psi_{fd}} = \frac{-K_2 K_3 K_4}{1 + T_3 s} \; . \tag{5.44}$$

According to [15] pg. 751, the s in (5.44) can be any one of the modes from an eigenvalue analysis of the plant matrix. If the machine is in steady state $(s = 0)$ or if s is a non-oscillating mode $(s = \sigma)$, (5.44) will be real and contribute only to synchronizing torque. For the machine to stay synchronized during steady state we need a positive net synchronizing torque:

$$
\begin{aligned}
\left.\Delta T_e\right|_{\Delta\delta,\text{ Steady State}} &= K_1 \Delta \delta + \left.\Delta T_e\right|_{\Delta\psi_{fd},\text{ Steady State}} \\
&= K_1 \Delta \delta + \frac{-K_2 K_3 K_4}{1 + T_3 (s = 0)} \Delta \delta \\
&= (K_1 - K_2 K_3 K_4)\, \Delta \delta
\end{aligned}
\tag{5.45}
$$

which means K_1 must be greater than $K_2 K_3 K_4$. If s is an oscillating mode $(s = \sigma \pm j\omega)$ it will contribute to damping torque as well during transition from one steady state to another.

This is because $j\Delta\delta$ is rotated $90°$ to be in phase with $\Delta\omega$. More specifically, according to (5.9) $s\Delta\delta = \omega_{base}\Delta\omega$. Reorganizing (5.44) to accomodate this scenario gives:

$$
\begin{aligned}
\Delta T_e\Big|_{\Delta\psi_{fd},\ \text{Osc. Mode}} &= \frac{-K_2K_3K_4}{1+T_3s}\Delta\delta \\
&= \frac{-K_2K_3K_4}{1+T_3s}\Delta\delta \times \frac{1-T_3s}{1-T_3s} \\
&= \left[\frac{-K_2K_3K_4}{1-(T_3s)^2}\right]\Delta\delta - \left[\frac{-K_2K_3K_4T_3}{1-(T_3s)^2}\right](s\Delta\delta) \\
&= \left[\frac{-K_2K_3K_4}{1-(T_3s)^2}\right]\Delta\delta + \left[\frac{K_2K_3K_4T_3\,\omega_{base}}{1-(T_3s)^2}\right]\Delta\omega\ .
\end{aligned}
\tag{5.46}
$$

If we wish to look at one of the oscillating modes directly:

$$
\begin{aligned}
\Delta T_e\Big|_{\Delta\psi_{fd},\ \text{Osc. Mode}} &= \left[\frac{-K_2K_3K_4}{1-(\sigma+j\omega_n)^2T_3^2}\right]\Delta\delta + \left[\frac{K_2K_3K_4T_3\,\omega_{base}}{1-(\sigma+j\omega_n)^2T_3^2}\right]\Delta\omega \\
&= \left[\frac{-K_2K_3K_4}{1-(\sigma^2-\omega_n^2)T_3^2}\right]\Delta\delta + \left[\frac{K_2K_3K_4T_3\,\omega_{base}}{1-(\sigma^2-\omega_n^2)T_3^2}\right]\Delta\omega\ .
\end{aligned}
\tag{5.47}
$$

Now for the machine to maintain stability during transition from one steady state to another we need positive net synchronizing and damping torque components from the dominant oscillating mode:

$$
\begin{aligned}
\Delta T_e\Big|_{Transition} &= K_1\Delta\delta + K_D\Delta\omega + \Delta T_e\Big|_{\Delta\psi_{fd},\ \text{Osc. Mode}} \\
&= K_1\Delta\delta + K_D\Delta\omega + \left[\frac{-K_2K_3K_4}{1-(\sigma^2-\omega_n^2)T_3^2}\right]\Delta\delta + \left[\frac{K_2K_3K_4T_3\,\omega_{base}}{1-(\sigma^2-\omega_n^2)T_3^2}\right]\Delta\omega \\
&= \left[K_1 - \frac{K_2K_3K_4}{1-(\sigma^2-\omega_n^2)T_3^2}\right]\Delta\delta + \left[K_D + \frac{K_2K_3K_4T_3\,\omega_{base}}{1-(\sigma^2-\omega_n^2)T_3^2}\right]\Delta\omega\ .
\end{aligned}
\tag{5.48}
$$

See section 5.5.1 for application of these criteria to the synchronous generator used in this project.

5.5   Aggregated Large Synchronous Generator (LSG)

The aggregated large synchronous generator (LSG) used in this project is three units in parallel of the machine given in chapter 3 of [15]. The machine is a 2-pole, 555 MVA, 3/60/24 kV, 0.9 PF (500 MW) steam turbine generator. The rotor inertia of this machine is given in per unit as $H = 3.525$ MWs/MVA. The base impedance for this machine is:

$$Z_{60\text{Hz}} = \frac{(24 \text{ kV})^2}{555 \text{ MVA}} \tag{5.49}$$
$$= 1.038 \,\Omega \,.$$

The machine impedances are given in the text in per unit on the 60 Hz base from (5.49) as:

$$\begin{aligned}
\text{Armature Winding d-axis Magnetizing Inductance } L_{ad} &= 1.66 \text{ pu} \\
\text{Armature Winding q-axis Magnetizing Inductance } L_{aq} &= 1.61 \text{ pu} \\
\text{Armature Winding Leakage Inductance } L_{al} &= 0.15 \text{ pu} \\
\text{Rotor Field Winding d-axis Leakage Inductance } L_{fdl} &= 0.16500 \text{ pu} \\
\text{Cage Winding d-axis Leakage Inductance } L_{kdl} &= 0.17130 \text{ pu} \\
\text{Cage Winding q-axis Leakage Inductance } L_{kql} &= 0.72520 \text{ pu} \\
\text{2nd Cage Winding q-axis Leakage Inductance } L_{k2ql} &= 0.12500 \text{ pu} \\
\text{Armature Winding Resistance } R_a &= 0.00300 \text{ pu} \\
\text{Rotor Field Winding Resistance } R_{fd} &= 0.00060 \text{ pu} \\
\text{Cage Winding d-axis Resistance } R_{kd} &= 0.02840 \text{ pu} \\
\text{Cage Winding q-axis Resistance } R_{kq} &= 0.00619 \text{ pu} \\
\text{2nd Cage Winding q-axis Resistance } R_{k2q} &= 0.02368 \text{ pu} \,.
\end{aligned} \tag{5.50}$$

We wish to operate the machine at 50 Hz in the constant torque region of operation. This can be accomplished by using the same volts/Hz ratio. The new operating voltage is therefore:

$$\begin{aligned}
\frac{E_{LSG}}{50 \text{ Hz}} &= \frac{24 \text{ kV}}{60 \text{ Hz}} \\
E_{LSG} &= 24 \text{ kV} \times \frac{50 \text{ Hz}}{60 \text{ Hz}} \\
&= 20 \text{ kV} \,.
\end{aligned} \tag{5.51}$$

Since the current rating must remain the same. The new power rating can be found as:

$$\begin{aligned}
\frac{\sqrt{3} \times 20 \text{ kV}}{S_{LSG}} &= \frac{\sqrt{3} \times 24 \text{ kV}}{555 \text{ MVA}} \\
S_{LSG} &= 555 \text{ MVA} \times \frac{20 \text{ kV}}{24 \text{ kV}} \\
&= 463 \text{ MVA}
\end{aligned} \tag{5.52}$$

resulting in a new single machine rating of 463 MVA, 3/50/20 kV, 0.9 PF (417 MW) for operation in a 50 Hz network. The new base impedance is:

$$Z_{50\text{Hz}} = \frac{(20 \text{ kV})^2}{463 \text{ MVA}} \tag{5.53}$$
$$= 0.864 \,\Omega \,.$$

The impedances in (5.50) must be converted to the 50 Hz base in (5.53) before being used in this project. The multiplier for this conversion can be found by combining (5.49) with (5.53):

$$
\begin{aligned}
\text{multiplier} &= \frac{Z_{60\text{Hz}}}{Z_{50\text{Hz}}} \\
&= \frac{1.038\,\Omega}{0.864\,\Omega} \\
&= 1.20\ .
\end{aligned}
\tag{5.54}
$$

The new machine impedances on the 50 Hz base from (5.53) are then:

$$
\begin{aligned}
\text{Armature Winding d-axis Magnetizing Inductance } L_{ad} &= 1.992 \text{ pu} \\
\text{Armature Winding q-axis Magnetizing Inductance } L_{aq} &= 1.932 \text{ pu} \\
\text{Armature Winding Leakage Inductance } L_{al} &= 0.18 \text{ pu} \\
\text{Rotor Field Winding d-axis Leakage Inductance } L_{fdl} &= 0.19800 \text{ pu} \\
\text{Cage Winding d-axis Leakage Inductance } L_{kdl} &= 0.20556 \text{ pu} \\
\text{Cage Winding q-axis Leakage Inductance } L_{kql} &= 0.87024 \text{ pu} \\
\text{2nd Cage Winding q-axis Leakage Inductance } L_{k2ql} &= 0.15000 \text{ pu} \\
\text{Armature Winding Resistance } R_a &= 0.00360 \text{ pu} \\
\text{Rotor Field Winding Resistance } R_{fd} &= 0.00072 \text{ pu} \\
\text{Cage Winding d-axis Resistance } R_{kd} &= 0.03408 \text{ pu} \\
\text{Cage Winding q-axis Resistance } R_{kq} &= 0.00743 \text{ pu} \\
\text{2nd Cage Winding q-axis Resistance } R_{k2q} &= 0.02842 \text{ pu}\ .
\end{aligned}
\tag{5.55}
$$

The aggregated synchronous generator model making up the onshore AC network in this project is three units in parallel of the machine described above. This triples the power rating and reduces the base impedance by a factor of three. In the per unit system, the machine impedances remain as stated in (5.55). The final LSG rating is therefore 1389 MVA, 3/50/20 kV with an inertia constant of 3.525 MWs/MVA.

5.5.1 Stability Characteristics of LSG with Manual Excitation

The state space plant matrix for the LSG according to (5.40) can be found with the MATLAB program in Appendix A. This plant matrix is:

$$
\mathbf{A} = \begin{bmatrix} a_{11} & a_{12} & a_{13} \\ a_{21} & 0 & 0 \\ 0 & a_{32} & a_{33} \end{bmatrix} = \begin{bmatrix} 0 & -0.3486 & -0.2983 \\ 314.2 & 0 & 0 \\ 0 & -0.4705 & -0.6470 \end{bmatrix}\ .
\tag{5.56}
$$

The plant matrix has one conjugate pair electromechanical oscillating mode and a non-oscillating mode:

$$\lambda = \sigma + j\,\omega_n$$
$$\lambda_{1,2} = -0.2012 \pm j\,10.4590 \tag{5.57}$$
$$\lambda_3 = -0.2446 + j\,0.0000\,.$$

In general, a stable system requires that σ is negative, which is true for the present scenario. The frequency of electromechanical oscillating mode $\lambda_{1,2}$ is 1.66 Hz. Another criteria associated with the field circuit is that the net steady state synchronizing torque of plant matrix $\mathbf{A}$ must be positive. This is found according to (5.45) as:

$$\Delta T_e\Big|_{\Delta\delta,\ \text{Steady State}} = (K_1 - K_2 K_3 K_4)\,\Delta\delta$$
$$= (2.4580 - 2.1033 \times 0.1755 \times 4.1436)\,\Delta\delta \tag{5.58}$$
$$= 0.9283\,\Delta\delta\,.$$

The net synchronizing and damping torque from the dominant oscillating mode during transition from one steady state to another must also be positive. This is found according to (5.48) as:

$$\Delta T_e\Big|_{Transition} = K_{S,net}\,\Delta\delta + K_{D,net}\,\Delta\omega$$
$$= 2.4521\,\Delta\delta + 2.8324\,\Delta\omega\,. \tag{5.59}$$

The machine meets the criteria associated with the field circuit given in section 5.4.1 and should therefore be able to retain synchronization during moderate load changes in the system.

5.5.2 Implementation of Manual Excitation in PSCAD/EMT$^{\text{TM}}$

Manual excitation is the application of a step change in voltage E_{fd} to the machine field winding. It is an open loop manual input to the system and there is no automatic voltage regulation providing a measured value for comparison to a reference. This means there is no error ΔE_{fd} while a control signal seeks a new steady state (ie: $\Delta E_{fd} = 0$ as in figure 5.5). Figure 5.6 is an implementation of manual excitaion in PSCAD/EMT$^{\text{TM}}$. It is a simple switch and two inputs at any synchronous generator. In this project, required excitation voltages for balanced system operation are estimated by vector analysis with the program in Appendix A and tuned by trial and error for specific load-frequency dynamic situations.
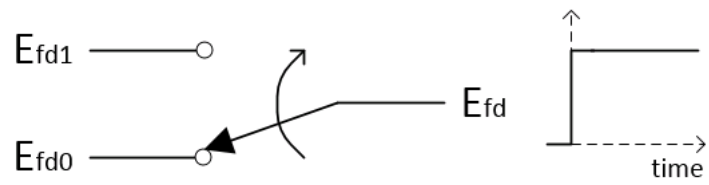
Figure 5.6: Manual Excitation: $\Delta E_{fd} = 0$

Chapter 6

Load Frequency Control

Load Frequency control is a method for balancing and regulating power demand between multiple synchronous generation units in an AC transmission system. It is built on the assumption that power is flowing through a primarily inductive transmission network (ie: high X/R ratio). This means frequency is constant throughout the system and is closely associated with power. This also means active power flow functions fairly independently of reactive power flow [15], Section 11.1. This chapter will introduce load frequency control according to Chapter 11 of [15] and how it was implemented in this project. It will study the dynamics associated with the turbines of the onshore AC system and how these dynamics interact with synchronous generator mechanical dynamics. It will also characterize the onshore AC system reference model according to an idealized turbine/generator transfer function of the Aggregated Large Synchronous Generator (LSG).

This project assumes steam turbine prime movers for the LSG and the Small Synchronous Generator (SSG). The simplifying assumption of non-reheat type turbines is also applied to the model allowing the turbine to be represented by a single time constant T_{CH} where "$_{CH}$" refers to steam chest. Figure 6.1 is the steam turbine transfer function. In the figure, ΔY represents the position of the steam input valve and ΔP_m represents the mechanical power output. According to Section 11.1.4 of [15], typical values for T_{CH} range from 0.2 to 0.3 seconds. The value of 0.3 seconds was chosen for this project.

$$\Delta Y \longrightarrow \boxed{\dfrac{1}{1+sT_{CH}}} \longrightarrow \Delta P_m$$
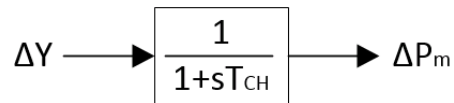
Figure 6.1: Steam Turbine Transfer Function

The steam turbine in figure 6.1 is regulated by a governor. The governor used in this project is developed according to Section 11.1.1 of [15]. The simplest form of regulation is referred to as isochronous control which means constant speed control for different loads and is typically used in small networks where only one synchronous generation source is present. It can be modelled as an integrator in a feedback loop around the turbine as in figure 6.2.
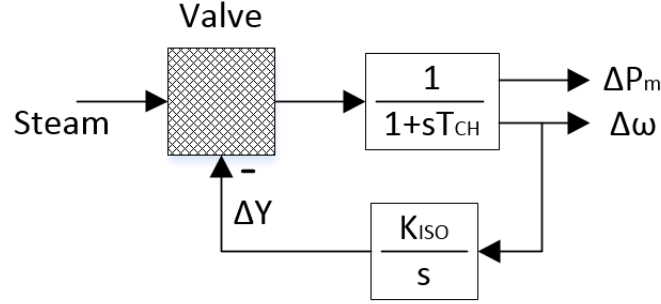
Figure 6.2: Steam Turbine with Isochronous Governor

For networks where more than one synchronous generation source is present, droop control is required. This allows for different power outputs from the individual synchronous generation sources according to a constant frequency. It is modelled as a proportional feedback loop around the isochronous integrator as in figure 6.3. The transfer function of the droop controller in figure 6.3 is:

$$\Delta Y = -\frac{K_{ISO}}{s}\left[\Delta\omega + R_{Pf}\,\Delta Y\right]$$

$$\Delta\omega = -\left[\frac{s}{K_{ISO}} + R_{Pf}\right]\Delta Y$$

$$\frac{\Delta Y}{\Delta\omega} = \frac{-1}{\frac{s}{K_{ISO}} + R_{Pf}} \tag{6.1}$$

$$= \frac{G_G}{1 + s\,T_G}$$

where G_G is the gain and T_G is the time constant of the governor. More specifically:

$$G_G = \frac{-1}{R_{Pf}}$$

$$T_G = \frac{1}{R_{Pf}\,K_{ISO}} \;. \tag{6.2}$$

Typical values for droop constant R_{Pf} range from 0.04 to 0.05 per unit on system power base. A droop of 5% was used for this study. A typical value of $T_G = 0.2$ seconds was also used.

We are building a transfer function that interacts with the synchronous generator mechanical system and external load changes seen at the terminals of the synchronous generator. Therefore, we can take the synchronous generator mechanical system block diagram from figure 5.3 and modify it for this purpose. First, we will exclude the $\Delta\delta$ feedback loop because we are only interested in the relationship between power and speed (or power and frequency). We will also replace K_D with D signifying the damping effects of load flow and neglecting
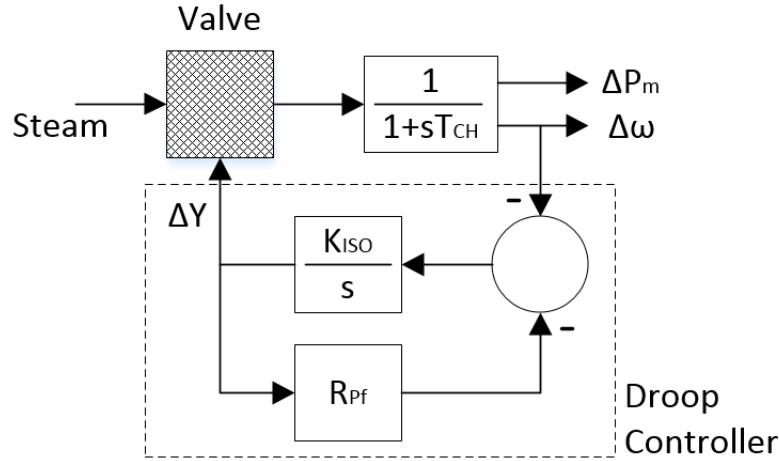
Figure 6.3: Steam Turbine with Droop Governor

the damping effects of internal machine characteristics such as field circuit or amortisseur windings. Figure 6.4 is the modified block diagram. It is the synchronous generator equation of motion (see also (5.8)) modified to receive load changes as input. In equation form this is:

$$
\begin{aligned}
\Delta\omega &= \frac{1}{Ms}\left[\Delta P_m - \Delta P_e\right] \\
&= \frac{1}{Ms}\left[\Delta P_m - \Delta P_L - D\Delta\omega\right]
\end{aligned}
\tag{6.3}
$$

where ΔP_L is the electrical power change at the machine terminals and $D\Delta\omega$ is the damping effect of the load flow. D is typically on the order of 1 to 2 p.u with load as base. Remember for network analysis that power is interchangeable with torque in the per unit system as explained in 5.1. It is now convenient to solve for $\Delta\omega$ of the synchronous generator:

$$
\begin{aligned}
Ms\,\Delta\omega &= \Delta P_m - \Delta P_L - D\Delta\omega \\
\left[D + Ms\right]\Delta\omega &= \Delta P_m - \Delta P_L \\
\Delta\omega &= \left[\frac{1}{D + Ms}\right]\left[\Delta P_m - \Delta P_L\right].
\end{aligned}
\tag{6.4}
$$

6.1 Idealized Load Frequency Transfer Function

In order to better understand and characterize the onshore AC system, we now wish to combine synchronous generator mechanical dynamics with turbine mechanical dynamics. This will allow us to define grid stiffness and initial frequency gradient or frequency sensitivity (which in this study will be referred to as frequency strength). For a simplified transfer
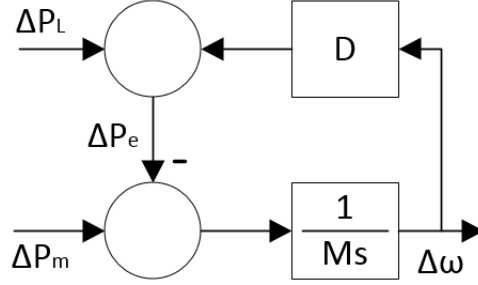
Figure 6.4: Synchronous Generator Mechanical System for Load Frequency Analysis

function we will assume an infinitely stiff shaft. This will have the effect of setting T_{CH} from figure 6.1 to zero (or $\Delta P_m = \Delta Y$). This will also allow us to neglect torsional dynamics by setting $\Delta\omega$ of the synchronous generator (equation (6.4)) equal to $\Delta\omega$ of the turbine (equation (6.1)). Combining (6.4) with (6.1) and setting $\Delta P_m = \Delta Y$ we have:

$$
\begin{aligned}
\Delta\omega &= \left[\frac{1}{D + Ms}\right]\left[\frac{-1}{R_{Pf}}\left(\frac{1}{1 + s\,T_G}\right)\Delta\omega - \Delta P_L\right] \\
^-\Delta P_L &= \left[D + Ms + \frac{1}{R_{Pf}}\left(\frac{1}{1 + s\,T_G}\right)\right]\Delta\omega \\
\frac{\Delta\omega}{\Delta P_L} &= \frac{-1}{D + Ms + \frac{1}{R_{Pf}}\left(\frac{1}{1 + s\,T_G}\right)} \times \frac{R_{Pf}(1 + s\,T_G)}{R_{Pf}(1 + s\,T_G)} \\
&= \frac{^-R_{Pf}(1 + s\,T_G)}{1 + R_{Pf}(D + Ms)(1 + s\,T_G)} \\
&= \frac{^-R_{Pf}(1 + s\,T_G)}{s^2\,R_{Pf}T_G M + s\,(R_{Pf}T_G D + R_{Pf}M) + R_{Pf}D + 1} \div \frac{R_{Pf}T_G M}{R_{Pf}T_G M} \\
&= \left[\frac{-1}{T_G M}\right]\left[\frac{1 + s\,T_G}{s^2 + s\left(\frac{D}{M} + \frac{1}{T_G}\right) + \left(\frac{D}{T_G M} + \frac{1}{R_{Pf}T_G M}\right)}\right]
\end{aligned}
\tag{6.5}
$$

and represents a system with two poles and a zero. Note that this transfer function does not consider the effects of inter-machine oscillations or power flow performance. Also, from this point forward $\Delta\omega$ will be considered interchangeable with Δf (section 11.1.3 of [15]) since it is being used to characterize the onshore AC system. Figure 6.5 is a block diagram of the idealized transfer function in (6.5).

6.1.1   Stiffness of the Onshore AC System

The steady state load frequency transfer function of the onshore AC system can be found by taking the limit of (6.5) as s goes to zero:

Figure 6.5: Turbine/Generator Idealized Transfer Function

$$\frac{\Delta f_{ss}}{\Delta P_L} = \lim_{s \to 0} \left[\frac{-1}{T_G M_{eq}}\right] \left[\frac{1 + s\,T_G}{s^2 + s\left(\frac{D_{eq}}{M_{eq}} + \frac{1}{T_G}\right) + \left(\frac{D_{eq}}{T_G M_{eq}} + \frac{1}{R_{eq}T_G M_{eq}}\right)}\right]$$

$$= \left[\frac{-1}{T_G M_{eq}}\right] \left[\frac{1}{\frac{D_{eq}}{T_G M_{eq}} + \frac{1}{R_{eq}T_G M_{eq}}}\right] \qquad (6.6)$$

$$= \frac{-1}{\frac{1}{R_{eq}} + D_{eq}}$$

where subscript "$_{eq}$" denotes a composite variable meaning it describes the entire network. The composite frequency response characteristic β_{eq} of the onshore AC system is then:

$$\beta_{eq} = -\frac{\Delta P_L}{\Delta f_{ss}}$$
$$= \frac{1}{R_{eq}} + D_{eq} \qquad (6.7)$$

and is commonly expressed in units: MW/Hz. According to section 11.1.3 of [15] this is sometimes also referred to as *stiffness* of the network. The variable R_{eq} is associated with the sum generating capacity of all sources contributing to regulation on the network. The variable D_{eq} is associated with the sum of all the loads on the network. In this project, R_{eq} is 0.05 per unit ($\frac{1}{R_{eq}} = 20$) and D_{eq} is 1.5 per unit. As a frame of reference, if we assume a lossless power system with load equal to the total capacity of the synchronous generation sources at 1489 MW, the stiffness of the onshore AC network is:

$$\beta_{eq} = \left[\frac{1}{0.05} + 1.5\right] \times \frac{1489 \text{ MW}}{50 \text{ Hz}}$$
$$= 640.3 \text{ MW/Hz} \qquad (6.8)$$

6.1.2   Frequency Strength of the Onshore AC System

The instantaneous load frequency transfer function of the onshore AC system can be found by taking the limit of (6.5) as s goes to ∞:
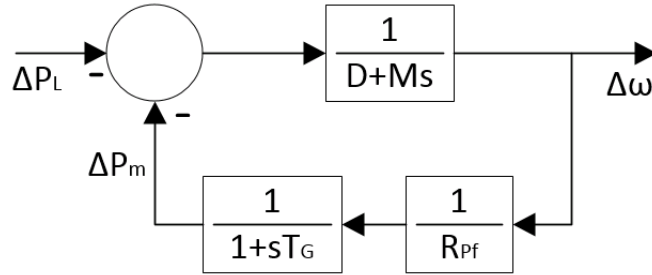
$$
\begin{aligned}
\frac{\Delta f}{\Delta P_L} &= \lim_{s \to \infty} \left[\frac{-1}{T_G M_{eq}} \right] \left[\frac{1 + s\,T_G}{s^2 + s\left(\frac{D_{eq}}{M_{eq}} + \frac{1}{T_G}\right) + \left(\frac{D_{eq}}{T_G M_{eq}} + \frac{1}{R_{eq} T_G M_{eq}}\right)} \right] \\
&= \left[\frac{-1}{T_G M_{eq}} \right] \left[\frac{s\,T_G}{s^2} \right] \\
&= \frac{-1}{s\,M_{eq}} \,.
\end{aligned}
\tag{6.9}
$$

By rearranging we have the initial frequency gradient of the onshore AC system:

$$
\begin{aligned}
\frac{s \Delta f}{\Delta P_L} &= \frac{-1}{M_{eq}} \\
\frac{\mathrm{d}}{\mathrm{d}t}[\Delta f] &= \frac{-1}{M_{eq}} \Delta P_L \,.
\end{aligned}
\tag{6.10}
$$

As M_{eq} increases, initial frequency gradient decreases making frequency more resilient (or less sensitive) to load disturbances. Therefore, as M_{eq} increases frequency can be considered stronger. Since the general definition of M is two times the inertia constant ($M = 2H$), a Composite Inertia Constant H_{eq} can be defined to quantify the frequency strength of the onshore AC system:

$$
H_{eq} = \frac{\text{total rotational inertia of AC system, MWs}}{\text{total generating capacity of AC system, MVA}}
\tag{6.11}
$$

and as H_{eq} increases, frequency strength increases. Choosing all the individual inertia constants to be 3.525 seconds, the LSG rating to be $3 \times 463 = 1389$ MW and the SSG rating to be 100 MW:

$$
\begin{aligned}
H_{eq} &= \frac{H_{LSG} \times S_{LSG} + H_{SSG} \times S_{SSG}}{S_{eq}} \\
&= \frac{3.525 \times 1389 + 3.525 \times 100}{1389 + 100} \\
&= 3.525 \text{ MWs/MVA}
\end{aligned}
\tag{6.12}
$$

6.1.3   Effective Inertia Constant (H_{DC})

Frequency strength is an important topic in this project as it measures the ability of the AC network to accommodate a DC link injecting power into it. The traditional idea is that

the AC network must have a certain amount of inertia so that the HVDC link will perform adequately. Similar to Composite Inertia Constant, section 10.6.5 of [15] defines Effective Inertia Constant as:

$$H_{DC} = \frac{\text{total rotational inertia of AC system, MWs}}{\text{total capacity of DC link, MW}} \ . \tag{6.13}$$

This quantifies frequency strength in terms of AC/DC system interaction. Repeating the calculation in (6.12) but on our HVDC link base we have:

$$\begin{aligned}
H_{DC} &= \frac{H_{LSG} \times S_{LSG} + H_{SSG} \times S_{SSG}}{P_{DC}} \\
&= \frac{3.525 \times 1389 + 3.525 \times 100}{400} \\
&= 13.1 \text{ MWs/MW}
\end{aligned} \tag{6.14}$$

and represents our reference system. The text recommends a value greater than 2 or 3 for connection of an HVDC link with line commutated converters. Although this project uses voltage source converters the H_{DC} concept is still relevant. Simulation has shown that with H_{DC} below 2 or 3 the onshore AC system can be unstable. The low H_{DC} scenario can therefore be used to demonstrate the ability of the Generator Response Following (GRF) method to increase frequency stability of the onshore AC network. In short, rather than requiring a higher H_{DC} from an onshore AC network, the GRF method can help increase the stability of a network with lower H_{DC} (see section 7.1). The traditional solution to this problem is to add synchronous condensers.

6.1.4 Global Frequency Response of the Onshore AC System

This section discusses global frequency response to load changes and what to expect when observing time-domain simulation results. A summary of the global characteristics associated with frequency response of the onshore AC system is listed here. These have already been chosen or calculated in previous sections.

- Composite Inertia Constant: $H_{eq} = 3.525$ seconds

- Composite Droop Regulation Constant: $R_{eq} = 0.05$ per unit

- Composite Damping Coefficient: $D_{eq} = 1.5$ per unit

Steady state frequency response to a load change is a function of AC grid stiffness and is derived from the idealized load frequency transfer function in (6.5). If we combine the steady state version of the transfer function in (6.6) with the definition of stiffness in (6.7) we have:

$$\Delta f_{ss} = \frac{-1}{\beta_{eq}} \Delta P_L \tag{6.15}$$

which can be used to quickly assess simulation results. Similarly, initial frequency gradient is a function of M_{eq} $(= 2H_{eq})$ and should have a certain amount of predictability for comparison to simulation. This can be found in (6.10) as the instantaneous version of the idealized load frequency transfer function. The full transfer function in (6.5) can also be used to anticipate the shape of the frequency response during transition to a new steady state. Figure 6.6 is the response of the system (characterized by the list given above) to a 1.0 per unit step load change. Initial gradient and final steady state are the same in each of the cases confirming the conclusions given in (6.10) and (6.15). Since we don't know the equivalent time constant associated with the global network, we can look at a range of possibilities. The time constant in the transfer function has been varied to demonstrate the influence on the shape of the frequency response. As time constant decreases, frequency tends to respond more like a single pole system.
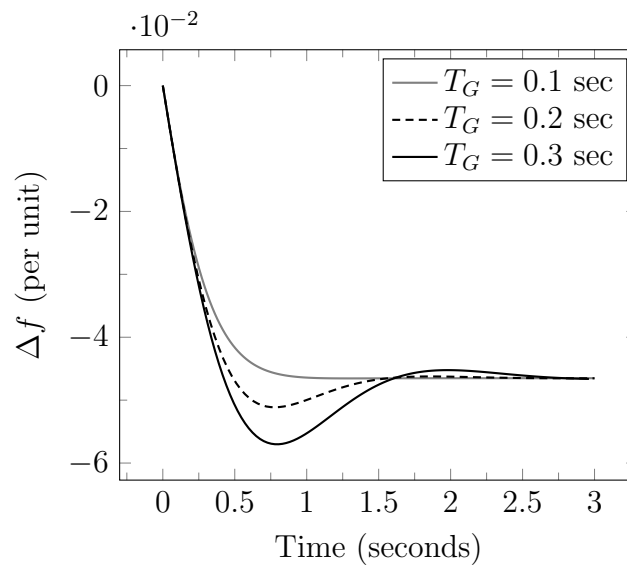
Figure 6.6: Global Frequency Response to Load Step Change of $\Delta P_L = 1$ p.u.

6.2   Implementation in PSCAD/EMT$^{\text{TM}}$

The synchronous generator model in PSCAD/EMT$^{\text{TM}}$has different sets of torque and speed inputs and outputs for different purposes. One set is for modelling the primary response functionality of the turbine and governor. Another set is for modelling the inertial response characteristics associated with the rotor mechanical system (ie: the swing equation) and the torsional dynamics of the shaft and turbine. The primary response of the steam turbine and governor was modelled with control blocks as in figure 6.3 with speed measurement taken from the generator as input. The inertial response of the rotor mechanical system was modelled with control blocks as in figure 6.7 which is an adaptation of figure 6.4 for relevant inputs. The PSCAD/EMT$^{\text{TM}}$synchronous generator model provides mechanical torque and electrical torque measurements for input to this diagram. Since this project assumes an infinitely stiff

shaft, torsional dynamics have been neglected. See 7.1.2 for further explanation of primary response and inertial response.
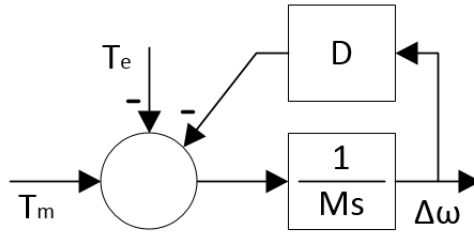
Figure 6.7: Synchronous Generator Mechanical System in PSCAD/EMT^{TM}

A program was also written in MATLAB to calculate and keep track of the many variables required for an implementation of these systems in PSCAD/EMT^{TM}. This program can be found in Appendix B and is used for tuning the PSCAD/EMT^{TM}simulation. It is summarized in the following sections.

6.2.1 Local Characteristics

Each generation source in the system has it's own droop constant to regulate power output based on frequency. Therefore, since we already chose the composite droop constant to be 0.05 per unit and assuming all generators in the system participate in regulation, the following needs to be true for the sum of the individual generator droop constants:

$$\frac{1}{R_{eq}} \times \frac{1489 \text{ MW}}{50 \text{ Hz}} = \frac{1}{R_{LSG}} \times \frac{1389 \text{ MW}}{50 \text{ Hz}} + \frac{1}{R_{SSG}} \times \frac{100 \text{ MW}}{50 \text{ Hz}} \ . \tag{6.16}$$

These droop constants represent R_{Pf} in figure 6.3 and must be on their respective machine bases for implementation in PSCAD/EMT^{TM}. If the windfarm is considered to be participating in regulation then:

$$\frac{1}{R_{eq}} \times \frac{1889 \text{ MW}}{50 \text{ Hz}} = \frac{1}{R_{LSG}} \times \frac{1389 \text{ MW}}{50 \text{ Hz}} + \frac{1}{R_{SSG}} \times \frac{100 \text{ MW}}{50 \text{ Hz}} + \frac{1}{R_{WTG}} \times \frac{400 \text{ MW}}{50 \text{ Hz}} \ . \tag{6.17}$$

Likewise, the damping coefficient D (in figure 6.7) is utilized at each of the individual machines and must therefore be on the individual machine base for implementation in PSCAD/EMT^{TM}. Since D_{eq} was chosen to be 1.5 per unit on a base representing all the loads on the AC network, the following needs to be true:

$$D_{eq} \times \frac{1489 \text{ MW}}{50 \text{ Hz}} = D_{LSG} \times \frac{1389 \text{ MW}}{50 \text{ Hz}} = D_{SSG} \times \frac{100 \text{ MW}}{50 \text{ Hz}} \ . \tag{6.18}$$

Time constants also have significance on a local scale. The two most important time constants used in the PSCAD/EMT$^{\text{TM}}$implementation of the system were given earlier. In summary, the turbine steam chest time constant T_{CH} was chosen to be 0.3 seconds and is the same for all generation units. All steam turbines are assumed to be of the non-reheat type for simplified modelling (reheat time constant of zero). Turbine governor time constant T_G was chosen to be 0.2 seconds and is the same for all generation units.

6.2.2   Local Power Change from Global Frequency Change

Once global steady state frequency is calculated in (6.15), the re-allocation of power output from nominal dispatch can be calculated at each of the individual generation sources. The conversion in (6.15) can be interpreted on a local scale with local R_n and D_n as defined in section 6.2.1 and frequency as input:

$$\Delta P_{LSG} = {}^{-}\beta_{LSG}\,\Delta f_{ss}$$
$$\Delta P_{SSG} = {}^{-}\beta_{SSG}\,\Delta f_{ss} \tag{6.19}$$
$$\Delta P_{WTG} = {}^{-}\beta_{WTG}\,\Delta f_{ss}$$

where:

$$\beta_{LSG} = \frac{1}{R_{LSG}} + D_{LSG}$$
$$\beta_{SSG} = \frac{1}{R_{SSG}} + D_{SSG} \tag{6.20}$$
$$\beta_{WTG} = \frac{1}{R_{WTG}}\;.$$

A diagram of this power re-allocation is given in figure 6.8. In the figure, initial frequency is a nominal value of 50Hz with a dispatch of rated power from each of the generation sources. Power is given in per unit so all machines can be drawn on the same scale and in the same diagram. More load is then added causing an under-frequency event and more power is allocated from the individual sources according to local characteristics. This diagram uses arbitrary scaling of the individual machines and does not reflect actual simulation results.
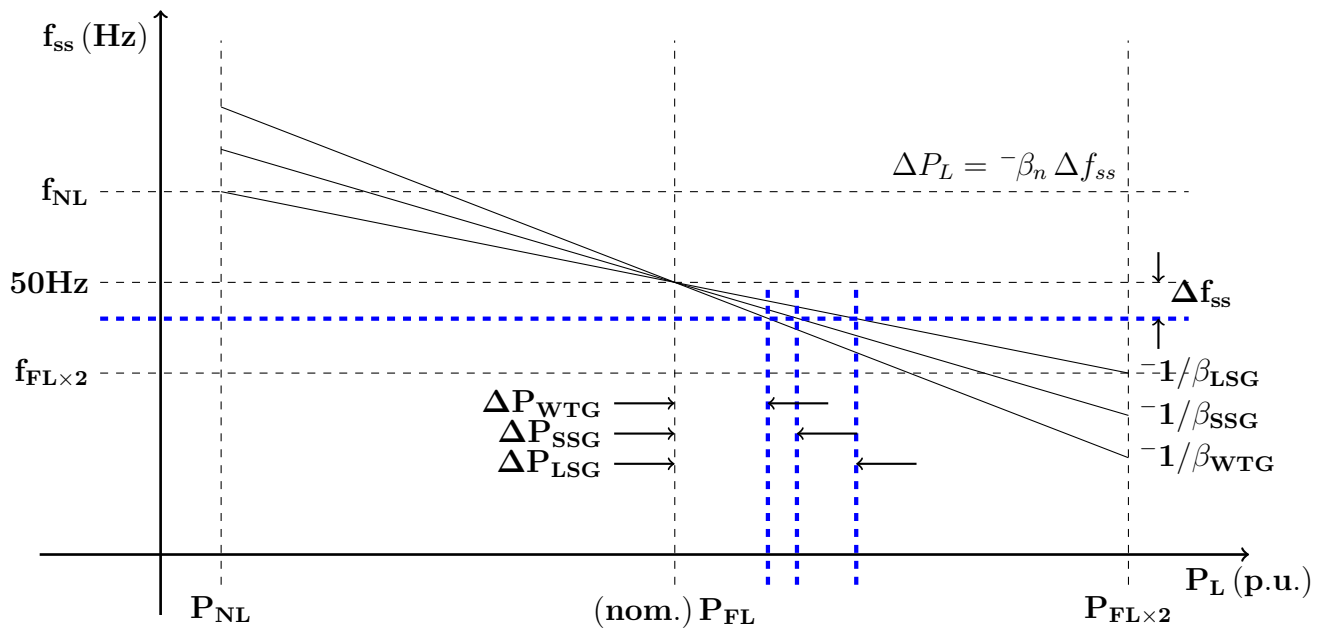
Figure 6.8: Local Re-Allocation of Power Output Due to Global Under-Frequency Event

Chapter 7

Generator Response Following and Wind Farm Controller

This chapter introduces the Generator Response Following (GRF) method. The general concept is that a SSG, located at a PCC with an OWF, responds in a typical way to changes in load in an onshore AC system employing load frequency control. This response can be measured and the information sent offshore allowing the OWF to mimic the load-sharing behavior of the SSG. 7.1 outlines what type of information is sent from the SSG to the OWF and how it is obtained. 7.2 outlines how the information is communication from source to destination. 7.3 outlines how the information is processed once it reaches the offshore windfarm.

7.1 Generator Response Following (GRF)

Historically, as discussed in section 6.1.3, connection of an HVDC link requires a minimum mechanical inertia directly coupled to the AC grid to maintain voltage and frequency stability. One way to quantify this inertia is to relate the total rotational kinetic energy of the AC system to the DC power capacity of the HVDC link. An Effective Inertia Constant is defined for this purpose in (6.13). The literature recommends H_{DC} greater than 2 or 3 for satisfactory operation of line commutated converters. Since this study uses voltage source converter technology, the Effective Inertia Constant is instead used to quantify the ability of the Generator Response Following (GRF) method to influence the performance of the interconnected AC system.

This section is structured as follows. 7.1.2 classifies the various types of frequency response relevant for this project. 7.1.1 defines mechanical and synthetic inertia relative to each other. 7.1.3 outlines the performance of the Small Synchronous Generator in terms of relevant information that can be used by the Offshore Windfarm.

7.1.1　Mechanical vs. Synthetic Inertia

A traditional solution to the problem of low Effective Inertia Constant is to add synchronous condensers to the AC network. This increases the mechanical inertia of the system but does not increase the power rating. Thus the frequency strength (defined in 6.1.2) of the AC system increases because the Composite Inertia Constant in (6.11) has increased. For our purposes, the mechanical inertia is quantified by the kinetic energy (KE) of the inertia constant definitions in (6.11) & (6.13). It is the integral of angular momentum relative to angular velocity:

$$KE = \int J\omega \, \mathrm{d}\omega$$
$$= \frac{1}{2}J\omega^2 \tag{7.1}$$

where J is the moment of the inertia and ω is the angular velocity of the rotor of the synchronous generation source. It is used in the equations of motion in 5.2 which assume a directly coupled (synchronized) rotor. In Section 5.2 as well as in (6.11) & (6.13), it is used in the per unit system with units MWs/MVA.

To facilitate the GRF method, KE can also be used to quantify the stabilizing effect of the electrical power injection from the Offshore Windfarm (OWF) at the Point of Common Coupling (PCC) with the onshore AC network. In other words, it can be used to quantify the synthetic inertia response of a WTG employing the GRF method. As will be elaborated in the following sections, the WTG power injection response is "following" the response of the SSG. The same per unit inertia constant can therefore be used to represent it and then to find a synthetic KE_{WTG} of the aggregated wind turbine generator (WTG):

$$H_{WTG} = H_{SSG}$$
$$\frac{KE_{WTG}}{P_{WTG}} = \frac{KE_{SSG}}{S_{SSG}} \tag{7.2}$$
$$KE_{WTG} = H_{SSG}\,P_{WTG}\,.$$

Without the GRF method, KE_{WTG} would be zero. With the GRF method, inertial response information is sent to the WTG and can be related to the rate of change of kinetic energy by the gain and time delay applied to it:

$$\frac{\mathrm{d}}{\mathrm{d}t}KE_{WTG} = \frac{K_{SSG}}{1 + sT_{SSG}}\,P_{iner} \tag{7.3}$$

where P_{iner} is the inertial response of the SSG defined in section 7.1.2, K_{SSG} is the gain applied to it and T_{SSG} is the time delay applied to it. This gain and delay must be optimized for the network by a tuning process demonstrated in section 8.3. A block diagram of this can also be seen in the fiber-optic channel of figures 1.1 & 1.2.
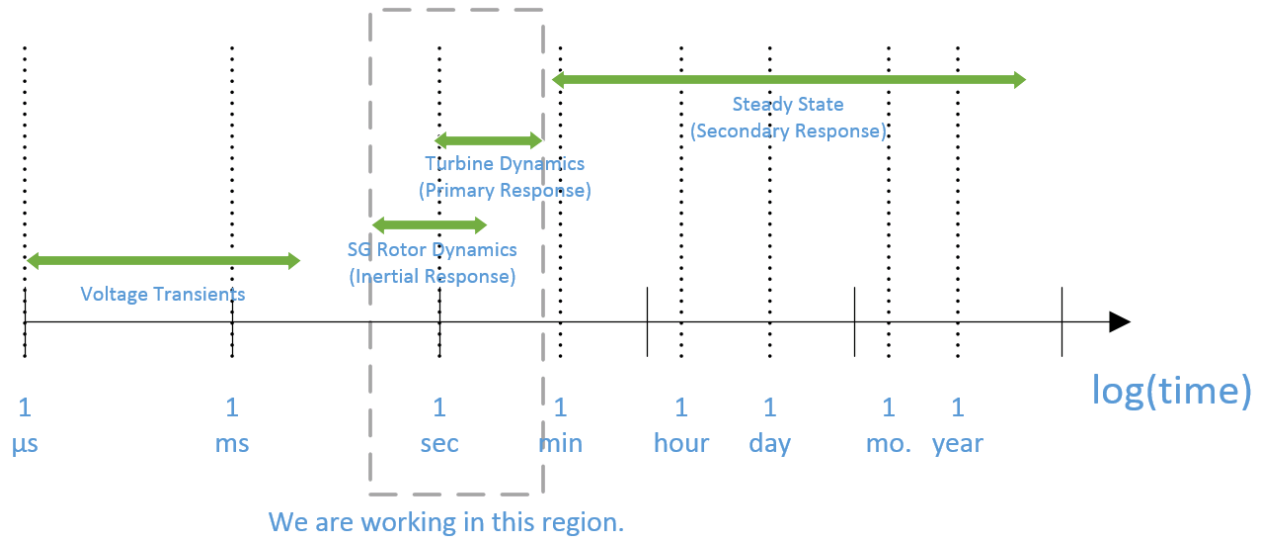
Figure 7.1: Relevant Timescales

7.1.2 Frequency Response Classifications

Figure 7.1 is a diagram of timescales which have significance in this project. In the middle are the dynamic timescale events that this project investigates. The primary response is the readjustment of the turbine to meet the new demand after a change in load on the system. The inertial response is slightly faster than the primary response and is associated with the kinetic energy stored in the rotor. It compensates for the temporary power imbalance that occurs between an instantaneous load change in the system and the time it takes for the turbine to readjust the power supply output to meet the new demand. Figure 7.2 defines primary response and inertial response in terms of block diagrams previously developed in this report. It is a combination of the synchronous generator small signal transfer function in figure 5.5 and the idealized turbine/generator transfer function for load-frequency control in figure 6.5. In figure 7.2, $\Delta\omega_r$ of the turbine is separated from $\Delta\omega_r$ of the synchronous generator signifying that primary response is different from inertial response. However, this project uses the simplifying assumption of an ideal (ie: infinitely stiff) shaft with no torsional dynamics which means the two $\Delta\omega_r$'s are in-fact equal. The simplifying assumption of manual excitation is represented by $\Delta E_{fd} = 0$.

On the left of figure 7.1 are the transient timescale events such as voltage transients and PWM switching operations. These are not relevant to the goals of this project, therefore they are neglected in the PSCAD/EMT$^{\text{TM}}$calculation by using larger timesteps. This lower resolution is a compromise that allows for faster simulation time with the software. On the right of figure 7.1 is steady state. Once steady state has been reached, secondary controls renormalize the system back to nominal (referred to as secondary response). This project studies the primary and inertial response associated with the load-frequency strategy outlined in chapter 6 and therefore is not concerned with secondary response.

It is also important to recognize that the size of the individual machine relative to the size
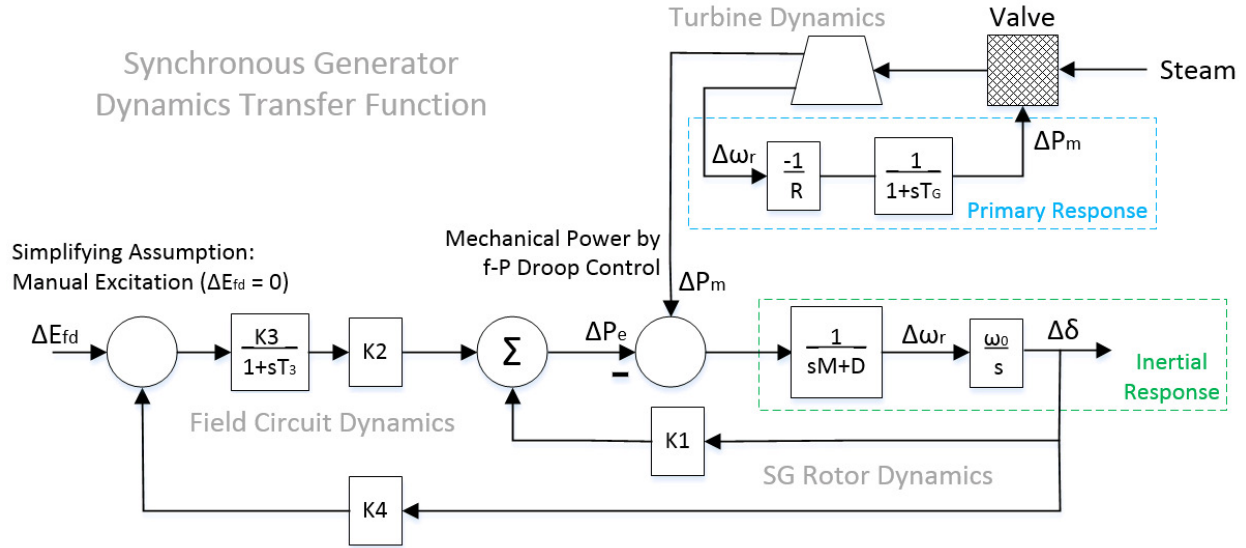
Figure 7.2: Primary Response vs. Inertial Response

of the system affects the load-frequency response as well. In the reference circuit used in this project, LSG makes up a large portion of the total onshore AC network power supply. It therefore dominates the frequency response of the system. This means that any inertial response from the LSG will be seen in the global frequency response waveform. On the other hand, SSG makes up a small portion of the total onshore AC network power supply. Therefore any inertial response from the SSG will be seen as a local power waveform. This topic is also mentioned in [15], chapter 11 (pg. 594). This is an important feature for implementation of the GRF method as the SSG inertial response can be taken as a local power measurement separate from the global frequency waveform during small load deviations from nominal (this effect can be observed in the weak grid power waveforms of figure 8.6). The inertial response of the SSG is therefore easy to separate from the primary response. It is taken from the swing equation for generators in (6.3) as:

$$P_{iner} = P_m - P_e \, . \tag{7.4}$$

This measurement can be taken in PSCAD/EMT^{TM}according to figure 6.7 or estimated in a practical application scenario as shaft torque minus terminal power. As stated in 5.1, power and torque can be considered interchangeable (in per unit) for power system studies. Figure 7.3 is an example of what an inertial response waveform looks like.

7.1.3   Small Synchronous Generator (SSG) and Initialization

The Small Synchronous Generator (SSG) is the same machine design as the LSG in section 5.5 but operated at a reduced load. This is done by operating it at a reduced voltage. The base impedance remains the same as for the LSG. For the purposes of this project the rating of
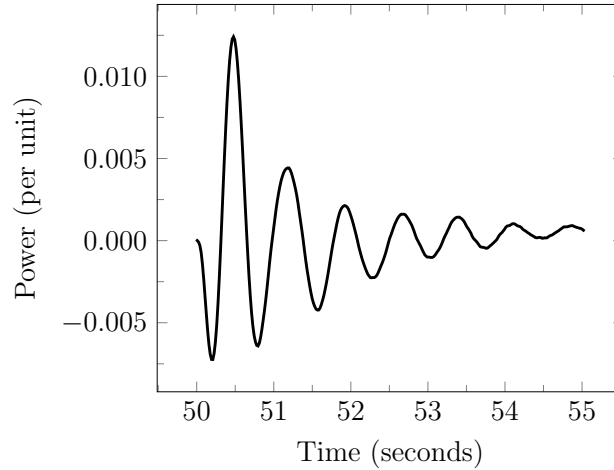
Figure 7.3: SSG Inertial Response Waveform

the SSG is 100 MVA. The new operating voltage can then be found with the base impedance in (5.53) as:

$$\begin{aligned}
100 \text{ MVA} &= \frac{(E_{SSG})^2}{Z_{50\text{Hz}}} \\
E_{SSG} &= \sqrt{100 \text{ MVA} \times Z_{50\text{Hz}}} \\
&= \sqrt{100 \text{ MVA} \times 0.864\,\Omega} \\
&= 9.295 \text{ kV} .
\end{aligned} \tag{7.5}$$

To summarize, the rating of the SSG is 100 MVA, 3/50/9.295 kV with an inertia constant of 3.525 MWs/MVA. It has the same stability characteristics as LSG.

SSG must also be synchronized to the grid to initialize the test system for time domain simulation of the Generator Response Following concept. According to section 6.2.1 of [21] this is referred to as paralleling with the grid. Before connecting to the bus, the SSG and the PCC must have the same:

- Voltage

- Frequency

- Phase Sequence

- Phase.

In our case, since we are initializing a system for load-frequency control as defined in chapter 6, the voltage and the phase sequence are the same but the frequency and the phase are not. Before closing the breaker, the LSG will be slightly overloaded and therefore operating below rated frequency. The SSG will unloaded and therefore operating at a very high frequency. The frequency at the PCC must therefore be monitored in comparison to the frequency at the

SSG. This is done by measuring the frequency at either side of the breaker and subtracting one from the other to observe the phase difference between them.

Figure 7.4 is a plot of the phase difference between the PCC and the SSG just before the breaker closes at 17.96 seconds. The measurement is taken with two phased locked loop measurement devices and the two phase angles are subtracted from each other. The discontinuities in the measurement are jumps between 0° and 360° and are insignificant. The breaker needs to be closed as the phase angle θ passes 0°. In this case, the breaker is closed at about 15° which is small enough for the machine to lock in to the grid frequency without slipping poles.

Figure 7.4: SSG Synchronization, Breaker Phase Difference ($H_{DC} = 13.1$)
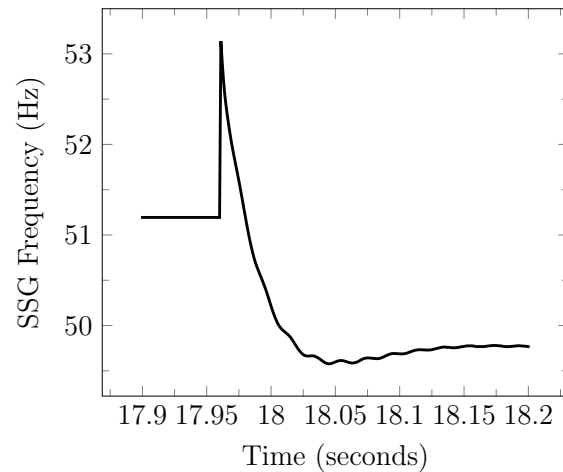
Figure 7.5: SSG Synchronization, SSG Frequency Zoom-In ($H_{DC} = 13.1$)

Figure 7.5 is a close-up of the SSG frequency during the synchronization. It dips down below rated frequency with a very steep slope as it seeks the grid frequency. Figure 7.6 is the SSG frequency superimposed over the grid frequency to demonstrate how quickly they synchronize and then settle to a new steady state. Now that all generation sources are supplying the load at rated conditions the network frequency converges to nominal operation at 50Hz. Figures 7.7 & 7.8 are the LSG and SSG power delivered to the load. SSG was operating at no-load and LSG was overloaded prior to the breaker closing. The droop controllers at each synchronous machine then determined the 100 MW load adjustment according to the theory and droop controller design parameters given in sections 6.1.4 & 6.2. A more detailed description of the theory and droop controller design applied specifically to this test circuit is given in section 8.1.

Figure 7.9 is the voltage during the transition. At the SSG, voltage was a bit high and steadily increasing prior to the breaker closing. This is because there was no load flow and no automatic voltage regulation. Once current starts flowing, there is not much problem maintaining steady state voltage. Once again, it should be emphasized that we are assuming manual excitation in this project to simplify the synchronous machine stability design. Voltage waveforms such as figure 7.9 may otherwise look very different.
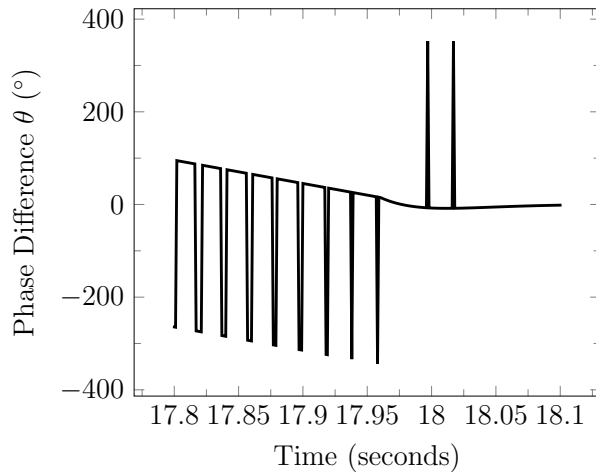
Figure 7.6: SSG Synchronization, Breaker Frequencies ($H_{DC} = 13.1$)

Figure 7.7: SSG Synchronization, LSG Power ($H_{DC} = 13.1$)
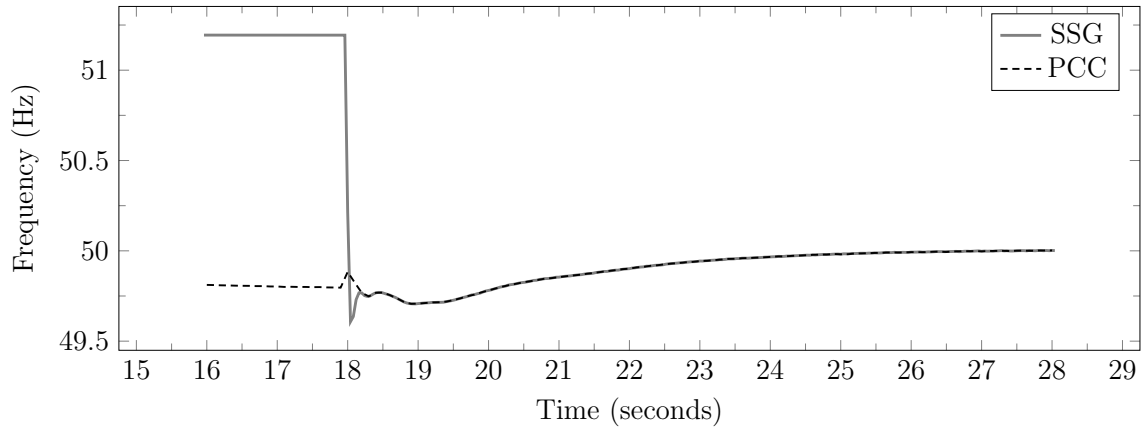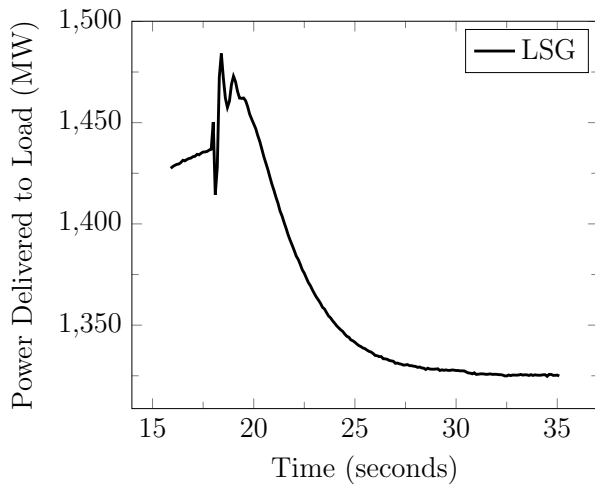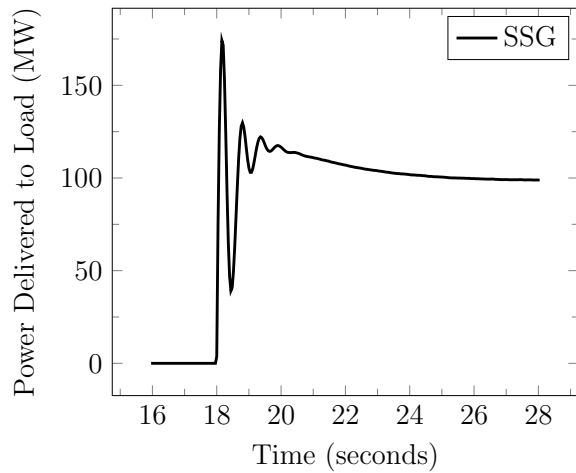
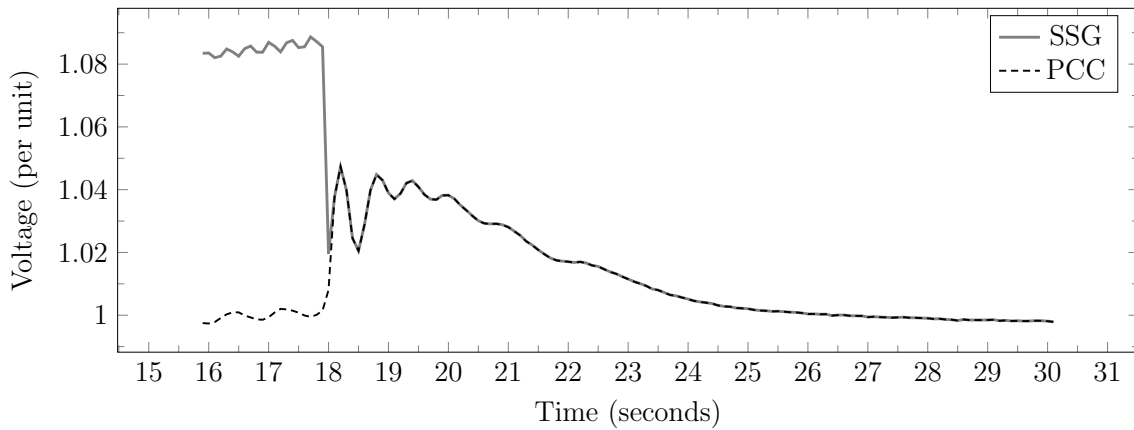Figure 7.8: SSG Synchronization, SSG Power ($H_{DC} = 13.1$)

Figure 7.9: SSG Synchronization, Breaker Voltages ($H_{DC} = 13.1$)

7.2   Communication Channels

In order to demonstrate the various design options available with the GRF method, both a communication-less and a fiber-optic communication channel are employed. Figures 1.1 & 1.2 of the reference circuit in section 1.4.2 are the onshore and the offshore network respectively and identify the path of these communication channels. Some characteristics identified in the following definitions have been previously developed and are referenced accordingly. The communication-less channel is defined in 7.2.1 and carries primary response information taken from the strong global frequency of the onshore AC grid. It is shown in figures 1.1 & 1.2 as a dotted line. The fiber-optic channel is defined in 7.2.2 and carries inertial response information taken directly from the SSG. This channel is shown in figures 1.1 & 1.2 as a dot-dash line.

7.2.1   Communication-less

According to [2], communication independent control schemes which rely only on local measurements must be developed. Rapid, reliable communication may be set up with the onshore AC grid through a cascaded droop control. In this way, frequency deviation information is transported from one AC grid to another with a voltage droop. Frequency regulation loops at the wind turbine level are then used to provide power increases or decreases based on AC collection grid frequency variations. This artificial coupling of the OWF to the main grid allows it to provide frequency support services as a traditional onshore windfarm would [2].

In this project, the communication-less channel is used to bring onshore frequency information to the offshore WTG for primary frequency regulation at the PCC. This is accomplished by exploiting the fact that V_{DC} is independent of power flow at GS-VSC (see section 4.2.1). Frequency is measured at the GS-VSC of the onshore AC grid and translated to voltage magnitude which is then applied to the DC transmission link (figure 4.7). DC current then compensates so that DC power can remain constant (figure 4.6). At WF-VSC, a feed-forward voltage associated with series line resistance is subtracted from the measured voltage. This allows the WF-VSC to read a voltage closer to that applied at GS-VSC before translating to frequency at the offshore AC collection grid (see figure 4.9). The AC voltage controls at WF-VSC provide a constant voltage magnitude and variable frequency source. This frequency is then received by the windfarm controller at the WTG which in-turn provides a primary response power flow. This controller is developed in section 7.3.2.

7.2.2   Fiber-Optic Communication

This method requires using the fiber-optic communication channel embedded in the sub-sea cable connection of a VSC-HVDC link to an OWF [5]. It should be noted that communication solutions can have performance and reliability problems. They can suffer from issues such as time delay, reduced data rate or complete loss of connection [2].

In this project, the fiber-optic channel provides the opportunity to separate primary response information from inertial response information. It is used to communicate inertial response information (as defined in section 7.1.2) from the SSG to the WTG. When properly applied to the overall power injection response of the OWF at the PCC, this inertial response information can have a stabilizing effect for the onshore AC network. This stabilizing effect has been quantified in section 7.1.1. The tuning process for application of the inertial response is demonstrated in section 8.3.

7.3 Windfarm

This section defines how the offshore windfarm is represented in this project. 7.3.1 outlines the aggregated wind turbine generator modelling technique. 7.3.2 develops the windfarm control strategy. These sections rely heavily on developments outlined in other parts of the report and therefore make many references.

7.3.1 Aggregated Wind Turbine Generator (WTG)

The aggregated wind turbine generator (WTG) in figure 1.2 is assumed to have a variable speed synchronous generator connected to the AC collection grid by a full scale back-to-back power converter and transformer as defined in section III-B of [23] and [6]. The power converter decouples generator speed from grid frequency and has full control over voltage magnitude on the grid side. These features allow the the WTG to be modelled as an ideal voltage source in this project. Since this is an aggregated representation of the WTG, an aggregated representation of the offshore cabling has also been defined in 4.2.2. This AC collection grid is a low X/R ratio system, power flow can therefore be regulated by changing voltage magnitude ([16], section 3.5.1). The ideal voltage source is fitted with controls that allow it to accept frequency information from the WF-VSC and vary the voltage magnitude relative to the WF-VSC voltage in order to deliver the requested power (see controller design in 7.3.2).

7.3.2 Windfarm Controller

The windfarm controller design in this project has two fundamental tasks: 1) Regulate power output based on information received from the two communication channels and 2) Enforce the decoupling of power and frequency. The first of these is the main task of the controller. It regulates power flow based on the assumption of an ideal voltage source (refer to 7.3.1) and a low X/R ratio network (defined in 4.2.2). The second task is necessary because the simplifying assumption of a resistive network for power regulation is not entirely true. There is still residual inductance in the network creating a minimal dependence between power and frequency. Since the controller power output depends on frequency information from the "communication-less" channel, power-frequency decoupling must be actively maintained.

The primary task of the windfarm controller is to regulate active power flow. The offshore AC collection grid has been defined in 4.2.2. Since this type of network has a low X/R ratio, power flow can be regulated according to the resistive network equation given in section 4.1.2, repeated here as:

$$
\begin{aligned}
S_{WTG} &= P_{WTG} + j\,Q_{WTG} \\
&= \left[\frac{E_{WTG}\,(E_{WTG} - E_{WF-VSC}\,\cos\delta)}{R_T}\right] + j\left[\frac{E_{WTG}\,E_{WF-VSC}\,\sin\delta}{R_T}\right]
\end{aligned}
\tag{7.6}
$$

where E_{WTG} is E_G from (4.4) and E_{WF-VSC} is E_{LD} from (4.4). As discussed in 3.2.5 & 4.2.3, E_{WF-VSC} can be regulated at 1 p.u. to facilitate the power regulation of the windfarm controller. Therefore, if we express (7.6) in per unit and assume δ to be small, it reduces to:

$$
S_{WTG} = \left[\frac{E_{WTG}\,(E_{WTG} - 1)}{R_T}\right] + j\left[\frac{E_{WTG}\,\delta}{R_T}\right].
\tag{7.7}
$$

As mentioned in section 7.3.1 the WTG is modelled as an ideal voltage source. Therefore, in order to regulate power according to (7.7), we use E_{WTG}. Figure 7.10 is the windfarm active power controller. It accepts frequency and power information from the two communication channels and calculates an active power reference. Notice that no time constants are used in the calculation of the active power reference. This branch of the windfarm controller assumes power is fully decoupled from frequency and therefore treats the frequency input as pure information. The PI controller then finds a value for E_{WTG} that matches the power measurement to the calculated reference.

The secondary task of the windfarm controller is to regulate reactive power flow in such a way that the effect of the residual inductance in the network is cancelled and power-frequency decoupling is maintained. This is accomplished by creating a dependence between reactive power and frequency. Frequency can be coupled to reactive power because δ is present in the Q_{WTG} component of (7.7). According to Section 3.4.3 of [16], this coupling equation is:
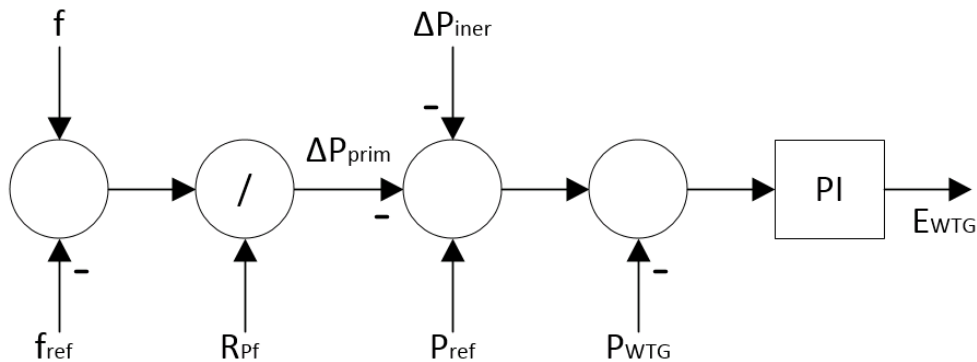
Figure 7.10: Windfarm Active Power Controller
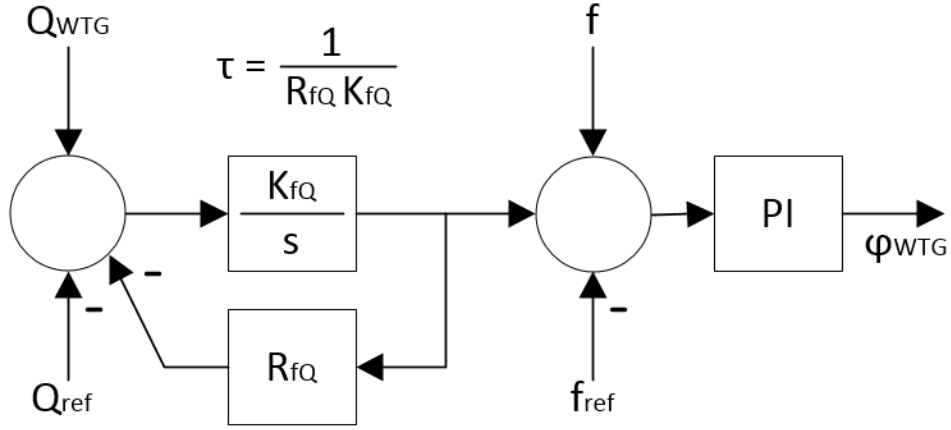
Figure 7.11: Windfarm Reactive Power Controller

$$\delta = \int \left[f_{WTG} - f_{WF-VSC} \right] dt$$
$$= \int \Delta f \, dt$$

(7.8)

where the frequencies are related to reactive power by $f = \frac{Q}{R_{fQ}}$, resulting in (expressed in derivative form):

$$\frac{\mathrm{d}\delta}{\mathrm{d}t} = \frac{Q_{WTG}}{R_{fQ}} - \frac{Q_{WF-VSC}}{R_{fQ}} \ .$$

(7.9)

Figure 7.11 is the reactive power regulation branch of the windfarm controller. Note that the output of the controller is power factor angle ϕ_{WTG}. Along with E_{WTG}, this is an input to the PSCAD/EMT$^{\mathrm{TM}}$ideal voltage source component that was chosen to represent the WTG. Reactive power is coupled to frequency by realizing the right side of (7.9). "$\frac{Q_{WTG}}{R_{fQ}}$" from (7.9) is the Qf droop controller at the WTG in figure 7.11. "$\frac{Q_{WF-VSC}}{R_{fQ}}$" from (7.9) represents the dynamics of the voltage source at WF-VSC freely regulating the frequency (see figure 4.9). The value of R_{fQ} at WTG is tuned experimentally to match those WF-VSC dynamics. The PI controller in figure 7.11 is essentially functioning as a plant. It is connecting the frequency regulation of the controller to an actual input (ϕ_{WTG}) for time domain simulation in PSCAD/EMT$^{\mathrm{TM}}$. Q_{ref} in figure 7.11 is chosen arbitrarily and can be zero.

Chapter 8

Simulation Results

Simulation results are presented in a way that outlines the different characteristics of the Generator Response Following method. First a primary response is given by the communication-less method. Then an inertial response is added in order to observe what happens relative to the original set of results. This data is split into two different scenarios, strong frequency grid and weak frequency grid. After final results have been presented, the optimization and variable selection process is outlined. Last, a few other waveforms are given which are relevant to the design process.

8.1   Primary Response from OWF

Figures 8.1 and 8.2 represent a primary response from the OWF by the "communication-less" channel for a strong frequency onshore grid scenario defined by

$$
\begin{aligned}
H_{DC} &= \frac{KE_{LSG} + KE_{SSG}}{P_{HVDC}} \\
&= \frac{H_{LSG}\,S_{LSG} + H_{SSG}\,S_{SSG}}{P_{HVDC}} \\
&= \frac{3.525 \times 1389 + 3.525 \times 100}{400} \\
&= 13.1\frac{MWs}{MW}
\end{aligned}
\tag{8.1}
$$

where KE is kinetic energy of the rotating mass in MWs, H is inertia constant in MWs/MVA, S is Apparent Power Rating in MVA and P is DC Power Rating in MW. Inertial response information was not sent to the windfarm for this example. This scenario is a simple asynchronous load change carried out by switching an additional resistance into the network parallel to the original load resistance at the PCC. The initial load is the rated load of the system and does not include transmission losses:

$$P_{LD,0} = 1800 \text{ MW}$$
$$R_{LD,0} = \frac{(245 \text{ kV})^2}{1800 \text{ MW}} \tag{8.2}$$
$$= 33.33 \, \Omega \, .$$

The final load adds a $1000 \, \Omega$ resistance in parallel to the original:

$$P_{LD,f} = (245 \text{ kV})^2 \times \left(\frac{1}{33.33 \, \Omega} + \frac{1}{1000 \, \Omega} \right) \tag{8.3}$$
$$= 1861 \text{ MW}$$

which again does not include transmission losses. As mentioned previously, this project assumes manual excitation from all synchronous generation sources in order to simplify the AC system stability design (see chapter 5). Manual excitation means there is no voltage regulation in the AC system. Therefore, manual step changes in excitation must be applied as inputs at LSG and SSG as described in section 5.5.2. In this project, these step changes are tuned by trial and error for any given load-frequency control scenario so that 1 p.u. voltage is always the final steady state at the load bus (PCC).
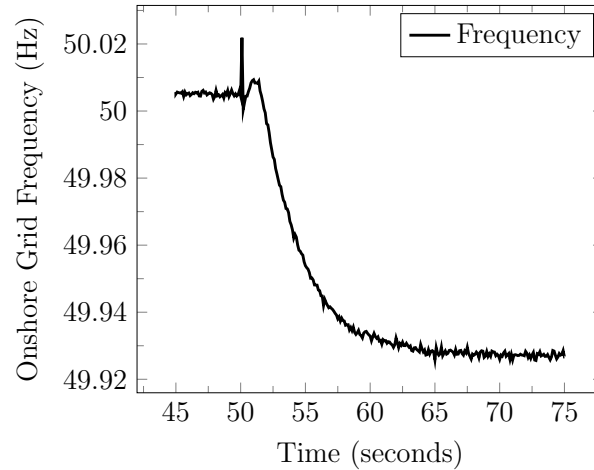

Figure 8.1: Grid Frequency with OWF Primary Response ($H_{DC} = 13.1$)

A theoretical calculation based on the theory outlined in chapter 6 is now also provided for comparison. It assumes the OWF contributes to system stiffness in terms of the regulation constant R_{eq} but not in terms of the AC damping coefficient D_{eq}. Our theoretical system stiffness as defined in section 6.1.1 is:
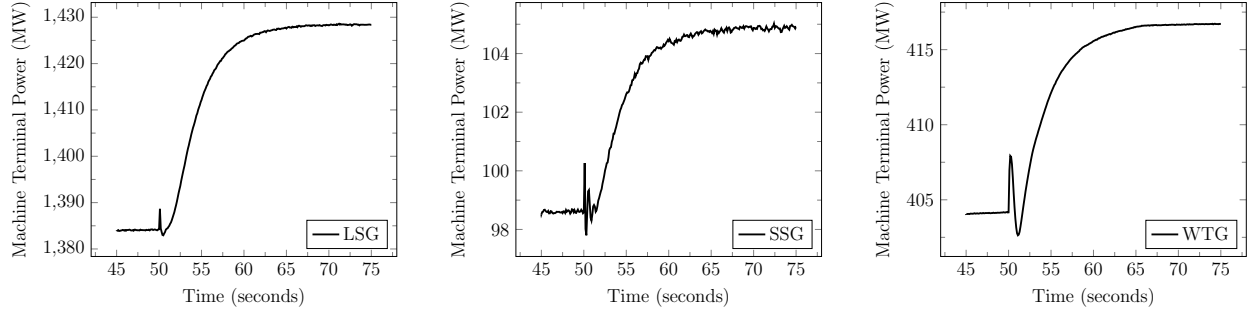
Figure 8.2: Power Injection with OWF Primary Response ($H_{DC} = 13.1$)

$$
\begin{aligned}
\beta_{eq} &= \frac{1}{R_{eq}} \times \frac{P_{LSG} + P_{SSG} + P_{WTG}}{50 \text{ Hz}} + D_{eq} \times \frac{P_{LD}}{50 \text{ Hz}} \\
&= \frac{1}{0.05} \times \frac{1389 \text{ MW} + 100 \text{ MW} + 400 \text{ MW}}{50 \text{ Hz}} + 1.5 \times \frac{1400 \text{ MW}}{50 \text{ Hz}} \\
&= \frac{1}{0.05} \times \frac{1889 \text{ MW}}{50 \text{ Hz}} + 1.5 \times \frac{1400 \text{ MW}}{50 \text{ Hz}} \\
&= 797.6 \, \frac{MW}{Hz} \ .
\end{aligned}
\tag{8.4}
$$

where D_{eq} is associated only with load supplied by AC generation. Our theoretical global frequency deviation combining (8.2), (8.3) and (8.4) according to section 6.1.4 is then:

$$
\begin{aligned}
\Delta f_{ss} &= \frac{-1}{\beta_{eq}} \left(P_{LD,f} - P_{LD,0} \right) \\
&= \frac{-1}{797.6 \text{ MW/Hz}} \left(1861 \text{ MW} - 1800 \text{ MW} \right) \\
&= {}^{-}0.076 \text{ Hz} \ .
\end{aligned}
\tag{8.5}
$$

Now, local calculations must be made to find the theoretical power deviation at each individual source. With some help from the load frequency design program in Appendix B regulation constants were chosen so that $R_{eq} = 0.05$ and the requirement given in (6.17) is observed:

$$
\begin{aligned}
\frac{1}{R_{eq}} \times \frac{1889 \text{ MW}}{50 \text{ Hz}} &= \left[\frac{1}{R_{LSG}} \times \frac{1389 \text{ MW}}{50 \text{ Hz}} \right] + \left[\frac{1}{R_{SSG}} \times \frac{100 \text{ MW}}{50 \text{ Hz}} \right] + \left[\frac{1}{R_{WTG}} \times \frac{400 \text{ MW}}{50 \text{ Hz}} \right] \\
\frac{1}{0.05} \times \frac{1889 \text{ MW}}{50 \text{ Hz}} &\approx \left[\frac{1}{0.0495} \times \frac{1389 \text{ MW}}{50 \text{ Hz}} \right] + \left[\frac{1}{0.0523} \times \frac{100 \text{ MW}}{50 \text{ Hz}} \right] + \left[\frac{1}{0.0510} \times \frac{400 \text{ MW}}{50 \text{ Hz}} \right] \\
755.6 \, \frac{MW}{Hz} &\approx \left[561.2 \, \frac{MW}{Hz} \right] + \left[38.2 \, \frac{MW}{Hz} \right] + \left[156.9 \, \frac{MW}{Hz} \right] \\
755.6 \, \frac{MW}{Hz} &\approx 756.3 \, \frac{MW}{Hz} \ .
\end{aligned}
$$

$$
\tag{8.6}
$$

Note that the per unit values from (8.6) are used in the PSCAD/EMT$^{\text{TM}}$model while the MW/Hz values are used for theoretical calculation. The load damping constants must be converted to individual machine bases from $D_{eq} = 1.5$ to meet the requirement defined in (6.18):

$$
\begin{aligned}
D_{eq} \times \frac{1489 \text{ MW}}{50 \text{ Hz}} &= \left[D_{LSG} \times \frac{1389 \text{ MW}}{50 \text{ Hz}}\right] = \left[D_{SSG} \times \frac{100 \text{ MW}}{50 \text{ Hz}}\right] \\
1.5 \times \frac{1489 \text{ MW}}{50 \text{ Hz}} &\approx \left[1.608 \times \frac{1389 \text{ MW}}{50 \text{ Hz}}\right] \approx \left[22.34 \times \frac{100 \text{ MW}}{50 \text{ Hz}}\right] \\
44.67 \, \frac{\text{MW}}{\text{Hz}} &\approx 44.67 \, \frac{\text{MW}}{\text{Hz}} \approx 44.68 \, \frac{\text{MW}}{\text{Hz}} \ .
\end{aligned}
\tag{8.7}
$$

Again, the per unit values from (8.7) are used in the PSCAD/EMT$^{\text{TM}}$model while the MW/Hz values are used for theoretical calculation. Change in local power output at each individual generation source can now be calculated from (8.5), (8.6) & (8.7) according to the local power equation in (6.19) & (6.20):

$$
\begin{aligned}
\Delta P_{LSG} &= \left(561.2 + 44.7\right)\frac{\text{MW}}{\text{Hz}} \times 0.076 \text{ Hz} \\
&= 46.0 \text{ MW} \\
\Delta P_{SSG} &= \left(38.2 + 44.7\right)\frac{\text{MW}}{\text{Hz}} \times 0.076 \text{ Hz} \\
&= 6.3 \text{ MW} \\
\Delta P_{WTG} &= \left(156.9\right)\frac{\text{MW}}{\text{Hz}} \times 0.076 \text{ Hz} \\
&= 12.2 \text{ MW} \ .
\end{aligned}
\tag{8.8}
$$

Table 8.1 summarizes the time domain results in figures 8.1 & 8.2 and the theoretical calculation in (8.5) & (8.8). Theory and simulation agree quite well with minimal error between the two. For comparison, time domain results from section 8.2 have also been included to observe the effects of an inertial response contribution from the OWF. With the inertial response in a strong grid scenario, the frequency deviation decreases, which in-turn decreases the output from the synchronous generation sources. The OWF then makes up the difference, supplying the power not supplied by the synchronous sources. With the inertial response in a weak grid scenario, this effect is amplified. The data represents an optimized scenario that contributes to the frequency stability of the onshore AC grid. Therefore the distorted steady state data given in the table may be an acceptable compromise in certain situations.

Method	Δf_{ss} (Hz)	ΔP_{LSG} (MW)	ΔP_{SSG} (MW)	ΔP_{WTG} (MW)	Total (MW)	Comments
Theory	-0.076	46.0	6.3	12.2	64.5	$H_{DC} = 13.1$
PSCAD	-0.077	44.1	6.3	12.5	62.9	$H_{DC} = 13.1$, Primary Response Only
PSCAD	-0.073	41.3	5.9	18.3	65.5	$H_{DC} = 13.1$, Primary & Inertial Response
PSCAD	-0.056	31.9	4.7	27.2	65.5	$H_{DC} = 0.92$, Primary & Inertial Response

Table 8.1: OWF Power Injection Summary

8.2 Primary & Inertial Response from OWF

Figures 8.3 & 8.4 represent a primary response combined with a synthetic inertia response from the OWF for a strong frequency onshore grid scenario as defined in (8.1). The response from section 8.1 has been superimposed over the plots for comparison. The most notable change is the increase in contribution from the WTG while the frequency deviation has decreased.
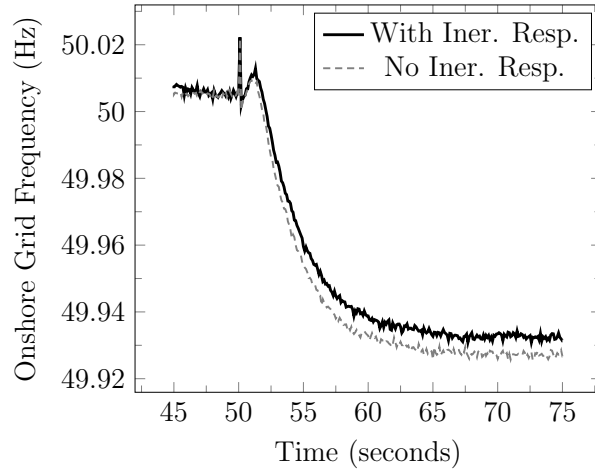
Figure 8.3: Grid Frequency with OWF Inertial Response ($H_{DC} = 13.1$)
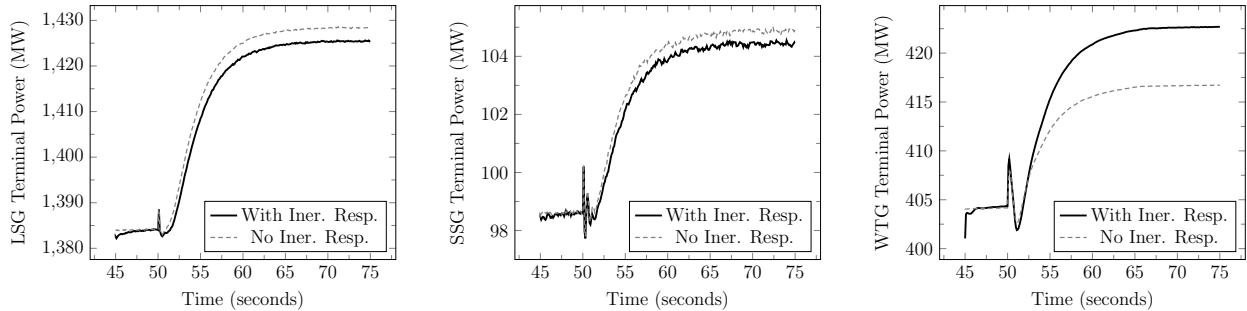
Figure 8.4: Power Injection with OWF Inertial Response ($H_{DC} = 13.1$)

Figures 8.5 & 8.6 represent a primary response combined with a synthetic inertia response from the OWF for a weak frequency onshore grid scenario defined by

$$
\begin{aligned}
H_{DC} &= \frac{KE_{LSG} + KE_{SSG}}{P_{HVDC}} \\
&= \frac{H_{LSG}\, S_{LSG} + H_{SSG}\, S_{SSG}}{P_{HVDC}} \\
&= \frac{0.01 \times 1389 + 3.525 \times 100}{400} \\
&= 0.92 \frac{MWs}{MW} \; .
\end{aligned}
\tag{8.9}
$$

In the figures, the background waveforms are the primary response for comparison. Since the frequency strength of the onshore AC network has been reduced we now see oscillations in the global frequency waveform due to the LSG inertial response. Oscillations in the individual power waveforms can also be observed depending on the size of the machine relative to the size of the whole test circuit. The waveforms in the foreground include the effects of the optimized synthetic inertia response. Gain and time delay of the inertia response information sent to the OWF from the SSG have been tuned in section 8.3. The process for the present test scenario has yielded a gain multiplier of 2.0 and a time delay of 0.01 seconds (see figures 8.7 & 8.8). A side effect of increasing the frequency strength of the onshore AC grid is an increased stiffness of the grid causing steady state values to deviate from those predicted by theory. The OWF then takes on the extra load that is no longer provided by the synchronous generation sources.
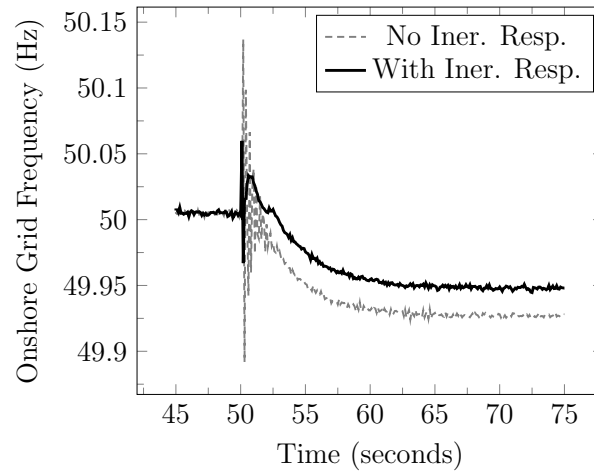
Figure 8.5: Grid Frequency with OWF Inertial Response ($H_{DC} = 0.92$)

8.3   Tuning and Interpreting Inertial Response

Application of gain and time delay to an inertial response signal may have an effect on AC system dynamic stability or steady state response. For the present study, gain multiplier and time delay were investigated by observing the effect on the onshore AC system frequency.
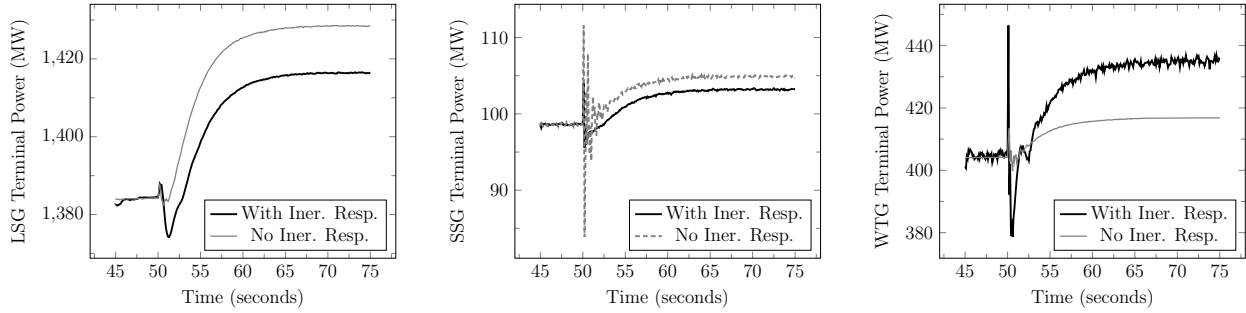
Figure 8.6: Power Injection with OWF Inertial Response ($H_{DC} = 0.92$)

Figures 8.7 & 8.8 are frequency plots for a range of gains and delays for a weak grid scenario defined by (8.9).

First, gain was held at 1.0 and a range of delays were simulated. Figure 8.7 is the transition point of the observed effect. Delays shorter than 0.01 seconds demonstrate a damping effect on the frequency waveform. Delays above 0.05 seconds do not. According to the data given in [24], latency of a fiber-optic communication channel about 400km in length can be calculated to approximately 200μs. Since this is well below the 0.01 seconds observed as being the transition point we can assume the latency associated with the presence of a fiber-optic cable in the system will have the desired damping effect on the frequency waveform. This effect is essentially a high pass filter and figure 8.9 is a diagram of this. The frequency of oscillation in the figure is about 5 Hz which has a period of 200ms. The cut-off frequency of the observed filtering effect begins to dampen the frequency waveform at about 20 Hz (0.05s) and the influence grows as the cut-off frequency increases to 100 Hz (0.01s).
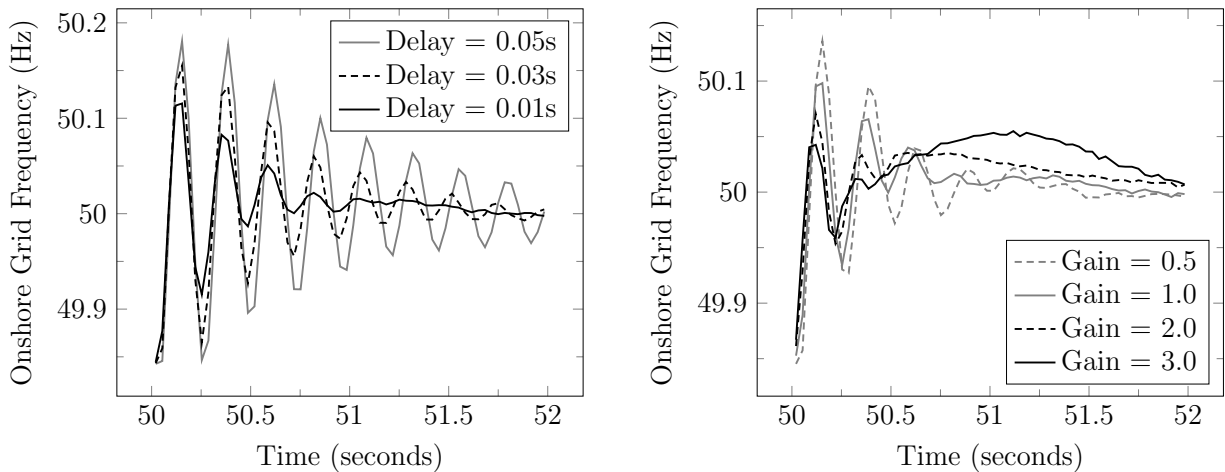
Figure 8.7: Delay Spectrum, Frequency Response (K = 2.0, $H_{DC} = 0.92$)

Figure 8.8: Gain Spectrum, Frequency Response ($\tau \leq 0.01$s, $H_{DC} = 0.92$)

Next, delay was held at 0.01 seconds and a range of gain multipliers were simulated. Figure 8.8 is the gain spectrum. The damping effect on the inertial response waveform increases as the gain multiplier increases. This suggests the frequency strength of the onshore AC grid is
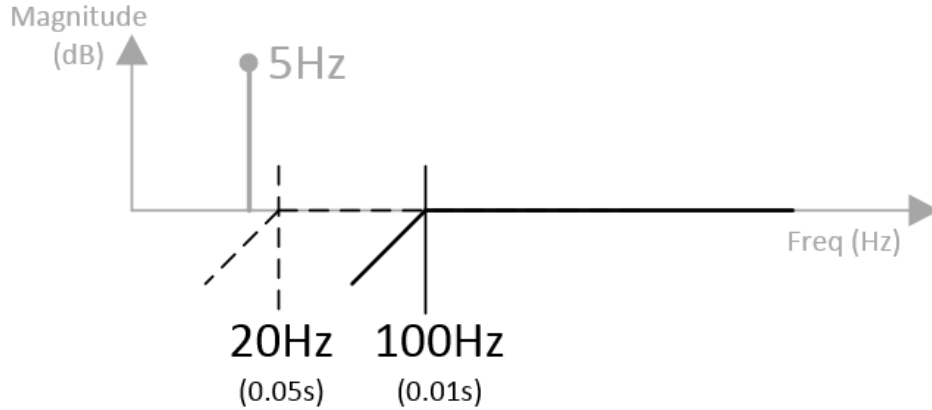
Figure 8.9: Filtering Effect of Delay Spectrum ($H_{DC} = 0.92$)

increasing as gain multiplier increases. Another harmonic appears in the waveform above a gain of 2.0 so a multiplier of 2.0 was chosen for this test scenario.

The spectrum in figure 8.10 is the same as in figure 8.8 except it is a strong frequency grid scenario and is plotted until steady state is reached. Steady state frequency response Δf_{ss} is decreasing as gain multiplier increases. We know from section 6.1.4 that AC grid stiffness increases as Δf_{ss} decreases and that this is associated with the primary responses of the generation in the system. In summary, AC grid stiffness is increasing as gain multiplier increases. We also know from the right side of figures 8.4 & 8.6 that the OWF is supplying the remainder of the load that the synchronous generation no longer provides due to the increase in stiffness.
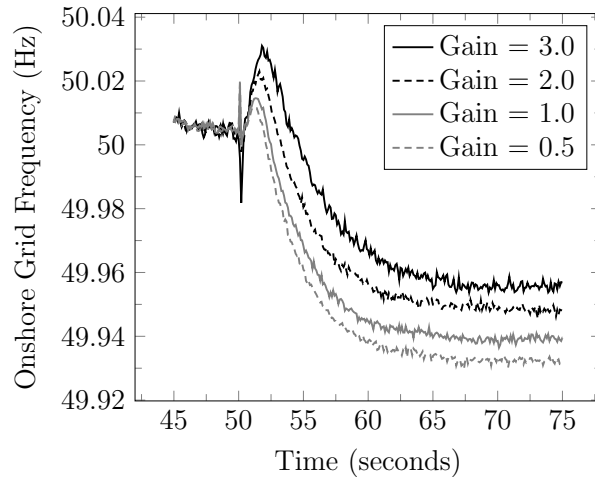
Figure 8.10: Gain Spectrum, Frequency Response ($\tau \leq 0.01$s, $H_{DC} = 13.1$)

We have been looking at trends and patterns in an attempt to balance and optimize the synthetic inertia effect of the GRF method. Now that it has been optimized, this effect might be quantified by setting $H_{WTG} = H_{SSG}$ in the per unit system. The associated kinetic

energy represented by this would then be:

$$KE_{WTG} = KE_{SSG} \, \frac{S_{WTG}}{S_{SSG}}$$
$$= H_{SSG} \, S_{WTG}$$
$$= 3.525 \text{ sec} \times 400 \text{ MW} \tag{8.10}$$
$$= 1410 \text{ MWs} \,.$$

However, since this is not mechanical inertia, the time rate of change of kinetic energy is more meaningful. The system must be designed so that the OWF power reserve is always greater than:

$$\frac{d}{dt} KE_{WTG} = \frac{K}{s\,\tau + 1} \, P_{iner}$$
$$= \frac{K/\tau}{s + 1/\tau} \, P_{iner}$$
$$= \frac{K}{\tau} \, P_{iner} \, e^{-t/\tau} \tag{8.11}$$
$$= \frac{2.0}{\tau \leq 0.01} \, P_{iner} \, e^{-t \,/\, (\tau \leq 0.01)}$$

where K and τ are the gain multiplier and time delay chosen above, P_{iner} is the inertial response power measurement at the SSG and $\frac{d}{dt} KE_{WTG}$ is the synthetic inertia response delivered to the WTG. A block diagram of (8.11) can also be found in the fiber-optic channel at the bottom of Figure 1.2.

Notice the amplitude modification applied to P_{iner} in (8.11) has time delay in the denominator. Although, the small delay associated with fiber-optic communication (appx. 200μs) has a very nice damping effect, a time delay that is too small may require too much power reserve from the OWF. For application of the method, time delay may be increased for a balance between the frequency stabilizing effect and a realistic power reserve.

8.4 Tuning the Communication-less Channel

As discussed in section 4.2.4 the communication-less channel is a cascaded droop, first converting onshore frequency deviation to HVDC voltage deviation (R_{Vf}), then to offshore frequency deviation (R_{fV}) and finally to power output at the windfarm controller (R_{Pf}). In 8.1 we chose $R_{WTG} = 0.051$ as our regulation constant for windfarm primary frequency response. Figure 8.11 is now a spectrum of OWF Power Injection plots and figure 8.12 is a spectrum of plots for DC Voltage at WF-VSC. These will be used for choosing R_{Vf} at GS-VSC.

According to (4.28), R_{WTG} is composed of the three cascaded regulation constants mentioned above. In this project, the initial estimate for these constants was:
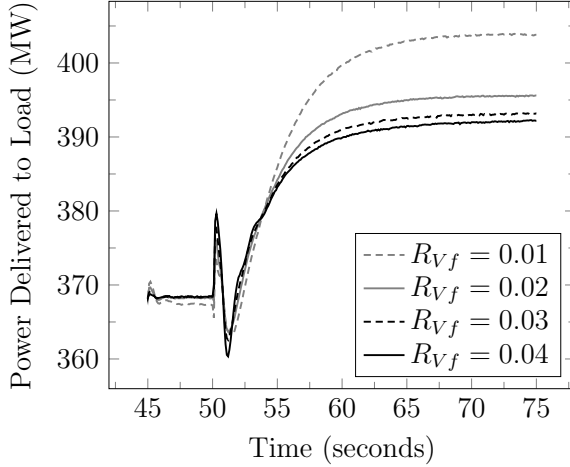
Figure 8.11: R_{Vf} Spectrum, WTG Power Injection ($H_{DC} = 13.1$)
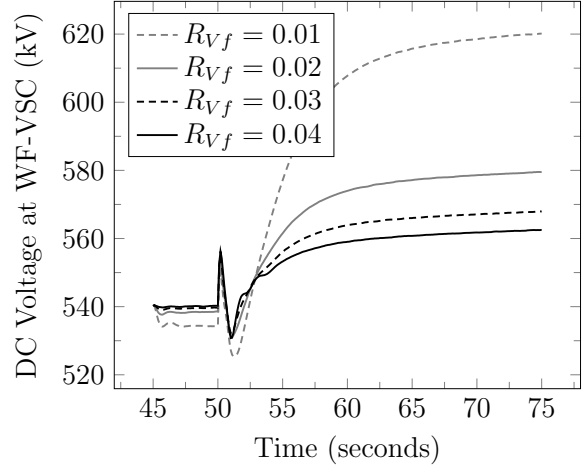
Figure 8.12: R_{Vf} Spectrum, v_{DC} at WF-VSC ($H_{DC} = 13.1$)

$$R_{WTG} = R_{Vf}\, R_{fV}\, R_{Pf}$$
$$0.051 = 0.05 \times 1.00 \times 1.02 \ . \tag{8.12}$$

In figure 8.11 each plot conforms to $R_{WTG} = 0.051$ by varying R_{Pf}. The integration constants (K) are also chosen so that $\tau = 50$ ms for each plot (see sections 4.2.3 & 4.2.4). In the figure, final steady state decreases as R_{Vf} increases. Increasing R_{Vf} beyond 0.06 leads to instability. In figure 8.12 we have a similar pattern, final steady state decreases as R_{Vf} increases. Again, further increase beyond 0.06 leads to instability. A rule of thumb has been given in section 2.3.4 to limit voltage deviations to approximately 15%. This would correspond to the "$R_{Vf} = 0.01$" scenario. Since this is certainly not the largest load change this system might encounter, a value greater than 0.01 should be chosen. Also, since steady states seem to converge to similar values above 0.02, this may be a good choice for the design. The choice of cascaded regulation constants for this project is therefore:

$$R_{WTG} = R_{Vf}\, R_{fV}\, R_{Pf}$$
$$0.051 = 0.02 \times 1.00 \times 2.55 \ . \tag{8.13}$$

Sample and Hold operations are then used as described in section 4.2.4 to further enhance the steady state stability.

8.5   Other Significant Waveforms

Figure 8.13 is the RMS voltage at the load bus (PCC). There is a small oscillation at steady state after primary response of the system to a load disturbance but it is stable at 1 pu magnitude. In this project, manual excitation has been assumed in order to simplify the

synchronous machine stability design (Chapter 5). This means there is no voltage regulation on the AC network. Simulation has therefore been performed keeping a close watch on PCC voltage as the accuracy of every simulation depends on this waveform converging to 1 pu. The voltage is controlled by adjusting the manual excitation input at LSG as described in section 5.5.2.
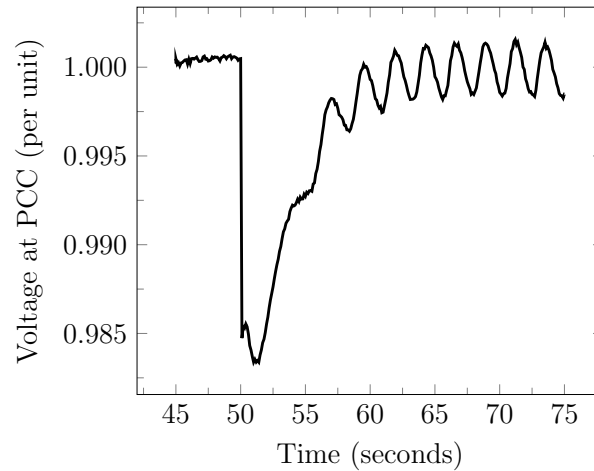
Figure 8.13: RMS Voltage at Load Bus ($H_{DC} = 13.1$)

Figures 8.14 & 8.15 are the first leg and the second leg of the communication-less channel respectively. They correspond to the scenario given in figures 8.3 & 8.4.
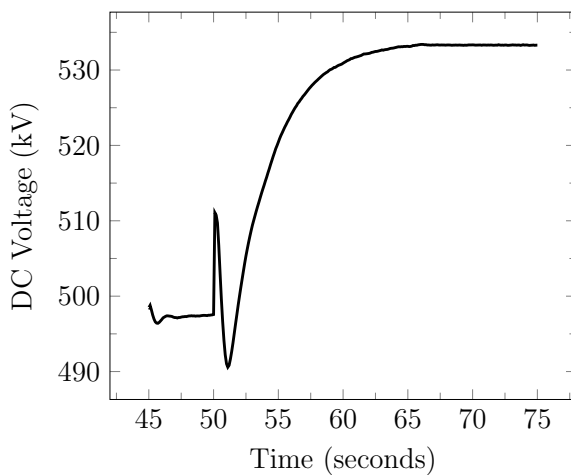
Figure 8.14: DC Voltage at GS-VSC ($H_{DC} = 13.1$)
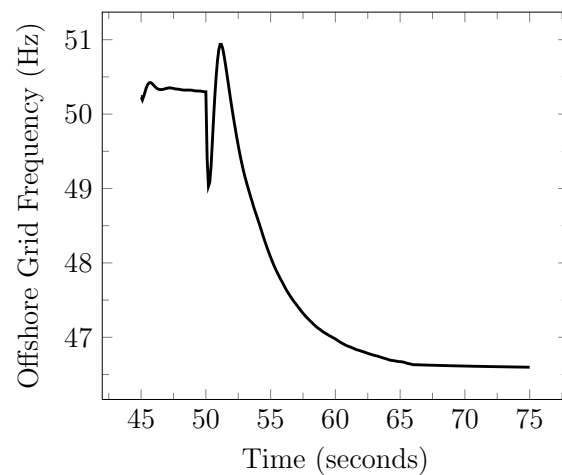
Figure 8.15: Frequency at WF-VSC ($H_{DC} = 13.1$)

As a comparison, onshore grid frequency deviation can be calculated from figure 8.14 and R_{Vf} chosen in (8.13):

$$\begin{aligned}
\Delta v_{DC} &= (533.3 \text{ kV} - 497.5 \text{ kV}) \,/\, 500 \text{ kV} \\
&= 35.8 \text{ kV} \,/\, 500 \text{ kV} \\
&= 0.0716 \text{ pu} \\
\Delta f &= {}^{-}\Delta v_{DC} \times R_{Vf} \times 50 \text{ Hz} \\
&= {}^{-}0.0716 \text{ pu} \times 0.02 \times 50 \text{ Hz} \\
&= {}^{-}0.072 \text{ Hz} \,.
\end{aligned} \tag{8.14}$$

Likewise, DC voltage deviation can be calculated from figure 8.15 and R_{fV} chosen in (8.13):

$$\begin{aligned}
\Delta f &= (46.6 \text{ Hz} - 50.3 \text{ Hz}) \,/\, 50 \text{ Hz} \\
&= {}^{-}3.7 \text{ Hz} \,/\, 50 \text{ Hz} \\
&= {}^{-}0.074 \text{ pu} \\
\Delta v_{DC} &= {}^{-}\Delta f \times R_{fV} \times 500 \text{ kV} \\
&= 0.074 \text{ pu} \times 1.00 \times 500 \text{ kV} \\
&= 37.0 \text{ kV}
\end{aligned} \tag{8.15}$$

and matches reasonably well with (8.14).

Chapter 9

Conclusion

9.1 Summary

The literature survey in chapter 2 explores various control strategies that have been proposed that enable VSC-HVDC connected offshore windfarms to provide synthetic inertia services to the onshore AC grid through active power injection. This includes dedicated control strategies at the grid-side VSC as well coordinated methods which utilize a combination of strategies across the decoupled asynchronous system to accomplish the desired outcome. Each method has advantages and disadvantages. Based on the survey, an optimized control strategy might have a synthetic inertial response which allows the designer to specify the inertia constant. The designer would have the freedom to increase the size of the inertia constant while keeping the DC link capacitor size within reason and without much dependence on DC voltage deviation limit. Ideally, this constant would be completely independent of capacitor size and DC voltage deviation. The method would also be able to contribute to the minimization of the steady state frequency deviation. The synthetic inertia design would be accomplished with minimal cost to the owner/operator and would not be site specific.

Generator Response Following is presented as a possible design solution which includes some of these desired characteristics. A theoretical outline of the Generator Response Following concept is also developed. The design solution is intended to outline the design possibilities available with communication channels that can function independently of each other. For example, simulation has been used to show that manipulating inertial response information, before combining with primary response, may be beneficial to onshore AC system dynamic stability (section 8.3). This effect may be quantified as an inertia constant but the time rate of change of the kinetic energy associated with that inertia constant may be more meaningful in this case. Simulation has also been used to show that the primary response feature contributes to steady state frequency regulation as power injection is adjusted based on this frequency. The method is therefore contributing to the AC system frequency stiffness. It should be emphasized that this study uses the simplifying assumption of manual excitation from all contributing synchronous machines.

For installation feasibility or economic reasons, a real world implementation of the concept

may be different from the above. For example, the installation of a SSG at the PCC for the sole purpose of providing inertial support to the OWF may not be economically practical. In this case, a synchronous condenser or a pre-existing synchronous generator located near the PCC might be used. Prior experience also suggests that the SSG can have a power rating as low as $5\% \times$ OWF power capacity and still be effective. A torque measurement at the shaft to separate primary response information from inertial response information also may not be realistic. Other possible implementations include a simple power measurement at the machine terminals or an offshore real-time calculation of a synchronous power flow response rather than "following" a measurement from another machine onshore. In summary, Generator Response Following is a promising method that can offer design flexibility for balancing economic needs with stability concerns when frequency support services are required from VSC-HVDC connected offshore windfarms.

9.2   Recommendations and Future Work

The data presented in section 8.3 suggests that as the frequency strength of the AC grid decreases and the GRF method is called upon to contribute to the frequency stability of the network, the frequency stiffness will be artificially increased as well. This means that the planned steady state frequency deviation of the AC grid load-frequency control may may need to be adjusted. The controller settings at the individual synchronous generation sources could be modified to accommodate a frequency stiffness that includes the effects of OWF power injection by the GRF method.

Most AC networks use Automatic Voltage Regulation to control the voltage magnitude of the source and load components on the system. In this project, it was decided that dynamic simulation of voltage regulation is a task far too complex for the allotted time. This study should be expanded to include the effects of Automatic Voltage Regulation and Power System Stabilization to be relevant for application of the method.

A real-time calculation of a synchronous power flow response at the OWF has also been suggested in place of the small synchronous generator. This method would have the obvious benefit of lower cost and would be a valid topic to investigate further.

Bibliography

[1] Zhu, J., Guerrero, J., Hung, W., Booth, C., Adam, G.. Generic inertia emulation controller for multi-terminal voltage-source-converter high voltage direct current systems. IET Renewable Power Generation 2014;8(7):740–748.

[2] Moreira, C., Gouveia, J., Silva, B.. Participation of multi-terminal hvdc grids in frequency regulation services. Institute of Electrical and Electronics Engineers Inc.; 2015, p. 202–209.

[3] Gonzalez-Longatt, F.. Frequency control and inertial response schemes for the future power networks. Green Energy and Technology 2014;:193–231.

[4] Li, Y., Zhang, Z., Yang, Y., Li, Y., Chen, H., Xu, Z.. Coordinated control of wind farm and vsc-hvdc system using capacitor energy and kinetic energy to improve inertia level of power systems. International Journal of Electrical Power and Energy Systems 2014;59:79–92.

[5] Martinez Sanz, I., Chaudhuri, B., Strbac, G.. Inertial response from offshore wind farms connected through dc grids. IEEE Transactions on Power Systems 2015;30(3):1518–1527.

[6] Tedeschi, E.. Elk-23 power electronics in future power systems. Norwegian University of Science and Technology, Trondheim, Norway. University Lecture; 2016.

[7] Dang, J., Tang, Y., Song, M., Ning, J., Fu, X.. Coordinated frequency control of thermal units with dc system in a wind-thermal-bundled system transmitted by high voltage direct current (hvdc) line. CRC Press/Balkema; 2015, p. 7–12.

[8] Yu, M., Dysko, A., Booth, C., Roscoe, A., Zhu, J.. A review of control methods for providing frequency response in vsc-hvdc transmission systems. Proceedings of the Universities Power Engineering Conference; 2014,.

[9] Elansari, A., Finney, S., Burr, J., Edrah, M.. Frequency control capability of vsc-hvdc transmission system. vol. 2015. Institution of Engineering and Technology; 2015,.

[10] Liu, X., Lindemann, A.. Coordinated control of vsc-hvdc connected offshore windfarms for enhanced ability of providing synthetic inertia. Institute of Electrical and Electronics Engineers Inc.; 2015,.

[11] Bauer, P.. Et4116 power electronics. Delft University of Technology, Delft, Netherlands. University Lecture; 2016.

[12] Mohan, N., Undeland, T., Robbins, W.. Power electronics, converters, applications and design, 3rd ed. John Wiley and Sons, Inc.; 2003.

[13] Blasko, V., Kaura, V.. A new mathematical model and control of a three-phase ac–dc voltage source converter. IEEE Transactions on Power Electronics 1997;12(1):116–122.

[14] Bajracharya, C., Molinas, M., Suul, J., Undeland, T.. Understanding of tuning techniques of converter controllers for vsc-hvdc. 2008,.

[15] Kundur, P.. Power system stability and control. McGraw-Hill, Inc.; 1994.

[16] Hatziargyriou, N.. Microgrids, architectures and control. John Wiley and Sons, Ltd.; 2014.

[17] Kim, C., Sood, V., Jang, G., Lim, S., Lee, S.. HVDC transmission, power conversion applications in power systems. John Wiley and Sons (Asia), Pte. Ltd.; 2009.

[18] Jóhannson, H.. 31750 - power system stability and control. Technical University of Denmark, Lyngby, Denmark. University Lecture; 2015.

[19] Haileselassie, T.. Control, dynamics and operation of multi-terminal HVDC transmission systems. PhD Thesis: Norwegian University of Science and Technology; 2012.

[20] Nexans, . Nexans submarine cables. 2013. URL: `https://www.nexans.co.uk/eservice/UK-en_GB/navigate_3495/Submarine_Medium_Voltage_cables.html#doc_and_info`.

[21] Sen, P.. Principles of electric machines and power electronics, 2nd ed. John Wiley and Sons, Inc.; 1997.

[22] Hoeijmakers, M.. Modelling of AC machines. Delft University of Technology; 2004.

[23] Blaabjerg, F., Liserre, M., Ma, K.. Power electronics converters for wind turbine systems. IEEE Transactions on Industry Applications 2012;48(2):708–719.

[24] Coffey, J.. Latency in optical fiber systems. 2017. URL: `www.commscope.com/Docs/Latency_in_optical_fiber_systems_WP-111432-EN.pdf`.

Appendix A

Machine Stability Program

This MATLAB program is based on the derivation in chapter 5. It is used to check the small signal stability of the synchronous machines used in this project so that they can withstand standard load disturbances without losing synchronization.

Load Inputs

```matlab
 1  function [Lad,Laq] = LoadParameters()
 2  global Lal Lfdl Lkdl Lkql
 3  global Req Leq1 Leq2 H KD
 4  global Ra Rfd Rkd Rkq
 5  global omega_sbase omega_r theta_0
 6  global Xeq1 Xeq2
 7  global Xdp Td0p
 8  global NAME
 9
10  theta_0 = 0 ;
11
12  % ORIGINAL INFORMATION IS FOR ONE UNIT
13  S_60 = 555E6 ;
14  V_60 = 24E3 ;
15  Z_60 = V_60^2 / S_60 ;
16
17  % MY MACHINE IS DERATED FOR 50Hz
18  f1 = 50 ;
19  S_50 = S_60 * f1/60 ;
20  V_50 = V_60 * f1/60 ;
21  Z_50 = V_50^2 / S_50 ;
22
23  Req = 0 ;
24  Leq1 = 0 ;
25  Leq2 = 0 ;
26  H = 3.525 ;
27  KD = 0 ;
28
```

```matlab
29  omega_sbase = 2*pi*f1 ; % RADIANS PER SECOND
30  Lad  = 1.66  *  Z_60/Z_50  ;
31  Laq  = 1.61  *  Z_60/Z_50  ;
32  Lal  = 0.15  *  Z_60/Z_50  ;
33  Lfdl = 1.65E-1 *  Z_60/Z_50  ;
34  Lkdl = 1.713E-1 *  Z_60/Z_50  ;
35  Lkql = 7.252E-1 *  Z_60/Z_50  ;
36  Lk2ql = 1.25E-1 *  Z_60/Z_50  ;
37
38  Ra  = 3.00E-3 *  Z_60/Z_50  ;
39  Rfd = 6.00E-4 *  Z_60/Z_50  ;
40  Rkd = 2.84E-2 *  Z_60/Z_50  ;
41  Rkq = 6.19E-3 *  Z_60/Z_50  ;
42  Rk2q = 2.368E-2 *  Z_60/Z_50  ;
```

Initialize State Vectors

```matlab
1  function  [ EBm, delta , e_fd , psi_fd , psi_ad , psi_aq , i_d , i_q , e_d , e_q ] = ...
2            initialize_state_vector(Et,Pt,Qt,Lad,Laq) % Q.3.1 , Q.3.2 , Q.3.3
3  global  Lal Lfdl Lkdl Lkql Rfd Ra
4  global  Leq1 Leq2 Xdp Xeq1 Xeq2
5  global  omega_sbase omega_r alpha theta_0
6
7  Xeq1 = omega_r*Leq1 ;
8  Xeq2 = omega_r*Leq2 ;
9  Xeq = Xeq1 + Xeq2 ;
10 Xd  = omega_r*(Lad + Lal) ; % [1 , equ  3.111  3.147]
11 Xq  = omega_r*(Laq + Lal) ; % [1 , equ  3.112  3.147]
12 Xad = omega_r*Lad ;
13 Xaq = omega_r*Laq ;
14
15 % [1 , equ  3.64  3.67  3.68  3.65  3.69]  Original for of the equations
16 % [1 , equ  3.92  3.98  3.99  3.93  3.100]  Modified for per unit respectively
17 LD_mat = [ -(Lad + Lal) Lad          Lad ; ...
18            -Lad          Lad + Lfdl Lad ; ...
19            -Lad          Lad         Lad + Lkdl ; ...
20            -Lad          Lad         Lad ] ; % Q.1.1 [ Line added for psi_ad]
21
22 LQ_mat = [ -(Laq + Lal) Laq ; ...
23            -Laq          Laq + Lkql ; ...
24            -Laq          Laq ] ; % Q.1.2 [ Line added for psi_aq]
25
26
27 %% CALCULATE STATE VECTORS
28
29 Itm = sqrt(Pt^2 + Qt^2)/Et ;
30 phi = -atan(Qt/Pt) ;
31 It = Itm*(cos(phi) + 1i*sin(phi)) ;
32 EB = Et - 1i*Xeq*It ;
33 Eq = Et + (Ra+1i*Xq)*It ;
34
```

```matlab
35  % FOR COMPARISON TO PSCAD, KUNDUR PG 100, 30JAN17RM
36  Xs = sqrt(Xd^2 + Xq^2) ;
37  Es = Et + (Ra+1i*Xs)*It ;
38  Ed = Et + (Ra+1i*Xd)*It ;
39  Efd_PSCAD = abs(Ed) ;
40  delta_PSCAD = abs(angle(Es)) ;
41
42  % REDEFINE THE VECTORS FOR GENERATOR CONVENTION RELATIVE TO Q-AXIS FOR
43  % COMPARISON TO KUNDUR EXAMPLE 12.3. ABSOLUTE VALUE OF ALL ANGLES IS USED
44  % HERE TO AVOID CONFUSION. THIS IS JUST FOR COMPARISON.
45  Etm = Et ;
46  EBm = abs(EB) ;
47  Eqm = abs(Eq) ;
48  phi = abs(phi) ;
49  delta_eq = abs(angle(EB)) ;
50  delta_sg = abs(angle(Eq)) ;
51  delta = delta_eq + delta_sg ;
52  delta_check = atan((Xq*Itm*cos(phi) - Ra*Itm*sin(phi)) ...
53                 / (Etm + Ra*Itm*cos(phi) + Xq*Itm*sin(phi))) ;
54
55  % It ASSUMES OVER-EXCITED PF
56  Eq = 1i*Eqm ;
57  Et = Etm*(cos(pi/2 - delta_sg) + 1i*sin(pi/2 - delta_sg)) ;
58  It = Itm*(cos(pi/2 - delta_sg - phi) + 1i*sin(pi/2 - delta_sg - phi)) ;
59  EB = EBm*(cos(pi/2 - delta) + 1i*sin(pi/2 - delta)) ;
60
61  e_d = real(Et) ;
62  e_q = imag(Et) ;
63  i_d = real(It) ;
64  i_q = imag(It) ;
65
66  i_fd = (e_q + Ra*i_q + Xd*i_d) / Xad ; % [1, equ 3.147]
67  e_fd = i_fd * Rfd ; % [1, pg 102]
68
69  % [1, pg 93] All amortisseur currents are zero in steady state
70  xD = LD_mat * [i_d i_fd 0]' ;
71  xQ = LQ_mat * [i_q 0]' ;
72  Te_PSCAD = xD(1)*i_q - xQ(1)*i_d ;
73
74  psi_fd = xD(2) ;
75  psi_ad = xD(4) ;
76  psi_aq = xQ(3) ;
77
78
79  %% SOME STATE VARAIBLE ASSIGNMENTS AND PRINTING
80
81  % Test of Function
82  fprintf('\n—————————————————————————')
83  fprintf('\nInitial values')
84  fprintf('\n—————————————————————————')
85  fprintf('\nIt = %.3f pu',Itm)
86  fprintf('\nphi = %.3f rad, %.3f deg',phi,phi/pi*180)
87  fprintf('\n—————————————————————————')
88  fprintf('\nEB = %.3f pu',EBm)
```

```
89   fprintf('\nEt = %.3f pu',Etm)
90   fprintf('\ndelta_eq = %.3f rad, %.3f deg',delta_eq,delta_eq/pi*180)
91   fprintf('\n————————————————————————')
92   fprintf('\nEq = %.3f pu',Eqm)
93   fprintf('\ndelta_sg = %.3f rad, %.3f deg',delta_sg,delta_sg/pi*180)
94   fprintf('\n————————————————————————')
95   fprintf('\ndelta = %.3f rad, %.3f deg\n',delta,delta/pi*180)
96   fprintf('\nEfd_PSCAD = %.3f pu',Efd_PSCAD)
97   fprintf('\ndelta_PSCAD = %.3f rad, %.3f deg',delta_PSCAD ...
98                                      ,delta_PSCAD/pi*180)
99   fprintf('\nTe_PSCAD = %.3f pu\n\n',Te_PSCAD)
100
101  fprintf('\ne_d  = %.3f pu',e_d)
102  fprintf('\ne_q  = %.3f pu',e_q)
103  fprintf('\ni_d  = %.3f pu',i_d)
104  fprintf('\ni_q  = %.3f pu',i_q)
105  fprintf('\ni_fd = %.3f pu\n\n',i_fd)
106
107  fprintf('\nPsi_d  = %.3f pu',xD(1))
108  fprintf('\nPsi_q  = %.3f pu',xQ(1))
109  fprintf('\nPsi_fd = %.3f pu',psi_fd)
110  fprintf('\nPsi_kd = %.3f pu',xD(3))
111  fprintf('\nPsi_kq = %.3f pu\n\n',xQ(2))
```

Main Program

```
1    clear all; close all; clc;
2
3    % Define global variables that are to be used in the simulation
4    global A B xD0 uD0
5    global Req H M KS KD
6    global Leq1 Leq2
7    global Lal Lfdl Rfd Ra
8    global omega_sbase omega_r alpha theta_0
9
10   %% INPUTS AND CONTROL VARIABLES
11
12   MODE = 1 ; % SPECIFY THE OSCILLATING MODE TO OBSERVE
13   omega_r = 1.00 ; % PER UNIT
14   Etmp = 1.00 ;
15   Ptmp = 1.0 ; % 0.9 ;
16   Qtmp = 0.04 ; % Ptmp/3 ;
17
18   Asat = 0.03215 ;
19   Bsat = 6.931 ;
20   psi_T1 = 0.8 ;
21
22
23   %% LOAD VARIABLES AND INITIALIZE STATE VECTORS
24
25   % Load Basic Parameters
```

```
26  [Ladu,Laqu] = LoadParameters ;
27
28  % THIS COUNTERBALANCES THE "NEGLECT P_PSI STATOR" SIMPLIFYING ASSUMPTIONS
29  % BY REMAINING 1.00 FOR ALL STATOR SMALL SIGNAL ASSOCIATIONS [KUNDUR, 5.1]
30  %
31  omega_rp = 1.00 ;
32
33  Xeq = omega_rp*(Leq1 + Leq2) ;
34  Xdu  = omega_rp*(Ladu + Lal) ; % [1, equ 3.111 3.147]
35  Xqu  = omega_rp*(Laqu + Lal) ; % [1, equ 3.112 3.147]
36  Xadu = omega_rp*Ladu ;
37  Xaqu = omega_rp*Laqu ;
38
39
40  %% UNSATURATED STATE VECTOR
41
42
43  Et0 = Etmp ; % PER UNIT
44  Pt0 = Ptmp ; % PER UNIT
45  Qt0 = Qtmp ; % PER UNIT, POSITIVE FOR OVEREXCITED
46  [EB0,delta_0u ,e_fd0u ,psi_fd0u ,psi_ad0u ,  ...
47   psi_aq0u ,i_d0u ,i_q0u ,e_d0u ,e_q0u] = ...
48   initialize_state_vector (Et0,Pt0,Qt0,Ladu,Laqu) ;
49
50
51  %% INITIAL SATURATED STATE VECTOR
52
53  Et0 = Etmp ; % PER UNIT
54  Pt0 = Ptmp ; % PER UNIT
55  Qt0 = Qtmp ; % PER UNIT, POSITIVE FOR OVEREXCITED
56
57  [KSD0,DUMMY] = SaturationFactor (Et0,Pt0,Qt0,Asat ,  ...
58                                  Bsat ,psi_T1 ,Ra,omega_rp*Lal) ;
59  [EB0,delta_0 ,e_fd0 ,psi_fd0 ,psi_ad0 ,psi_aq0 ,i_d0 ,i_q0 ,e_d0 ,e_q0] = ...
60   initialize_state_vector (Et0,Pt0,Qt0,KSD0*Ladu,KSD0*Laqu) ;
61
62  Efd0 = e_fd0/Rfd * omega_r*Ladu ; % EQU 12.116 b32, THIS IS UNSATURATED
63  Eq0s = e_fd0/Rfd * omega_r*KSD0*Ladu ; % EQU. 3.171, THIS IS SATURATED
64
65
66  %% FINAL SATURATED STATE VECTOR
67
68  Etf = Etmp ;
69  Ptf = Ptmp ;
70  Qtf = Qtmp ; % POSITIVE FOR OVEREXCITED
71
72  [KSDF,KSDI] = SaturationFactor (Etf,Ptf,Qtf,Asat ,  ...
73                                  Bsat ,psi_T1 ,Ra,omega_rp*Lal) ;
74  [EBf,delta_f ,e_fdf ,psi_fdf ,psi_adf ,psi_aqf ,i_df ,i_qf ,e_df ,e_qf] = ...
75   initialize_state_vector (Etf,Ptf,Qtf,KSDF*Ladu,KSDF*Laqu) ;
76
77  Efdf = e_fdf/Rfd * omega_r*Ladu ; % EQU 12.116 b32, THIS IS UNSATURATED
78  Eqfs = e_fdf/Rfd * KSDF*omega_r*Ladu ; % EQU. 3.171, THIS IS SATURATED
79
```

```
80
81  %% INCREMENTAL SATURATION
82
83  % STATE MATRICES USE KSDI INCREMENTAL SATURATION AND OSCILLATE ABOUT KSDF
84  % TOTAL SATURATION
85  Lads = KSDI*Ladu ;
86  Laqs = KSDI*Laqu ;
87  Xds  = omega_rp*(Lads + Lal) ; % [1, equ 3.111 3.147]
88  Xqs  = omega_rp*(Laqs + Lal) ; % [1, equ 3.112 3.147]
89  Xads = omega_rp*Lads ;
90  Xaqs = omega_rp*Laqs ;
91
92
93  %% CALCULATE STATE MATRICES (EQU. 12.115,116)
94
95  M = 2*H ;
96  RT = Req + Ra ;
97  Ladsp = 1/(1/Lads + 1/Lfdl) ;
98  Xdsp = omega_rp*(Ladsp + Lal) ; % 12.105
99  XTd = Xeq + Xdsp ; % 12.105
100 XTq = Xeq + Xqs ;
101 D = RT^2 + XTd*XTq ;
102
103 m1 = EBf * (XTq*sin(delta_f) - RT*cos(delta_f)) / D ; % 12.108
104 n1 = EBf * (RT*sin(delta_f) + XTd*cos(delta_f)) / D ;
105 m2 = XTq * Lads / (D * (Lads + Lfdl)) ;
106 n2 = RT * Lads / (D * (Lads + Lfdl)) ;
107 K1 = n1 * (psi_adf + i_df*Laqs) - m1 * (i_qf*Ladsp + psi_aqf) ; % 12.113
108 K2 = n2 * (psi_adf + i_df*Laqs) - m2 * (i_qf*Ladsp + psi_aqf) ...
109     + i_qf*Ladsp/Lfdl ; % 12.113
110
111 Kfd1 = omega_sbase * Rfd / Lfdl ;
112 a11 = -KD/M ; % OMEGA
113 a12 = -K1/M ;
114 a13 = -K2/M ;
115 a21 = omega_sbase ; % DELTA
116 a22 = 0 ;
117 a23 = 0 ;
118 a31 = 0 ; % PSI_FD
119 a32 = -Kfd1 * m1 * Ladsp ;
120 a33 = -Kfd1 * (1 - Ladsp/Lfdl + m2*Ladsp) ;
121
122 b11 = 1/M ; % OMEGA
123 b12 = 0 ;
124 b21 = 0 ; % DELTA
125 b22 = 0 ;
126 b31 = 0 ; % PSI_FD
127 b32 = omega_sbase*Rfd/Ladu ;
128
129 A = [ a11 a12 a13 ; a21 a22 a23 ; a31 a32 a33 ] ; % [omega delta psi_fd]
130 B = [ b11 b12 ; b21 b22 ; b31 b32 ] ; % [omega delta psi_fd]
131
132
133 %% SMALL SIGNAL INITIAL VALUES
```

```
134
135  % ASSUMPTIONS:
136  %
137  % - MANUAL EXCITATION (CONSTANT VOLTAGE)
138  % - CONSTANT TORQUE CONTROL
139
140  omega_0 = omega_r ;
141  omega_f = omega_r ; % THIS CAN CHANGE FOR LOAD SHARING
142
143  omega_D0 = -(omega_f - omega_0) ;
144  delta_D0 = -(delta_f - delta_0) ;
145  psi_fdD0 = -(psi_fdf - psi_fd0) ;
146
147  TM_D = 0 ; % ZERO FOR CONSTANT TORQUE CONTROL: -(Ptf - Pt0) ;
148  EfdD = 0 ; % ZERO FOR MANUAL EXCITATION: -(e_fdf - e_fd0) ;
149
150  xD0 = [omega_D0 delta_D0 psi_fdD0]' ; % [ omega delta psi_fd ]
151  uD0 = [TM_D EfdD]' ;
152
153
154  %% STABILITY DESIGN / GENERATOR DESIGN PRACTICE
155
156  % NOTES:
157  %
158  % - THIS SECTION CALCULATES THE EIGENPROPERTIES
159  % - CALCULATIONS FOR DESIGN PRACTICE WITH TRANSFER FUNCTIONS IS ALSO
160  %   INCLUDED
161
162  % FROM GENERATOR SMALL SIGNAL LINEARIZATION
163  K3 = -b32/a33 ;
164  T3 = -1/a33 ;
165  K4 = -a32/b32 ;
166
167  [Phi,Lambda] = eig(A) ;
168  lambda = diag(Lambda) ;
169  sigma = real(lambda) ;
170  omega_n = imag(lambda) ;
171
172  % KUNDUR, PPG 712, 713, 723 - 726
173  f_n = omega_n/(2*pi) ; % natural frequency
174  epsilon = -sigma ./ sqrt(sigma.^2 + omega_n.^2) ; % damping ratio
175  omega_d = omega_n .* sqrt(1 - epsilon.^2) ;
176  theta = acos(epsilon) ; % damping angle
177  tau = 1/abs(sigma) ; % decay time constant
178
179  % MAKE SOME COMPARISONS AND PRINT THEM
180  KNUM = K2*K3*K4 ;
181  KDEN = 1 - (sigma(MODE)^2 - omega_n(MODE)^2)*T3^2 ;
182  KSfd = -KNUM / KDEN ;
183  KDfd = KNUM * T3 * omega_sbase / KDEN ;
184
185  KS_SS = K1 - KNUM ; % STEADY STATE SYNCHRONIZING TORQUE COEFFICIENT
186  KSnet = K1 + KSfd ;
187  KDnet = KD + KDfd ;
```

```matlab
188
189   fprintf('\nEVALUATE STABILITY: ')
190   fprintf('\n-SPECIFY WHICH OSCILLATING MODE TO OBSERVE')
191   fprintf('\n———————————————————————————— ')
192   fprintf('\nTORQUE COMPONENTS IN STEADY STATE')
193   fprintf('\nMUST BE NON-NEGATIVE: ')
194   fprintf('\nKS_SS = %.4f ',KS_SS)
195   fprintf('\nKD = %.4f ',KD)
196
197   fprintf('\n———————————————————————————— ')
198   fprintf('\nTRANSIENT TORQUE COMPONENTS IN  OSCIL ')
199   fprintf('\n-LATING MODE %i  DUE TO FIELD  CIRCUIT ',MODE)
200   fprintf('\nKSfd  = %.4f ',KSfd)
201   fprintf('\nKDfd  = %.4f ',KDfd)
202
203   fprintf('\n———————————————————————————— ')
204   fprintf('\nNET TORQUE COMPONENTS DURING')
205   fprintf('\nTRANSIENT MUST BE NON-NEGATIVE: ')
206   fprintf('\nKSnet = %.4f ',KSnet)
207   fprintf('\nKDnet = %.4f ',KDnet)
208
209   fprintf('\n———————————————————————————— ')
210   fprintf('\nDOUBLE CHECK EIGENVALUES OF OSCILLATING')
211   fprintf('\nMODE %i ',MODE)
212   fprintf('\nomega_n = %.2f and %.2f ',sqrt(KSnet*omega_sbase/M)  ...
213                                      ,omega_n(MODE))
214   fprintf('\nepsilon = %.4f and %.4f ',0.5*KDnet/sqrt(KSnet*omega_sbase*M)  ...
215                                      ,epsilon(MODE))
216
217   fprintf('\n———————————————————————————— ')
218   fprintf('\nALL sigmas MUST BE NEGATIVE: ')
219   lambda
220
221   fprintf('———————————————————————————— ')
222   fprintf('\nDAMPING RATIO LESS THAN 0.1  IS A')
223   fprintf('\nSTABILITY CONCERN: ')
224   epsilon
225
226   fprintf('———————————————————————————— ')
227   fprintf('\nMACHINE LOAD ANGLE MUST BE LESS THAN  90 ')
228   fprintf('\nDEGREES (TOTAL LOAD ANGLE MUST BE LESS ')
229   fprintf('\nTHAN THAT BEYOND WHICH POWER DECREASES). ')
230   fprintf('\nBE SURE TO ADD PEAK TRANSIENT OSCILLATION ')
231   fprintf('\nTO THIS FINAL STEADY STATE VALUE: ')
232   fprintf('\ndelta_0 = %.2f ',delta_0 * 180/pi)
233   fprintf('\ndelta_f = %.2f\n\n ',delta_f * 180/pi)
```

Appendix B

Load-Frequency Control Program

This MATLAB program is based on the derivation in chapter 6. It is used to calculate the numerous PSCAD/EMT™inputs for the task of testing, tuning and troubleshooting the reference circuit.

Main Program

```matlab
1  clear all ; close all ; clc ;
2
3  % NOTES:
4  %
5  % -THIS PROGRAM IS DESIGNED TO GIVE PSCAD INPUTS AS WELL AS THEORETICAL
6  %  CALCULATIONS
7  % -VALIDATED AGAINST KUNDUR EX'S 11.1 AND 11.2, 05FEB17RM
8  % -NOMENCLATURE: UNDERSCORE AT END OF VARIABLE NAME MEANS PER UNIT
9
10 fprintf('\nTHIS PROGRAM CONVERTS REGULATION CONSTANTS BASED ON')
11 fprintf('\nGENERATION RESERVE, WHICH IS A GOOD IDEA FOR A REAL')
12 fprintf('\nWORLD DESIGN. HOWEVER, IF YOU JUST WANT A SIMPLE')
13 fprintf('\nCALCULATION, SET "GEN_RES" TO RATED LOAD.\n\n')
14
15 % PROCESS:
16 %
17 % STEP 00: D AND R FOR USE WITH INDIVIDUAL MACHINE TxFx's
18 % STEP 01: GLOBAL FREQUENCY CHANGE (STEADY STATE)
19 % STEP 02: INDIVIDUAL POWER CHANGE (STEADY STATE)
20 % STEP 03: INDIVIDUAL DYANAMICS (INDIVIDUAL EVENT BUT COMPOSITE FREQUENCY
21 %          RESPONSE IS AN INPUT)
22
23 % INPUTS
24 f1 = 50 ;
25 NUM = 5 ; % NUMBER OF MACHINES PARTICIPATING IN REGULATION
26 Mx_LSG1 = 461.8 ; % MVA
27 Mx_LSG2 = Mx_LSG1 ; % MVA
28 Mx_LSG3 = Mx_LSG1 ; % MVA
```

```
29  Mx_SSG = 98.9 ; % 0.05 * Mx_WTG ; % MVA
30  Mx_WTG = 406.2 ;
31  % MW [FROM WF-VSC, THE CLOSEST PART OF WHAT I AM DEFINING AS "WINDFARM"]
32  GEN_TOTL = Mx_LSG1 + Mx_LSG2 + Mx_LSG3 + Mx_SSG + Mx_WTG ;
33  % MVA, TOTAL GENERATION CAPACITY PARTICIPATING IN REGULATION
34
35  D_ = 1.5 ; % TYPICAL IS 1.0 TO 2.0 [PER UNIT LOAD / PER UNIT FREQUENCY]
36  R_eq_ = 0.05 ; % TYPICAL IS 0.04 TO 0.05 [PER UNIT FREQUENCY / PER UNIT
37                  % SPINNING RESERVE GENERATION PARTICIPATING IN REGULATION]
38  T_G = 0.2 ; % GOVERNOR TIME CONSTANT [GLOBAL FOR NOW]
39  DEAD_BAND = 1.00 ; % REGULATION PARTICIPATION DUE TO DEADBAND
40
41  H_LSG1_ = 3.525 ; % MWs / MVA
42  H_LSG2_ = H_LSG1_ ;
43  H_LSG3_ = H_LSG1_ ;
44  H_SSG_ = 3.525 ;
45  H_WTG_ = 0 ; % SYNTHETIC AND CAN BE GIVEN A VALUE LATER
46                  % [ZERO IS OK IF H_DC > 2 OR 3]
47  KE_AC_TOTL = H_LSG1_*Mx_LSG1 + H_LSG2_*Mx_LSG2 + H_LSG3_*Mx_LSG3 + ...
48                  H_SSG_*Mx_SSG ;
49
50  LD_INIT = 1890.4 ; % MW
51  LD_FINL = 1961.3 ; % MW
52  DLTA_PL = LD_FINL - LD_INIT ; % MW
53
54
55  %% STEP 00: D AND R FOR USE WITH INDIVIDUAL MACHINE TxFx's
56
57  if    DLTA_PL < 0 ;
58      % MW, SPINNING RESERVE GENERATION PARTICIPATING IN REGULATION
59      GEN_RESV = GEN_TOTL ; % INITIAL LOAD + UNUSED RESERVE
60  else  GEN_RESV = GEN_TOTL - LD_INIT ; % UNUSED RESERVE
61  end; GEN_RESV = GEN_RESV * DEAD_BAND ; % BASE FOR R_eq PER UNIT
62
63  if GEN_RESV < 0 ;
64      fprintf('\n!! WARNING !! NO GENERATION RESERVE AVAILABLE FOR')
65      fprintf('\n                    REGULATION. FOR CALCULATION PURPOSES')
66      fprintf('\n                    THE GENERATION RESERVE HAS BEEN')
67      fprintf('\n                    ARBITRARILY SET TO %.0f.',LD_INIT)
68      GEN_RESV = LD_INIT ; % MW
69  end
70
71  GEN_RESV = LD_INIT ; % MW
72
73  % INSTRUCIONS: USE THESE VARIABLES TO TUNE THE OUTPUT OF THE PROGRAM
74  MOD_LSG = 0.81 ;
75  MOD_SSG = 4.0 ;
76  MOD_WTG = 0.95 ;
77
78  MOD_LSG1 = NUM * MOD_LSG ;
79  D_LSG1_ = (D_ / MOD_LSG1) * LD_FINL / Mx_LSG1 ;
80  % PER UNIT Mx CAPACITY / PER UNIT FREQUENCY
81  R_LSG1_ = (R_eq_ * MOD_LSG1) * Mx_LSG1 / GEN_RESV ;
82  % PER UNIT FREQUENCY / PER UNIT Mx CAPACITY
```

```
 83 | T_ISO_LSG1 = T_G * R_LSG1_ ; % 1/K_ISO (FOR PSCAD)
 84 |
 85 | MOD_LSG2 = NUM * MOD_LSG ;
 86 | D_LSG2_ = (D_ / MOD_LSG2) * LD_FINL / Mx_LSG2 ;
 87 | R_LSG2_ = (R_eq_ * MOD_LSG2) * Mx_LSG2 / GEN_RESV ;
 88 | T_ISO_LSG2 = T_G * R_LSG2_ ;
 89 |
 90 | MOD_LSG3 = NUM * MOD_LSG ;
 91 | D_LSG3_ = (D_ / MOD_LSG3) * LD_FINL / Mx_LSG3 ;
 92 | R_LSG3_ = (R_eq_ * MOD_LSG3) * Mx_LSG3 / GEN_RESV ;
 93 | T_ISO_LSG3 = T_G * R_LSG3_ ;
 94 |
 95 | MOD_SSG = NUM * MOD_SSG ;
 96 | D_SSG_ = (D_ / MOD_SSG) * LD_FINL / Mx_SSG ;
 97 | R_SSG_ = (R_eq_ * MOD_SSG) * Mx_SSG / GEN_RESV ;
 98 | if ~R_SSG_ ; R_SSG_ = Inf ; end
 99 | T_ISO_SSG = T_G * R_SSG_ ;
100 |
101 | MOD_WTG = NUM * MOD_WTG ;
102 | D_WTG_ = (D_ / MOD_WTG) * LD_FINL / Mx_WTG ;
103 | R_WTG_ = (R_eq_ * MOD_WTG) * Mx_WTG / GEN_RESV ;
104 | if ~R_WTG_ ; R_WTG_ = Inf ; end
105 |
106 |
107 | %% STEP 01: GLOBAL FREQUENCY CHANGE
108 |
109 | % --INPUT: LOAD CHANGE [DLTA_PL]
110 | % --OUTPUT: COMPOSITE(STEADY STATE) FREQUENCY CHANGE [DLTA_fss]
111 |
112 | % CONVERSIONS
113 | D = D_ * LD_FINL / f1 ; % MW/Hz
114 | R_LSG1 = R_LSG1_ * f1 / Mx_LSG1 ; % Hz/MW
115 | R_LSG2 = R_LSG2_ * f1 / Mx_LSG2 ; % Hz/MW
116 | R_LSG3 = R_LSG3_ * f1 / Mx_LSG3 ; % Hz/MW
117 | R_SSG = R_SSG_ * f1 / Mx_SSG ; % Hz/MW
118 | R_WTG = R_WTG_ * f1 / Mx_WTG ; % Hz/MW
119 |
120 | % COMPOSITE FREQUENCY RESPONSE CHARACTERISTIC AND STEADY STATE RESPONSE
121 | R_eq = 1 / (1/R_LSG1 + 1/R_LSG2 + 1/R_LSG3 + 1/R_SSG + 1/R_WTG) ; % Hz/MW
122 | R_eq1_ = R_eq_ ;
123 | R_eq2_ = R_eq * GEN_RESV / f1 ;
124 | BETA = 1/R_eq + D ; % MW/Hz
125 | DLTA_fss = -DLTA_PL / BETA ; % Hz [b/c lim s->0]
126 |
127 | fprintf('\n\nDESIGN THE MACHINE REGULATION CONSTANTS')
128 | fprintf('\nSO THAT R_eq1 APPROXIMATELY EQUALS R_eq2:')
129 | fprintf('\n——————————————————————————————')
130 | fprintf('\nR_eq1 = %.4f',R_eq1_)
131 | fprintf('\nR_eq2 = %.4f\n\n',R_eq2_)
132 |
133 | % COMPOSITE INERTIA CONSTANT AND INITIAL FREQUENCY GRADIENT
134 | KE_eq = (KE_AC_TOTL + H_WTG_*Mx_WTG) ; % MWs
135 | H_eq = KE_eq / GEN_TOTL ; % MWs/MVA
136 | M_eq = 2*H_eq ; % MWs/MVA
```

```
137  f_grad = −DLTA_PL / (2*KE_eq) ; % Hz/sec [b/c lim s−>Inf]
138
139  fprintf('\nFREQUENCY OBSERVATIONS: ')
140  fprintf('\n——————————————————————————————')
141  fprintf('\nINITIAL FREQUENCY GRADIENT: %.4f Hz/sec',f_grad)
142  fprintf('\nFINAL STEADY STATE FREQUENCY: %.3f Hz\n\n',DLTA_fss)
143
144  % EFFECTIVE INERTIA CONSTANT
145  H_DC = KE_AC_TOTL / Mx_WTG ; % MWs/MVA
146
147  fprintf('\nH_DC SHOULD BE GREATER THAN 2.0 OR 3.0:')
148  fprintf('\n——————————————————————————————')
149  fprintf('\nH_DC = %.1f\n\n',H_DC)
150
151
152  %% STEP 02: INDIVIDUAL POWER CHANGE
153
154  % −INPUT: COMPOSITE(STEADY STATE) FREQUENCY CHANGE [DLTA_fss]
155  % −OUTPUT: INDIVIDUAL STEADY STATE POWER CHANGE FOR EACH MACHINE
156
157  % INDIVIDUAL BETA
158  BETA_LSG1 = 1/R_LSG1 + D/MOD_LSG1 ; % MW/Hz
159  BETA_LSG2 = 1/R_LSG2 + D/MOD_LSG2 ;
160  BETA_LSG3 = 1/R_LSG3 + D/MOD_LSG3 ;
161  BETA_SSG = 1/R_SSG + D/MOD_SSG ;
162  if R_SSG==Inf ; BETA_SSG = 0 ; end
163  BETA_WTG = 1/R_WTG + D/MOD_WTG ;
164  if R_WTG==Inf ; BETA_WTG = 0 ; end
165
166  % INDIVIDUAL DELTA PL
167  PL_LSG1 = −DLTA_fss * BETA_LSG1 ; % MW
168  PL_LSG2 = −DLTA_fss * BETA_LSG2 ;
169  PL_LSG3 = −DLTA_fss * BETA_LSG3 ;
170  PL_SSG = −DLTA_fss * BETA_SSG ;
171  PL_WTG = −DLTA_fss * BETA_WTG ;
172
173  PL_TOTL = PL_LSG1 + PL_LSG2 + PL_LSG3 + PL_SSG + PL_WTG ;
174
175  fprintf('\nTHESE INDIVIDUAL POWER CHANGES SHOULD ADD')
176  fprintf('\nUP TO THE TOTAL POWER CHANGE: \nACTUAL: %.1f MW',DLTA_PL)
177  fprintf('\nTOTAL:   %.1f MW',PL_TOTL)
178  fprintf('\n——————————————————————————————')
179  fprintf('\nLSG1 STEADY STATE POWER CHANGE: %.1f MW',PL_LSG1)
180  fprintf('\nLSG2 STEADY STATE POWER CHANGE: %.1f MW',PL_LSG2)
181  fprintf('\nLSG3 STEADY STATE POWER CHANGE: %.1f MW',PL_LSG3)
182  fprintf('\nSSG STEADY STATE POWER CHANGE:   %.1f MW',PL_SSG)
183  fprintf('\nWTG STEADY STATE POWER CHANGE:   %.1f MW\n\n',PL_WTG)
184
185  fprintf('\nFOR THE COMMUNICATION−LESS CHANNEL, ')
186  fprintf('\nTHE FOLLOWING EQUATION SHOULD HOLD: ')
187  fprintf('\n[R_Pf,SG = R_Vf,SG x R_fV,WG x R_Pf,WG]')
188  fprintf('\nTHIS PROGRAM SUGGESTS THE FOLLOWING: ')
189  fprintf('\n——————————————————————————————')
190  fprintf('\nLEG 01: R_Vf,SG OF GS−VSC IS: %.4f',sqrt(R_WTG_))
```

```matlab
191  fprintf('\nLEG 02: R_fV,WG OF WF-VSC IS: 1.0000 ')
192  fprintf('\nLEG 03: R_Pf,WG OF WTG IS:     %.4f\n\n',sqrt(R_WTG_))
193
194  %% STEP 03: SMALL SIGNAL DYNAMICS TRANSFER FUNCTION
195
196  T = 0.2 ; % T_G ;
197  M = 7.05 ;
198  D = 1.5 ; % D_LSG1_ ;
199  R = 0.05 ; % R_LSG1_ ;
200
201  G = -1/(T*M) ;
202
203  N1 = T ;
204  N0 = 1 ;
205  NUM = [N1 N0] ; % N1*s + N0
206
207  D2 = 1 ;
208  D1 = D/M + 1/T ;
209  D0 = D/(T*M) + 1/(R*T*M) ;
210  DEN = [D2 D1 D0] ; % D2*s^2 + D1*s + D0
211
212  H = G * tf(NUM,DEN) ;
213  [y,t] = step(H,3) ;
214
215  opts = bodeoptions('cstprefs');
216  opts.FreqUnits = 'Hz';
217  figure ; bode(H,opts) ; grid on ;
218
219  figure ; plot(t,y) ; grid on ;
220  csvwrite('SG_Turbine_Step.csv',[t y]) ;
```